INFORMATION TO USERS

This manuscript has been reproduced from the microfilm master. UMI films the text directly from the original or copy submitted. Thus, some thesis and dissertation copies are in typewriter face, while others may be from any type of computer printer.

The quality of this reproduction is dependent upon the quality of the copy submitted. Broken or indistinct print, colored or poor quality illustrations and photographs, print bleedthrough, substandard margins, and improper alignment can adversely affect reproduction.

In the unlikely event that the author did not send UMI a complete manuscript and there are missing pages, these will be noted. Also, if unauthorized copyright material had to be removed, a note will indicate the deletion.

Oversize materials (e.g., maps, drawings, charts) are reproduced by sectioning the original, beginning at the upper left-hand corner and continuing from left to right in equal sections with small overlaps.

Photographs included in the original manuscript have been reproduced xerographically in this copy. Higher quality 6" x 9" black and white photographic prints are available for any photographs or illustrations appearing in this copy for an additional charge. Contact UMI directly to order.

Bell & Howell Information and Learning
300 North Zeeb Road, Ann Arbor, MI 48106-1346 USA
800-521-0600

Positronium Hyperfine Splitting Corrections Using Non-Relativistic QED

Seyyed Mohammad Zebarjad
Centre for High Energy Physics
Department of Physics, McGill University
Montréal, Québec

November 1997

A Thesis submitted to the
Faculty of Graduate Studies and Research
in partial fulfillment of the requirements of the degree of
Doctor of Philosophy

Contents

List of Figures

List of Tables

Abstract

We use Nonrelativistic Quantum Electrodynamics (NRQED) as an effective field theory to calculate the single photon annihilation contribution to the positronium hyperfine splitting (HFS) in its ground state at order $\mathcal{O}(\alpha^6)$. Our analytical result completes the hyperfine splitting calculation to order $m_e\alpha^6$. Using NRQED, we derive the Lamb shift of a scalar-scalar bound state and $\mathcal{O}(\alpha^5)$ hyperfine splitting of positronium for a general excited state. Using the same technique, we also rederive the Lamb shift of Hydrogen atom and $\mathcal{O}(\alpha^5)$ HFS of positronium in its ground state.

Résumé

Nous utilisons Électro-Dynamique Quantique Non-Relativistique (NRQED) comme théorie des champs effective afin de calculer la contribution de l'anihilation d'un seul photon au découplage hyperfin du positronium dans son état de base à l'ordre $O(\alpha^6)$. Ce résultat analytique complète les calculs du découplage hyperfin à l'ordre $m_e\alpha^4$. En utilisant toujours NRQED, nous dérivons le décalage de Lamb de l'état scalaire-scalaire lié ainsi que le découplage hyperfin du positronium pour un état excité général n et l à l'ordre $O(\alpha^5)$. Finalement, nous utilisons la technique NRQED pour redériver le décalage de Lamb de l'atome d'hydrogène ainsi que le découplage hyperfin du positronium à son état de base.

Acknowledgement

I would like to thank my supervisor, Professor Clifford Burgess for his scientific and financial support. I have learned a lot from the courses I took with him and I am sure this work would have been impossible without his help. I would like to thank him for his patience and wish him the best in his research and his personal life.

I was definitely lucky to have met Dr. Patrick Labelle who introduced me the wonderful world of NRQED. He shared with me his invaluable experiences and knowledge of NRQED. I am sure, it would be very difficult, if not impossible, for me to have learnt all this material by myself. This last year of my studies during which I have worked with him has been the best time I have ever had in my life. I cannot thank him enough for his kindness and patience and I am certain he will one day make it to the top.

I also thank Professors R.C. Myers and C.S. Lam for the informative courses I took with them.

I would like to highly appreciate the financial support of the Ministry of Culture and Higher Education of Iran, without which this work would not have been feasible. I also thank Dr. Reza Hoseini, Dean of Higher Education Advisory, who has been taking care of all students affairs.

I should also thank Dr. A.H. Hoang for his collaboration to part of the hyperfine splitting calculation and also for his excellent suggestions concerning chapter(5) of this thesis.

My thanks also to Martin Kamela and Chris Roderick who helped me with the proofread of the manuscript, and Stéphane Legault for translating the abstract into French.

No doubt the smooth running of business in our physics Department

would not be possible without the skills of secretaries, Mrs. Paula Domingues, Joanne Longo, Diane Koziol, Elizabeth Sharon, and the expertise of the computer system managers, Mr. Paul Mercure and Juan Gallego, all of whom I wish to thank.

I am greatly indebted to my wife, Roza Aleyasin, and my daughters, Fatemeh and Marzieh, whose patience helped me to bear all the difficulties of these years. They invested five of the best years of their lives in my thesis without complaining about the extraordinary weather of Montreal or nagging about being away from our relatives. I hope that one day I can make it up to them. Special thanks to my parent, Khadijeh Semati, S. Mohesn Zebarjad, for their constant encouragment.

I am deeply greatful to my friend Dr. Omid Hamidi-Ravari with whom I had many unforgettable times in Physics Department and am eagerly waiting for his special ceremony in Kerman City.

It would not be fair to end this acknowledgment without mentioning the name of my friends with whom we had so much fun in Montreal: Dr. Garousi, Dr. Desfouli, Mr. Sabouri, Fatemeh Mirbagheri, Mostafa Mousavi.

Statement of Original Contributions

In this thesis, we calculate an analytical result for $\mathcal{O}(\alpha^6)$ hyperfine splitting of positronium in its ground state coming from single photon annihilation. We also calculate the $\mathcal{O}(\alpha^5)$ hyperfine splitting of positronium for a general excited state, and the Lamb shift for a bound state of two scalars. The above calculations are performed by using Non-Relativistic Quantum Electrodynamics (NRQED). Also, for the first time we recover old results such as the Lamb shift in Hydrogen atom, and the hyperfine splitting of the positronium ground state, by using NRQED techniques. All of these applications of NRQED are new, although some (not all) have been computed in other ways. This thesis completes the $\mathcal{O}(\alpha^6)$ hyperfine splitting of positronium is the first such calculation, which can be considered as a new test of QED.

Chapters (2), (3) and (4) (except sections (2.3), (2.4)) is an excerpt from our papers[14][16][17], written in collaboration with Prof. C.P. Burgess and Dr. P. Labelle. Chapter (5), which is completely written by myself, has not yet been submitted to journal, although we have published the results in the Phys. Rev. Lett.[19].

I have taken an active role in all the above calculations. Some parts of them have been checked by Dr. P. Labelle who also proposed this line of research.

Chapter 1

Motivation and Outline of this Thesis

The detailed comparisons between the heroic precision calculations using Quantum Electrodynamics (QED) and equally heroic precision measurements represent one of the pinnacles of twentieth-century physics. On the theoretical side, comparisons involving the energy levels of bound states, such as hydrogen or positronium, pose a particular challenge. This is because of the necessity of incorporating the small radiative corrections of relativistic QED into the nonperturbative treatment required for the bound state itself. Important conceptual progress in handling bound states in QED was made several years ago, by Caswell and Lepage[1], with the development of non-relativistic QED (NRQED), which consists of an application of effective-field-theory ideas to atomic physics applications of QED.

NRQED starts with the recognition that much of the complication of QED bound-state calculations arises because the fine-structure constant,[1] $\alpha = e^2/4\pi$, enters into observables in two conceptually different ways. First, α enters as the small parameter which controls the higher-order QED radia-

[1]We use throughout units for which $\hbar = c = 1$.

tive corrections. Second, α enters from the appearance in these calculations of three separate scales: the electron mass, m, the bound-state momentum, mv, and the bound-state energy, mv^2, once it is recognized that $v = O(\alpha)$ in the bound state. While much of the higher-order QED radiative corrections involve scales at, or above, m, where relativistic kinematic is important, the complications associated with handling the bound states all arise at the lower two scales, mv and mv^2.

NRQED takes advantage of this hierarchy of scales to efficiently separate the radiative corrections from the bound-state physics. First one accurately integrates out all physics associated with momenta $p \gtrsim O(m)$, obtaining an effective theory of non-relativistic particles whose interactions are organized according to their suppression by powers of the two independent small parameters, α and v. This effective theory is then used to systematically compute bound-state properties, at which point v becomes of order α. Keeping v and α independent until this last step makes the bookkeeping more straightforward. The additional bonus is that bound-state calculations are much easier to do within the effective theory because its non-relativistic framework permits the direct application of well-tested techniques based on Schrödinger's equation.

Any effective field theory relies on the existence of a hierarchy of scales, it e.g., in the case $M_1 \sim mv \ll M_2 \sim m$, in a physical problem. The heart of the effective theory's utility lies in its power-counting rules, which identify how to systematically isolate the complete contributions to any observable to any fixed order in the small ratio, M_1/M_2. NRQED is no exception in this regard, with the power-counting rules identifying the suppression of observables in powers of $v \sim \alpha$. It is the recent development of NRQED power-counting rules [2][3][4][6], which now makes it possible to directly identify the $O(\alpha^n)$

contributions to any atomic-physics observable. These rules have recently been demonstrated in practice in some illustrative papers[12][13][22][23][16] [17].

Although contributions order by order in α can also be obtained by other methods, the virtue of NRQED lies in its simplicity, which potentially makes more complicated calculations feasible. It also permits the very simple extension of low-order results to bound states involving particles of other spins [14].

It is noteworthy to mention that the effective field theory approach to non-relativistic systems is becoming standard in the literature for quarkonium systems, the strongly-interacting anologues of positronium. One can find a lot of papers about the corresponding effective field theory of Non-Relativistic Quantum Chromodynamics (NRQCD). In addition, NRQED and NRQCD are closely related to Heavy Quark Effective Theory (HQET), the effective theory applicable to systems with a single nonrelativistic particle.

Despite all these developments in effective theory approches, the power of NRQED approach has still not been fully appreciated by the atomic physics community. Therefore, our goal in presenting this thesis is twofold:

1. Using NRQED we **simplify** and **systematically** rederive many old well-known calculations such as:

   - Order α^4 energy correction of positronium, scalar-scalar and fermion-scalar bound state.
   - Order α^5 Lamb shift of hydrogen atom.
   - Order α^5 hyperfine splitting (HFS) of the ground state of positronium.

   Besides building confidence in our results, these calculations include

new results for intermediate steps in our calculations, in which we perform the matching of QED to NRQED at next-to-leading order (NLO) and next-to-next-to-leading order [2] (NNLO) in α. Only a small part of this matching is already available in the literature, and the remainder, which we present here for the first time, will have applications to many other higher-precision NRQED calculations.

2. Using NRQED we obtain new results to prove its **power** with respect to the conventional calculations:

   - Order α^5 hyperfine splitting of general excited states of positronium.
   - Order α^6 hyperfine splitting of positronium in its ground state .

Our result for the $\mathcal{O}(\alpha^6)$ permits the first-ever analytical calculation of the complete $O(m\alpha^6)$ contribution to positronium hyperfine splitting (HFS) [19]. To see the importance of this calculation let us explain the situation in more detail.

The theoretical expression for HFS of positronium in its ground state is

$$\Delta E_{hfs} = m_e \alpha^4 \left[\frac{7}{12} - \frac{\alpha}{\pi}\left(\frac{8}{9} + \frac{1}{2}\ln 2\right) + \alpha^2 \left(\frac{5}{24}\ln \alpha^{-1} + K\right) - \frac{7}{8\pi}\alpha^3 \ln^2 \alpha^{-1} + \mathcal{O}(\alpha^3)\right], \quad (1.0.1)$$

where ΔE_{hfs} is the energy difference between the triplet (ortho) and singlet (para) ground state of positronium, and K is defined by

$$K \equiv K_1(1\text{-}\gamma \text{ ann}) + K_2(2\text{-}\gamma \text{ ann}) + K_3(3\text{-}\gamma \text{ ann}) + K_4(\text{non-annihilation}) \quad (1.0.2)$$

[2] In this thesis, we use the abbreviations NLO and NNLO for Next-to-leading order and Next-to-Next-to-leading order respectively. We also use HFS for hyperfine splitting.

Using NRQED we provide, for the first time, an analytical[3] calculation of K_1(1-γ ann). Apart from K_1(1-γ ann), all the contributions to K coming from the non-annihilation, and the two- and three-photon annihilation processes have been calculated before (see Table 5.1).

In this thesis, we first rederive the α^4 and α^5 corrections of the Eq.(1.0.1) using NRQED as an effective field theory. We then calculate K_1(1-γ ann), the single-photon annihilation contribution to the constant K, completing the theoretical formula in Eq.(1.0.1).

The outline of this thesis is as follows:

- Chapter(2)

  In this chapter we introduce NRQED by briefly reviewing the NRQED Lagrangian. We then discuss the matching procedure, section(2.2), which is required to obtain some of the NRQED couplings to leading order in α. We review NRQED propagators in section(2.3). Section(2.4) gives a quick summary of NRQED power counting, as obtained in Ref.[2]. These power counting rules are then used to systematically identify all possible contributions to some particular bound state calculations which we present in chapters (3), (4) and (5).

- Chapter(3)

  Here we show how the NRQED Lagrangian, with the coefficients fixed at the leading order, gives the full O(α^4) order bound state energy shift for positronium. We also calculate this energy level shift for the cases where either or both particles have spin zero. This is the simplest application of NRQED as an effective field theory in bound state calculations.

[3] An independent numerical calculation of K_1(1-γ ann) appeared at the same time as our analytical expression.

- Chapter(4)

  In section(4.1), we first summarize the next-to-leading order matchings for two-fermi operators which are already given in the literature. We then explain how these matchings can be used to calculate the Lamb shift in the hydrogen atom, as well as in scalar-scalar bound states. The reader will surely enjoy these derivations and prefer them over more traditional ones based on the Bethe-Salpeter equation. Section(4.2) is devoted to Next-to-Leading order matching of four-fermi operators. Some of these matchings are new and have not been published previously. The main result of this section is that the complete $O(m\alpha^5)$ contribution in NRQED is obtained using precisely the same graphs as for the $O(m\alpha^4)$ contribution, but with coupling constants which are matched to relativistic QED at higher order in α. These results are then brought together to give the hyperfine splitting for both the ground state and the excited states of positronium.

- Chapter(5)

  In chapter(5) we first perform a matching at NNLO for the spin-1 annihilation operator. This is then followed by the calculation of all the bound state diagrams relevant to obtaining an analytical result for the $\mathcal{O}(\alpha^6)$ hyperfine splitting (HFS) of positronium in its ground state. This is finally used to determine, for the first time, the the unknown coefficient K_1(1-γ ann) which we introduced in Eq.(1.0.1).

Chapter 2

Introduction to NRQED

As explained in the introductory chapter NRQED is an efficient adaptation of QED which simplifies the handling of power counting, cancellation of divergences, and gauge invariance in bound state problems. In this chapter we introduce the NRQED Lagrangian and evaluate the various coefficients appearing in the Lagrangian by "matching" them to QED. NRQED Feynman rules are described in section (2.2) followed by a discussion of propagators in section (2.3). We then turn to power counting in section(2.4), which is the core of this chapter. We give some examples to clarify how the power counting rules work.

2.1 NRQED Lagrangian.

We start with the Lagrangian density of NRQED as applied to non-relativistic electrons and positrons, which is obtained from full QED by integrating out all virtual physics at scales greater than the electron mass, $\Lambda \gtrsim m$.

The fields representing the low energy degrees of freedom in this theory are ψ, χ and A_μ, which respectively represent the particles and photons with energy less than m. For example, in the case of positronium ψ and

χ would be the non-relativistic electron and positron, while in the case of the Hydrogen atom, would be the electron and proton. The Lagrangian is: $\mathcal{L} = \mathcal{L}_{photon} + \mathcal{L}_{2-Fermi} + \mathcal{L}_{4-Fermi} + \cdots$, with: [1]

$$\begin{aligned}
\mathcal{L}_{2-Fermi} &= \psi^\dagger \Big\{ iD_t + \frac{\mathbf{D}^2}{2m} + \frac{\mathbf{D}^4}{8m^3} + c_1 \boldsymbol{\sigma}\cdot\mathbf{B} + c_2\Big(\mathbf{D}\cdot\mathbf{E} - \mathbf{E}\cdot\mathbf{D}\Big) \\
&\quad + c_3 \boldsymbol{\sigma}\cdot\Big(\mathbf{D}\times\mathbf{E} - \mathbf{E}\times\mathbf{D}\Big) + \ldots \Big\}\psi \\
&\quad + \text{same terms with } \psi \to \chi, \\
\mathcal{L}_{4-Fermi} &= c_4\, \psi^\dagger \boldsymbol{\sigma}\sigma_2 \chi^* \cdot \chi^T \sigma_2 \boldsymbol{\sigma} \psi + c_5\, \psi^\dagger \sigma_2 \chi^* \cdot \chi^T \sigma_2 \psi \\
&\quad + c_6\Big(\psi^\dagger \sigma_2 \boldsymbol{\sigma} \mathbf{D}^2 \chi^* \cdot \chi^\dagger \sigma_2 \boldsymbol{\sigma} \psi + \text{h.c.}\Big) + \ldots \\
\mathcal{L}_{photon} &= \frac{1}{2}(\mathbf{E}^2 - \mathbf{B}^2) + c_9 A^0(\mathbf{k}) \frac{\mathbf{k}^4}{m^2} A^0(\mathbf{k}) \\
&\quad - c_{10} A^i(k) \frac{\mathbf{k}^4}{m^2} A^j(k) \left(\delta_{ij} - \frac{k_i k_j}{\mathbf{k}^2}\right) + \ldots
\end{aligned} \tag{2.1.1}$$

Here $\mathbf{D} = i(\mathbf{p} - q\mathbf{A})$ and $D_t = \partial_t + iqA_0$, and the components of the vector $\boldsymbol{\sigma}$ are the the usual Pauli spin matrices

$$\sigma_1 = \begin{pmatrix} 0 & 1 \\ 1 & 0 \end{pmatrix} \quad \sigma_2 = \begin{pmatrix} 0 & -i \\ i & 0 \end{pmatrix} \quad \sigma_3 = \begin{pmatrix} 1 & 0 \\ 0 & -1 \end{pmatrix},$$

and the q is the electric charge.

For the NRQED we define perturbation calculations by splitting the Lagrangian density, $\mathcal{L}$, into an unperturbed and perturbed part: $\mathcal{L} = \mathcal{L}_0 + \mathcal{L}_{int}$, where

$$\begin{aligned}
\mathcal{L}_0 &= \mathcal{L}_{0,particles} + \mathcal{L}_{0,photon} \\
&= \Big\{ \psi^\dagger \Big(i\partial_t - \frac{\mathbf{p}^2}{2m}\Big)\psi + \chi^\dagger \Big(i\partial_t - \frac{\mathbf{p}^2}{2m}\Big)\chi \Big\} + \frac{1}{2}\Big(\mathbf{E}^2 - \mathbf{B}^2\Big)
\end{aligned}$$

The Feynman rules corresponding to this Lagrangian are listed in Fig.(2.1).

[1] We omit the four fermion terms proportional to c_7 and c_8 which are listed in ref.[2], because they are redundant in the sense that they may be expressed in terms of those we display.

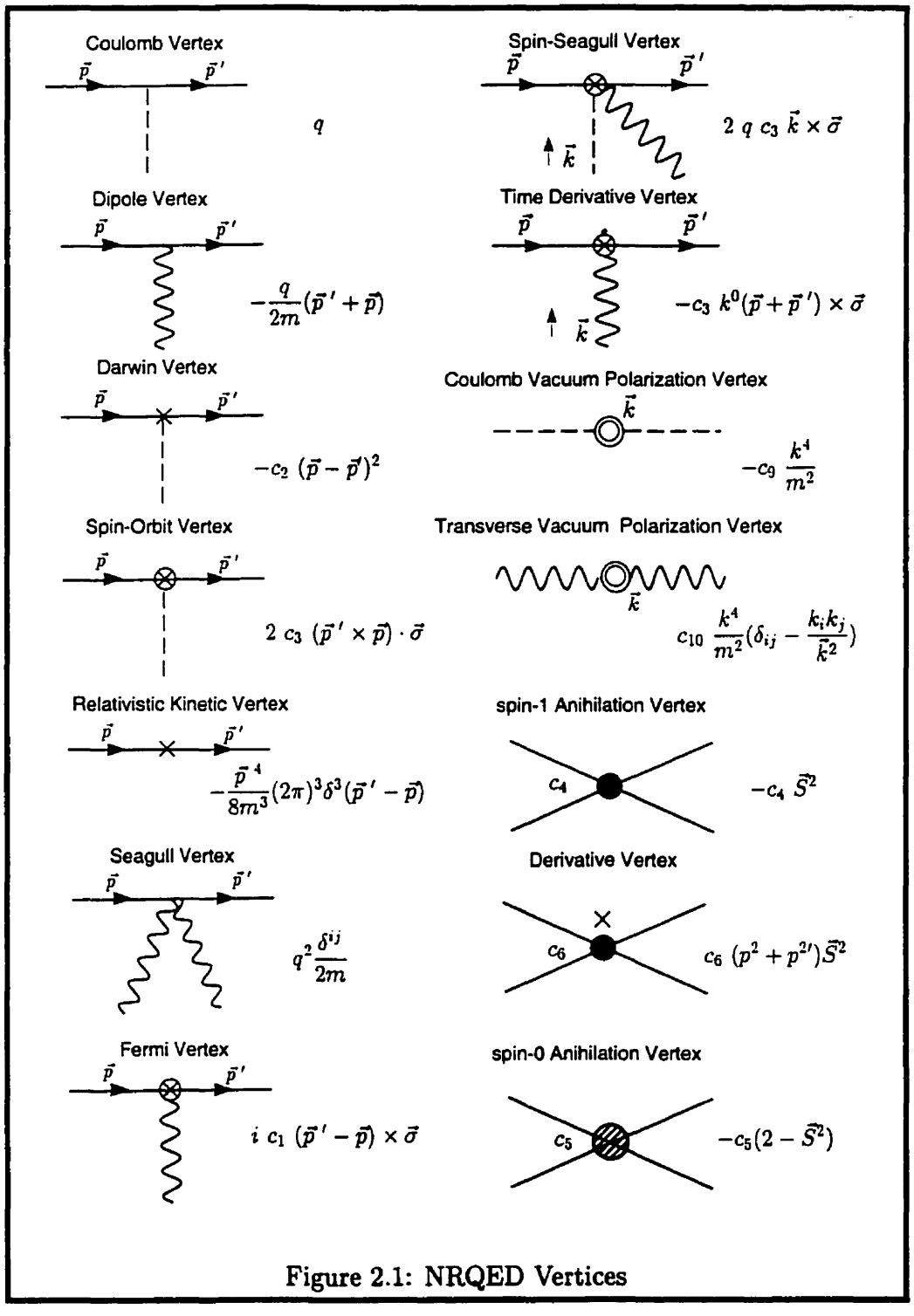

Figure 2.1: NRQED Vertices

For the photon we choose the Coulomb gauge. This is the most efficient gauge to study non-relativistic bound states since it permits the isolation of the Coulomb interaction (which must be treated non-perturbatively) from all other interactions (which can be treated as perturbations).

2.2 Matching at Leading Order.

The various coefficients, c_i, appearing[2] in Eq.(2.1.1) are calculable functions of α and m which are obtained by integrating out scales larger than m using QED. They may be conveniently determined by computing scattering processes for free electrons and positrons[3] using both QED and the NRQED Lagrangian, Eqs.(2.1.1). Equating the results to a fixed order in α and v:

$$\begin{array}{ccc} \text{QED scattering amplitudes} & & \text{NRQED scattering} \\ \text{expanded in powers of } \mathbf{p}/m & = & \text{amplitudes,} \end{array}$$

completely determines the constants c_i to this order. This is the so-called matching procedure. Notice that no bound state physics enters at this stage of the calculation.

Performing the matching operation at tree-level in QED gives the lowest-order results in α [1]. We present these calculations in detail in subsequent sections (see sections (2.2.1), (2.2.2) and (5.1)), but present here the leading order results:

$$\begin{aligned} c_1^{(0)} = \frac{q}{2m}, \qquad c_2^{(0)} = \frac{q}{8m^2}, \qquad c_3^{(0)} = \frac{iq}{8m^2}, \\ c_4^{(0)} = -\frac{\pi\alpha}{m^2}, \qquad c_6^{(0)} = -\frac{2\pi\alpha}{3m^4}, \end{aligned} \tag{2.2.2}$$

[2]There is no need to put any coefficients, c_i, for D_t and $\mathbf{D}^2$, since we can absorb them into the parameters m and q. The Relativistic Kinetic Vertex is $-\frac{\mathbf{p}^4}{8m^3}$ by Lorentz invariance and for the applications of this thesis Lorentz invariance ensures the coefficient of $\mathbf{D}^4$ is uncorrected in powers of α.

[3]Since in this thesis we mainly concentrate on positronium, we take the electron and the positron as the particles in the matching procedure. One should be careful in applying these results for other types of spin 1/2 particles.

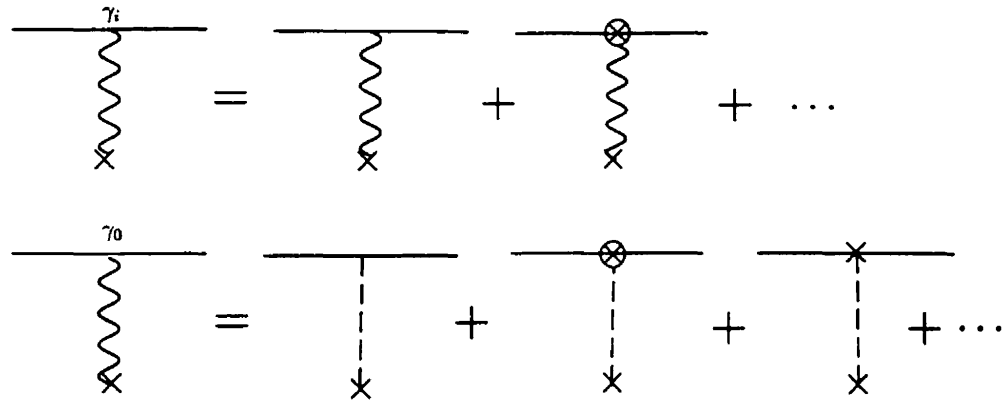

Figure 2.2: The matchings which determine $c_1^{(0)}$, $c_2^{(0)}$ and $c_3^{(0)}$. The graphs on the LHS represent QED Feynman rules, while those on the right are for NRQED.

and

$$c_5^{(0)} = c_9^{(0)} = c_{10}^{(0)} = 0. \tag{2.2.3}$$

The superscript "(0)" indicates that the coefficient is a tree-level result.

2.2.1 Two-Fermi Operators

The coefficients of two-fermi operators, c_1, c_2 and c_3, appearing in Eq.(2.1.1) can be fixed by considering the scattering of an electron by an external field A_μ. This is illustrated, at tree level, in Fig.(2.2). In writing the LHS we use the following representation of the Dirac spinor, u, in terms of a two-component spinor, ξ:

$$u(p) = \sqrt{\frac{E+m}{2E}} \begin{pmatrix} \xi \\ \frac{\boldsymbol{\sigma}\cdot\mathbf{p}}{E+m}\xi \end{pmatrix} \tag{2.2.4}$$

where ξ is normalized to unity. We then expand the vertex of Fig.(2.2) in powers of $\frac{\mathbf{p}}{m}$, leading to:

$$(QED)_{1st-row} \;=\; \bar{u}(p')q\gamma_i u(p)$$

$$= -q\,\xi'^{\dagger}\,\frac{\mathbf{p}+\mathbf{p}'}{2m}\,\xi + iq\,\xi'^{\dagger}\,\frac{(\mathbf{p}'-\mathbf{p})\times\boldsymbol{\sigma}}{2m}\,\xi + \mathcal{O}(\mathbf{p}^2/m^2)$$

$$(QED)_{2nd-row} = \bar{u}(p')q\gamma_0 u(p)$$

$$= q\,\xi'^{\dagger}\,\xi + iq\xi'^{\dagger}\,\boldsymbol{\sigma}\cdot\frac{(\mathbf{p}'\times\mathbf{p})}{4m^2}\,\xi - q\,\xi'^{\dagger}\,\frac{(\mathbf{p}-\mathbf{p}')^2}{8m^2}\,\xi + \mathcal{O}(\mathbf{p}^3/m^3). \qquad (2.2.5)$$

Using the Feynman rules of NRQED shown in Fig.(2.1), we can easily find the right-hand side of Fig.(2.2) to same order in $(\mathbf{p}/m)$:

$$(NRQED)_{1st-row} = -q\,\xi'^{\dagger}\,\frac{\mathbf{p}+\mathbf{p}'}{2m}\,\xi + ic_1\,\xi'^{\dagger}\,(\mathbf{p}'-\mathbf{p})\times\boldsymbol{\sigma}\,\xi$$

$$(NRQED)_{2nd-row} = q\,\xi'^{\dagger}\,\xi + 2c_3\,\xi'^{\dagger}\,\boldsymbol{\sigma}\cdot(\mathbf{p}'\times\mathbf{p})\xi - c_2\xi'^{\dagger}\,(\mathbf{p}-\mathbf{p}')^2\,\xi \qquad (2.2.6)$$

Equating Eqs.(2.2.5) and (2.2.6), we obtain the coefficients $c_1^{(0)}$, $c_2^{(0)}$ and $c_3^{(0)}$ in Eq.(2.2.2). We refer to this as "tree level matching" because only tree level QED diagrams are involved (similarly, n-loop matching will refer to the number of loops "n" in the QED diagrams). The one-loop matching introduces $\mathcal{O}(\alpha)$ corrections to the coefficients, c_i.

It should be emphasized that the matching calculation does not involve any bound states at all, since it is done using only the scattering of free electrons and positrons. Matching is also the only stage of the calculation which involves QED diagrams. Once the coefficients of the NRQED Lagrangian are obtained in this way only they are used in the subsequent bound-state calculations. This separation of the matching from the bound-state calculations lies at the heart of NRQED's simplicity. For example, this separation permits the use of different gauges in the relativistic and non-relativistic parts of the calculation, since the gauge choice used for NRQED is independent of the gauge used in QED, so long as one computes only gauge-invariant quantities. This permits the convenience of using a covariant gauge, like Feynman

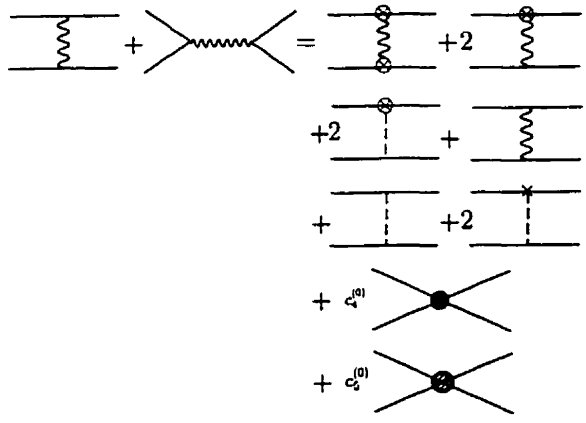

Figure 2.3: The matching which determines $c_1^{(0)}$, $c_2^{(0)}$, $c_3^{(0)}$, $c_4^{(0)}$ and $c_5^{(0)}$.

gauge, in the QED part of the calculation while keeping Coulomb gauge for NRQED calculations.

2.2.2 Four-Fermi Operators

To see how the effective four-fermi couplings, $c_4^{(0)}$ and $c_5^{(0)}$, arise, we repeat the previous procedure for tree level e^+e^- scattering in both QED and NRQED. In this case the tree level photon-exchange graphs are automatically reproduced by their NRQED counterparts due to the just obtained matching results for $c_1^{(0)}$, $c_2^{(0)}$, and $c_3^{(0)}$. That means the t-channel QED diagram cancels the NRQED t-channel graphs in Fig.(2.3) [4]. This leaves $c_4^{(0)}$ and $c_5^{(0)}$, to reproduce the effect of only the annihilation graph in Fig.(2.3). This must be reproduced by an effective interaction because the photon which is exchanged must necessarily involve a four-momentum of order m, and so cannot appear in the effective theory. For simplicity, in performing this matching we evalu-

[4]Indeed, for non-relativistic electrons and photons the energy of the exchanged photon is much below the electron mass and so this scattering is described by the same t-channel graph in NRQED. As a result, tree-level t-channel photon exchange does not contribute to any of the NRQED four-fermi operators in the matching process.

ate all diagrams at threshold — *i.e.* all the diagrams have vanishing external three momentum in the center-of-mass frame of the electron-positron pair. We emphasize that this choice of external momentum is purely for convenience, and the matching could equally well be performed with non-zero (but non-relativistic) three-momenta for the electron and positron, giving precisely the same NRQED coefficients. Using the QED Feynman rules, the scattering amplitude for the annihilation diagram at threshold gives

$$(QED) = \bar{v}(0) q\gamma_\mu u(0) \left(\frac{-1}{m^2}\right) \bar{u}(0) q\gamma_\mu v(0), \tag{2.2.7}$$

where $u(0)$ and $v(0)$ denote the electron (positron) spinor at threshold:

$$u(0) = \begin{pmatrix} \xi_1 \\ 0 \end{pmatrix} \quad , \quad v(0) = \begin{pmatrix} 0 \\ -i\sigma_2 \xi_2^* \end{pmatrix}.$$

The matrix element reads explicitly

$$\begin{aligned} (QED) &= \frac{q^2}{4m^2} \left(\xi_2^T \sigma_2 \boldsymbol{\sigma} \xi_1\right) \cdot \left(\xi_1^\dagger \boldsymbol{\sigma} \sigma_2 \xi_2^*\right) \\ &= \frac{q^2}{4m^2} \left[\frac{3}{2}\left(\xi_2^\dagger \xi_2\right)\left(\xi_1^\dagger \xi_1\right) + \frac{1}{2}\left(\xi_2^\dagger \boldsymbol{\sigma} \xi_2\right) \cdot \left(\xi_1^\dagger \boldsymbol{\sigma} \xi_1\right)\right] \end{aligned} \tag{2.2.8}$$

where we have used a Fierz re-shuffling on the second equality. We recognize the right-hand side of Eq.(2.2.8) to be the matrix element between ξ_1 and ξ_2 of the following operator:

$$\frac{q^2}{4m^2} \frac{(3 + \boldsymbol{\sigma}_1 \cdot \boldsymbol{\sigma}_2)}{2} = \frac{q^2}{4m^2} \mathbf{S}^2. \tag{2.2.9}$$

Here $\mathbf{S} = \mathbf{s}_1 + \mathbf{s}_2$, with $\mathbf{s}_i = \frac{1}{2}\boldsymbol{\sigma}_i$ is the total intrinsic spin operator, and the subscript "i" of $\boldsymbol{\sigma}_i$ denotes upon which particle the corresponding Pauli matrix acts. Recall from Fig.(2.1) that the sum of spin-1 and spin-0 Annihilation vertices at tree level is

$$-c_4^{(0)} \mathbf{S}^2 - c_5^{(0)} (2 - \mathbf{S}^2). \tag{2.2.10}$$

Equating Eqs.(2.2.9) and (2.2.10) for spin-singlet and spin-triplet state, we obtain $c_4^{(0)} = -q^2/4m^2$ and $c_5^{(0)} = 0$. Therefore, we have obtained the coefficients $c_4^{(0)}$ and $c_5^{(0)}$ in Eqs.(2.2.2) and (2.2.3).

2.3 NRQED Propagators.

More complicated scattering amplitude involve e^+e^- lines, which we now discuss. It is much simpler and powerful to work with old fashioned Rayleigh-Schrödinger perturbation theory (in which one indicates explicitly if an internal particle has positive or negative energies), than with covariant time-ordered perturbation theory. In addition, the use of the Coulomb gauge for the photon makes computations in the effective theory much easier to handle. In old fashion perturbation theory (OFPT) [10] all particles are on-shell but energy is not conserved at the vertices, and all the diagrams have an explicit direction along which time flows. That means Coulomb photons propagate instantaneously (*i.e.* along vertical lines in our diagrams since we choose the time axis to point to the right) and transverse photons propagate in the time direction. In OFPT [10] the propagator for each intermediate state is:

$$\frac{1}{E_0 - E_{intermediate}} \tag{2.3.11}$$

In this expression E_0 is the total unperturbed energy of the state of interest and $E_{intermediate}$ is the energy of the particles present in the intermediate state. For example, for a bound state having principle quantum number n, nuclear charge Z and reduced mass $\mu = m_1 m_2/(m_1 + m_2)$, E_0 would be $-Z^2\mu\alpha^2/(2n^2)$ and $E_{intermediate}$ is $p_1^2/(2m_1^2) + p_2^2/(2m_2)$, with $p^2/(2m^2)$ counting for each fermion. When there are photons in the intermediate state, we have the following cases, depending on whether we follow $\mathbf{A}_i$ or A_0:

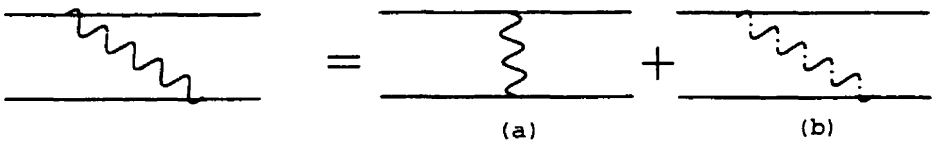

Figure 2.4: Separation of a transverse photon into a soft, instantaneous contribution (represented by a vertical line) and an ultra-soft propagator (represented by the broken wavy line).

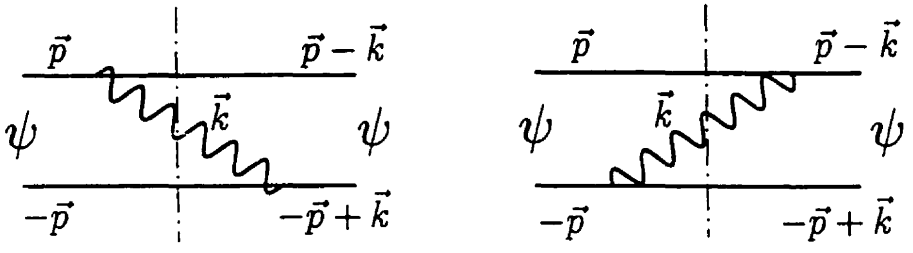

Figure 2.5: The two non-covariant perturbation theory diagrams which correspond to a single covariant diagram using time-ordered propagator.

1. Non-Coulomb photon ($\mathbf{A}_i$):

   In this case the propagator, Eq.(2.3.11), should be modified for each photon to:

$$\frac{1}{E_0 - E_{intermediate}} \times \frac{1}{2\sqrt{\mathbf{k}^2+\lambda^2}}\left(\delta_{ij} - \frac{k_i k_j}{\mathbf{k}^2+\lambda^2}\right), \qquad (2.3.12)$$

   where λ is a regulator for infrared (IR) divergences and we should also consider the photon energy, $|\mathbf{k}|$, in the intermediate state energy, $E_{intermediate}$. As is shown in [2], the power of NRQED is enhanced if one separates the general photon propagator into the "soft" transverse photons (having energies of order $\gamma \equiv Z\mu\alpha$) and the "ultra-soft" photons (with $E \simeq \gamma^2/\mu$) because the counting rules differ for the two types of photons. Soft photons are represented by vertical lines (*i.e.* they interact instantaneously), Fig.(2.4(a)) and therefore never appear

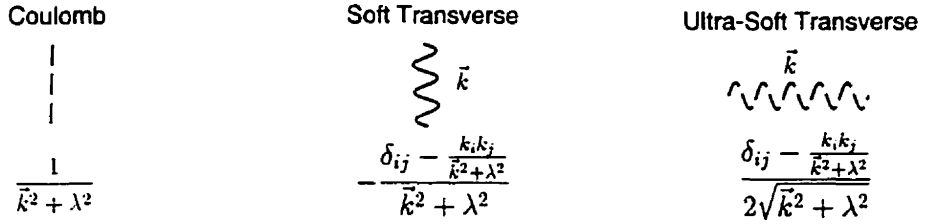

Figure 2.6: Photon propagators.

in intermediate states. On the other hand, ultra-soft photons propagate in the time direction, Fig.(2.4(b)).

It is shown in Ref[2] that when we have soft photon in intermediate state, Eq.(2.3.12) reduces to

$$\frac{-1}{\mathbf{k}^2+\lambda^2}\left(\delta_{ij}-\frac{k_ik_j}{\mathbf{k}^2+\lambda^2}\right) \tag{2.3.13}$$

It is easy to prove this equation. Consider the diagrams shown in Fig.(2.5). Using Eq.(2.3.12), we calculate the sum of the intermediate propagators of these two diagrams:

$$\frac{1}{2|\mathbf{k}|}\left(\delta_{ij}-\frac{k_ik_j}{\mathbf{k}^2}\right)\left(\frac{1}{\frac{-\gamma^2}{2\mu}-\frac{(\mathbf{p}-\mathbf{k})^2}{2m_1}-\frac{\mathbf{p}^2}{2m_2}-|\mathbf{k}|}+\frac{1}{\frac{-\gamma^2}{2\mu}-\frac{\mathbf{p}^2}{2m_1}-\frac{(\mathbf{p}-\mathbf{k})^2}{2m_2}-|\mathbf{k}|}\right) \tag{2.3.14}$$

For a soft photon, since $|\mathbf{k}| \sim Z\mu\alpha$, we can ignore the other terms in denominator with respect to $|\mathbf{k}|$. Therefore we obtain Eq.(2.3.13) with $\lambda = 0$.

2. Coulomb Photon (A_0):

   In this case the Coulomb propagator is given by $1/(\mathbf{k}^2+\lambda^2)$.

Fig.(2.6) summarizes these three types of photon propagators.

2.4 NRQED Power Counting

The essence of any effective field theory is its power-counting rules, since these are what permit the systematic calculation of observables to any order in small ratios of scales. Unfortunately, power counting in NRQED is slightly more complicated than in many effective field theories because of the appearance of 'ultra-soft' photons. Recall that the charged particles in a QED bound state typically have momenta $p \sim m\alpha$ and energy $E \sim m\alpha^2$. Photons can therefore be emitted with momenta equal to *either* of these scales. Photons having momenta, k, (and energy ω) of order $m\alpha$ (soft photon) do not pose any problems for power-counting, but those having $k, \omega \sim m\alpha^2$ — the 'ultra-soft' ones — do. Physically, such ultra-soft photons represent the effects of retardation in the effective theory.

Fortunately, these ultra-soft photons have wavelengths which are also large compared to the size of the bound state, and so their effects can be organized into slightly more complicated power-counting rules using what amounts to a multipole expansion in their couplings to the charged particles. In the final analysis, this multipole expansion introduces extra suppression by powers of α into interaction vertices involving ultra-soft photons. (Their contribution to the hyperfine splitting starts at order $m\alpha^6$ [2].)

When the dust settles, the power-counting result has an appealingly simple form [2]. Consider computing a contribution to a bound-state observable using the NRQED Lagrangian, Eq.(2.1.1), in perturbation theory. We face two possibilities, which are treated separately in the next two sections:

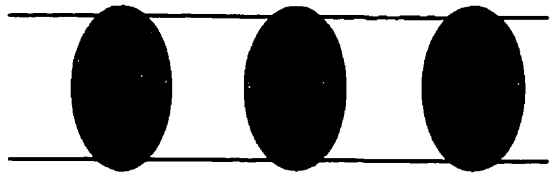

Figure 2.7: Generic NRQED diagrams in the presence of soft photons only.

2.4.1 Soft Photons

When only soft photons are present – *i.e.* when retardation effects are neglected – all NRQED diagrams reduce to a set of instantaneous interactions, giving graphs as in Fig.(2.7). There are several quantities which determine the size of the contribution of any such graph to bound-state observables [2]. One of these is N, the number of electron-positron propagators separating the instantaneous interactions[5]. The other two quantities are related to the powers of α and $1/m$ which appear in each of the coupling constants, c_i, of the NRQED Lagrangian. Suppose the particles in the bound state have masses m_1 and m_2, with charges $q_1 = e$ and $q_2 = Ze$ respectively. Define, then, κ and ρ to be, respectively, the total number of powers of $1/m_1$, $1/m_2$ which appear in the vertices of the graph of interest. Finally, denote by n_i the number of powers of α which appear in vertex "i" . a_i similarly denotes the number of powers of Z in a vertex. Suppose N, κ, ρ, $\sum_i n_i$ and $\sum_i a_i$, with the sum over all vertices, are known for any particular NRQED graph. Then the contribution of this graph to the energy-level shift in a bound state is of order[2]:

$$\frac{\mu^{\kappa+\rho+1}}{m_1^{\kappa} m_2^{\rho}} Z^{\eta} \alpha^{\zeta}, \tag{2.4.15}$$

[5] N is denoted N_{TOP} in ref. [2].

times a possible factor of $\ln(Z\mu\alpha)$. Here $\mu = m_1 m_2/(m_1+m_2)$ is the reduced mass and ζ and η are defined to be

$$\zeta = 1+\kappa+\rho-N+\sum_i n_i, \tag{2.4.16}$$

$$\eta = 1+\kappa+\rho-N+\sum_i a_i \tag{2.4.17}$$

The proof of Eq.(2.4.15) is as follows. When we have only soft photons then the only dynamically relevant energy scale in the NRQED graph is the typical bound state three momentum $\gamma \equiv Z\mu\alpha$. The masses of the constituents factor out trivially of any NRQED diagram. Indeed, the masses appear only as an overall factor in the rules for the vertices and in the propagators[6]. Thus, for any particular NRQED graph, there is an overall factor $1/(m_1^\kappa m_2^\rho \mu^{-N})$. Since the NRQED graphs have dimensions of energy, integration of three momentum in these graph should give us a factor $\gamma^{\kappa+\rho-N+1}$. That means we obtain

$$\frac{\mu^{\kappa+\rho+1}}{m_1^\kappa m_2^\rho}\Big(Z\alpha\Big)^{1+\kappa+\rho-N} \tag{2.4.18}$$

There are also additional powers of Z and α coming from the charges of vertices, $\sum_i a_i$ and $\sum_i n_i$, which we should add to the above equation. This completes the proof of Eq.(2.4.15).

To understand how to work with these rules, let us consider Fig(2.9(a)) for positronium. Since $m_1 = m_2 = m$, $\mu = m/2$ and $Z = 1$, Eq.(2.4.15) reduces to $m\alpha^\zeta$. From the Fig.(2.9(a)) we can see that $N = 2$, $\kappa+\rho = 7$, $\sum_i n_i = 2$. Therefore this figure will contribute to the order of $m\alpha^8$ in the bound state calculation.

Although the quantity N enters in Eqs.(2.4.16) and (2.4.17) with a negative sign, inserting additional interactions (and so increasing N) typically

[6]The propagator for the two bound particles is given simply by $\frac{-1}{(\mathbf{p}^2+\gamma^2)/2\mu}$.

involves sufficient additional vertices to ensure that the net contribution to ζ increases and that the contribution from the diagram is therefore further suppressed. The only exception to this statement is the case of repeated insertions of the Coulomb interaction, which increases N, $\sum_i n_i$ and $\sum_i a_i$ by 1 but leaves $\kappa + \rho$ unchanged (recall the Coulomb interaction does not contain any powers of inverse mass). Therefore, adding any number of Coulomb interactions to a given diagram leaves the value of ζ unchanged, indicating that one cannot perturb in the Coulomb interaction, which must be summed up to all orders. This is accomplished by using Schrödinger wave-functions for the external lines of the bound state diagrams and the non-relativistic Schrödinger-Coulomb propagator for intermediate states. On the other hand, it is easy to see that adding any other interaction increases the value of ζ since all the other interactions contain powers of $1/m$. Consequently There are only a finite number of graphs which can contribute for a given positive choice of ζ.

2.4.2 Ultra-Soft Photons

For the diagrams containing ultra-soft photon we must extend the counting rules presented in the previous section. This is accomplished in Ref.[2][6], but because a full explanation of this counting would take too long, we simply state here the final result.

A diagram containing ultra-soft photons contributes to order

$$\frac{\mu^{\kappa+\rho+1}}{m_1^{\kappa} m_2^{\rho}} Z^{\tilde{\eta}} \alpha^{\tilde{\zeta}} \tag{2.4.19}$$

where we define $\tilde{\zeta}$ and $\tilde{\eta}$ to be

$$\tilde{\zeta} = 1 + \kappa + \rho - N + 2N_\gamma + \sum_i \mathcal{M}_i \tag{2.4.20}$$

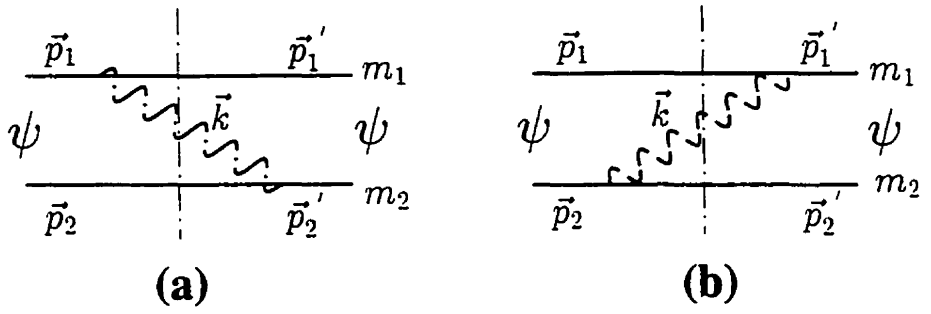

Figure 2.8: Two non-covariant perturbation theory diagrams corresponding to a transverse photon exchange.

$$\tilde{\eta} = 1 + \kappa + \rho - N + \sum_i a_i + 2N_\gamma + \sum_i \mathcal{M}_i \tag{2.4.21}$$

where N_γ is the number of ultra-soft photons in the diagram and $\mathcal{M}_i$ is order of multipole expansion to which the i^{th} vertex has been expanded. The sum in $\sum_i \mathcal{M}_i$ is over all the vertices connected to ultra-soft photon. To explain what we mean by multipole expansion, consider diagrams shown in Fig.(2.8)[7]:

- Zeroth order of multipole expansion

  Zeroth order term in multipole expansion is obtain by setting $\mathbf{p}_1' = \mathbf{p}_1$ and $\mathbf{p}_2' = \mathbf{p}_2$ in NRQED vertices. For example, for Fig.(2.8(a)) the zeroth order term is:

$$Fig.(2.8(a))\Big|_0 = \int \frac{d^3\mathbf{p}}{(2\pi)^3} \quad \Big\{\psi^*(\mathbf{p}_1', \mathbf{p}_2')\Big(\frac{q_1(\mathbf{p}_1 + \mathbf{p}_1')_i}{2m_1}\Big)\Big(\frac{q_2(\mathbf{p}_2 + \mathbf{p}_2')_i}{2m_2}\Big) \frac{1}{2|\mathbf{k}|}\Big(\delta_{ij} - \frac{k_i k_j}{\mathbf{k}^2}\Big)\Big(\frac{1}{\frac{-\gamma^2}{2\mu} - \frac{\mathbf{p}_1'^2}{2m_1} - \frac{\mathbf{p}_2^2}{2m_2} - |\mathbf{k}|}\Big) \psi(\mathbf{p}_1, \mathbf{p}_2)\Big|_{\mathbf{p}_1 = \mathbf{p}_1' = -\mathbf{p}_2 = -\mathbf{p}_2' = \mathbf{p}}\Big\} \tag{2.4.22}$$

In the case of the Fermi vertex, this gives zero since the NRQED Feyn-

[7]These two diagrams are considered into one diagram in covariant perturbation theory.

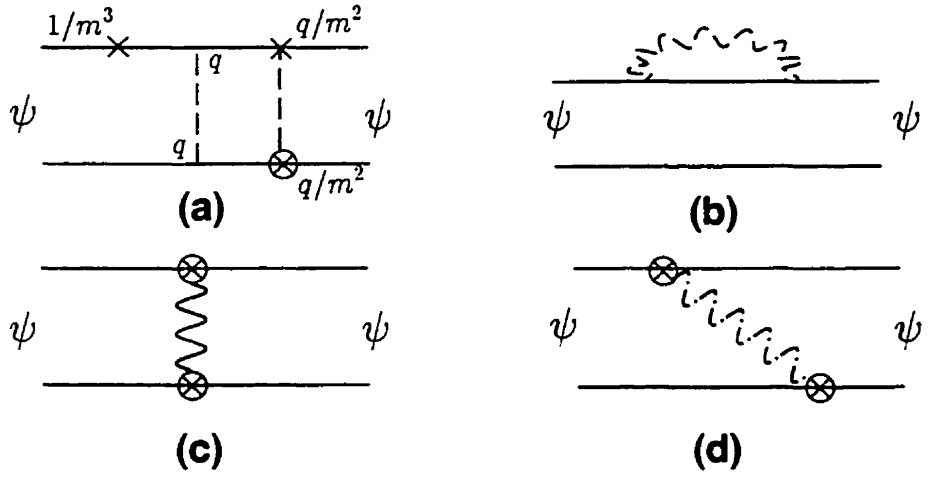

Figure 2.9: Generic bound state potentials.

man rule is proportional to $\mathbf{p}' - \mathbf{p} = \mathbf{k}$. This means that the first nonzero contribution is of the first order in the multipole expansion.

- Higher order multipole expansion

  To obtain the higher order terms in the multipole expansion, one provides a factor $(\pm\mathbf{k}\cdot\boldsymbol{\nabla}_{\mathbf{p}_i'})^n/n!$ for each vertex connected to an ultra-soft photon, where n is the order of interest in the multipole expansion, and a plus(minus) sign is used if the photon is absorbed(emitted). The gradient must be taken with respect to the three momentum of the fermion line on the right of the vertex. It is necessary to distinguish between the momentum of the fermion before and after the interaction, even though we have to set them equal in the end.

In this thesis we do not need to go beyond the zeroth order in the multipole expansion. We now give a few examples of the use of Eqs.(2.4.20)) and (2.4.21).

As a first example consider the interaction Fig.(2.9(b)) in hydrogen, $m_1 =$

m_e and $m_2 = m_p$, where the ultra-soft photon, Eqs.(2.4.20) and (2.4.21), is connected to an electron line. In this diagram, $\kappa = 0$ and $\rho = 1$ (there is one factor of $1/m$ on each vertex), $\sum_i n_i = 1$ (a factor e on each vertex), $N = 1$, $N_\gamma = 1$ and, if the zeroth order in the multipole expansion (or in the Taylor expansion) is used, $\mathcal{M}_1 = \mathcal{M}_2 = 0$. This leads to a contribution of order α^5. The mass dependence is found to be μ^3/m_e^2 and the Z dependence is, from (2.4.21), Z^4. This diagram therefore contributes to order

$$\frac{\mu^3 Z^4}{m_e^2}\alpha^5. \tag{2.4.23}$$

In fact, this result is enhanced by a logarithm $\ln(Z\alpha)$ and contributes to the Lamb shift.

Consider now Fig.(2.9(c)) in positronium so that $Z = 1$ and $m_1 = m_2 = m_e$. In this diagram, the transverse photon is soft (represented by a vertical line). We can therefore use Eqs.(2.4.16) and (2.4.17). One has $\sum_i n_i = 1$ and $\kappa = \rho = 1$. If the tree level expressions are used for the coefficients, then this diagram contributes to order $m_e\alpha^4$. The same diagram will contribute to a higher order in α if the loop corrections to the coefficients of the Fermi vertices are considered (the one-loop correction being, from Eq.(4.1.2), $\alpha/2\pi$).

As a final example, consider Fig.(2.9(d)) in positronium where $m_1 = m_2 = m_e$ and $Z = 1$. Here the photon is ultra-soft. As mentioned previously, the first non-vanishing contribution from this diagram contains two factors of $\mathbf{k}$ (one from each spin vertex) so that $\sum_i \mathcal{M}_i$ is equal to at least two. $N = 1$, $N_\gamma = 1$ and the other coefficients are as in Fig.(2.9(c)), if the tree level coefficients are used. One then finds that this diagram will contribute to order $m_e\alpha^7$.

Summary

In this chapter, we have reviewed the following preliminary subjects in a NRQED calculation:

- The NRQED Lagrangian:

  We wrote the most general Lagrangian which respects low energy symmetries such as parity and gauge invariance.

- Matching at the leading order:

  The unknown coefficients in the NRQED Lagrangian are evaluated by matching the QED to NRQED at leading order in α at threshold.

- Power counting:

  It was shown that we have two types of counting rules in a bound state system for soft and ultra-soft photons. Since there are an infinite number of vertices in an effective field theory, it is extremely important to decide which ones contribute to our problem. Using power-counting rules allows us to make that decision.

Now we are ready to do the simplest calculations in the bound state by using NRQED as an effective field theory. We will calculate the full $\mathcal{O}(\alpha^4)$ energy shift of positronium, scalar-scalar and fermion-scalar in a bound state.

Chapter 3

Leading-Order Bound State Energy Shift.

The $\mathcal{O}(\alpha^4)$ correction to the binding energy of an electrostatically bound system of two spin-$\frac{1}{2}$ particles is a well-understood problem in quantum mechanics. Recently, corrections at the same order to the energy of states involving two spin-0 particles or a spin$\frac{1}{2}$- spin 0 bound state, have been calculated [18] using Bethe-Salpeter methods. In this chapter we reproduce these results for the full $\mathcal{O}(\alpha^4)$ energy corrections for the above systems, using NRQED. The purpose in so doing is to test NRQED against standard results, and to develop some techniques for later use in our calculations.

3.1 Positronium Energy Shift to Order α^4.

All NRQED calculations can be divided into three steps.

- First use the counting rules to identify the diagrams which contribute to the order of interest. This first step not only permits the identification of the relevant diagrams, but it also fixes the order (in the number of loops) at which the coefficients, c_i, of the NRQED Lagrangian must be matched.

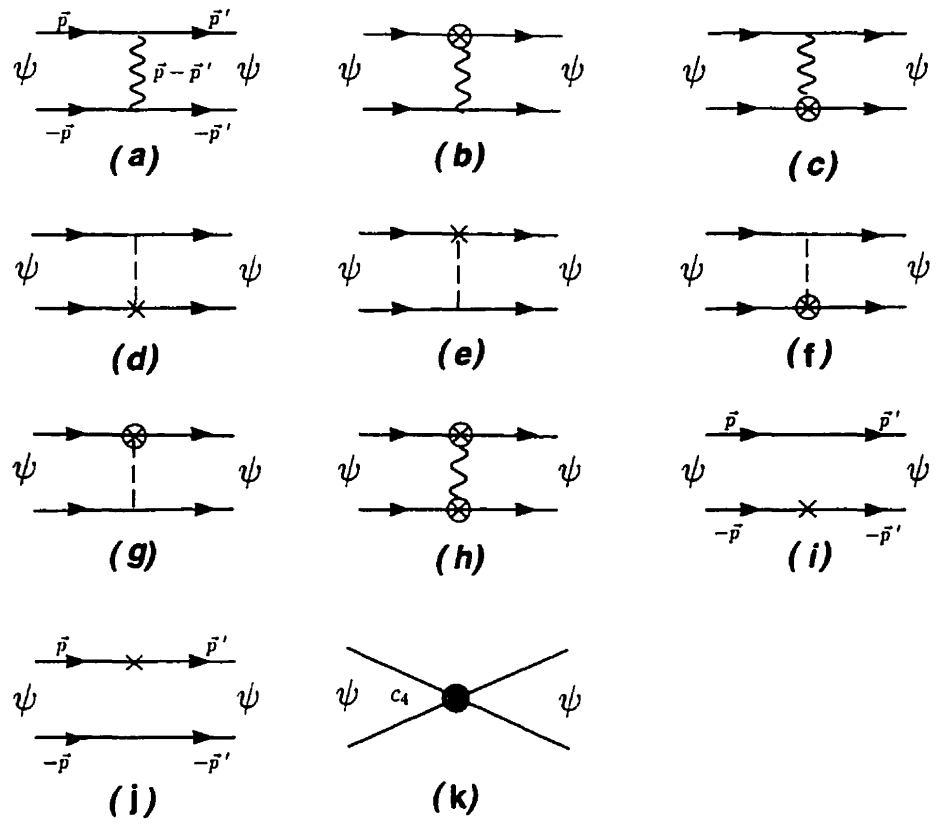

Figure 3.1: The lowest order diagrams contributing to the fermion-fermion bound state energy.

- Second, match the coefficients to the order indicated by step one.
- Finally, evaluate the relevant NRQED bound state diagrams.

We are now in a position to perform these steps for the calculation of the full $\mathcal{O}(\alpha^4)$ corrections to all energy levels of a spin $\frac{1}{2}$-spin $\frac{1}{2}$ bound state. We first consider the general case where the two fermion masses are different .

To find all the NRQED diagrams which contribute to order α^4 we start from the counting rules:

- Soft photons

  Recall that soft photons contribute to order :

$$\frac{\mu^{\kappa+\rho+1}}{m_a^{\kappa} m_b^{\rho}} Z^{\eta} \alpha^{\zeta}, \tag{3.1.1}$$

  where

$$\zeta = 1 + \kappa + \rho - N + \sum_i n_i \tag{3.1.2}$$

  Since we want to calculate to the order α^4, we put $\zeta = 4$, and obtain the following constraint: $\kappa + \rho - N + \sum_i n_i = 3$. Considering first the case where $N = 0$, we are left with the condition $\kappa + \rho + \sum_i n_i = 3$. There are five possible solutions for this condition which correspond to the diagrams shown in Fig.(3.1):

  1. $\kappa = 2$, $\rho = 0$ and $\sum_i n_i = 1$, Figs.(3.1 (e), (g)).
  2. $\kappa = 0$, $\rho = 2$ and $\sum_i n_i = 1$, Figs.(3.1 (d), (f)).
  3. $\kappa = 1$, $\rho = 1$ and $\sum_i n_i = 1$, Figs.(3.1 (a), (b), (c), (h), (k)).
  4. $\kappa = 0$, $\rho = 3$ and $\sum_i n_i = 0$, Fig.(3.1 (i)).
  5. $\kappa = 3$, $\rho = 0$ and $\sum_i n_i = 0$, Fig.(3.1 (j)).

  As the reader can easily check, all the diagrams having $N \geq 1$, contribute at least to $\mathcal{O}(\alpha^5)$.

- Ultra-soft photons

  From Eq.(2.4.20), one can see that diagrams with ultra-soft photons start at $\mathcal{O}(\alpha^5)$, and so are irrelevant at the order of current interest.

All the diagrams which contribute to this problem are therefore shown in Fig.(3.1). It is important to notice that the annihilation diagram in Fig.(3.1(k))

will contribute to the energy shift only when the particles involved are anti-particles of one another, and so have the same masses. The wave-function, $\psi(\mathbf{p})$, is the product of the Schrödinger wave-function in momentum space and a two component, dimensionless spinor. The spinor part acts on each fermion line. For a spin $\frac{1}{2}$-spin $\frac{1}{2}$ bound state, this becomes a tensor product of two such spinors. There would be of course no spinors for a bound state of two scalars.

Let us start the α^4 calculation by considering the contribution of diagram Fig.(3.1(a)) to the energy shift: (in this chapter we replace all c_i's by their tree-level values.)

$$\begin{aligned}
\Delta E_a &= \int \frac{d^3p d^3p'}{(2\pi)^6}\psi^*(\mathbf{p}')\left[\left(\frac{e}{2m_a}(\mathbf{p}+\mathbf{p}')_i\right)\left(\frac{Ze}{2m_b}(\mathbf{p}+\mathbf{p}')_j\right)\right. \\
&\qquad \left. \times\frac{-1}{(\mathbf{p}-\mathbf{p}')^2}\left(\delta_{ij}-\frac{(\mathbf{p}-\mathbf{p}')_i(\mathbf{p}-\mathbf{p}')_j}{(\mathbf{p}-\mathbf{p}')^2}\right)\right]\psi(\mathbf{p}') \\
&= \frac{-Ze^2}{4m_a m_b}\int\frac{d^3p d^3p'}{(2\pi)^6}\psi^*(\mathbf{p}')\left[\frac{(\mathbf{p}+\mathbf{p}')^2}{(\mathbf{p}-\mathbf{p}')^2}-\frac{(\mathbf{p}^2-\mathbf{p}'^2)^2}{(\mathbf{p}-\mathbf{p}')^4}\right]\psi(\mathbf{p}) \\
&= \frac{\mu^3(Z\alpha)^4\delta_{\ell,0}}{n^3 m_a m_b}+\frac{\mu^3(Z\alpha)^4}{m_a m_b n^4}-\frac{3\mu^3(Z\alpha)^4}{2m_a m_b(\ell+1/2)n^3}, \qquad (3.1.3)
\end{aligned}$$

where we considered the charges to be $q_1 = -e$ and $q_2 = Ze$ and we have used $\gamma = Z\mu\alpha$.

Another spin independent contribution comes from the diagram with a Darwin vertex on one of the fermion line and a Coulomb vertex on the other fermion line, Fig.(3.1(d)). This diagram leads to an energy shift equal to

$$\begin{aligned}
\Delta E_e &= \int\frac{d^3p' d^3p}{(2\pi)^6}\psi^*(\mathbf{p}')\left[\frac{e(\mathbf{p}-\mathbf{p}')^2}{8m_a^2}\,Ze\,\frac{1}{(\mathbf{p}-\mathbf{p}')^2}\right]\psi(\mathbf{p}) \\
&= \frac{Ze^2}{8m_a^2}|\psi(0)|^2=\frac{\mu^3(Z\alpha)^4}{2m_a^2 n^3}\delta_{l,0} \quad , \qquad (3.1.4)
\end{aligned}$$

where m_a and m_b are the fermions' masses. Notice also that the cancellation of the Darwin vertex with the Coulomb propagator means that this interaction will be represented by a delta function in configuration space. We

obtain the same result for the Fig.(3.1(d)). Therefore, we have

$$\Delta E_d + \Delta E_e = \frac{\mu^3 (Z\alpha)^4}{2m_a^2 n^3}\delta_{l,0} + \frac{\mu^3 (Z\alpha)^4}{2m_b^2 n^3}\delta_{l,0} \quad . \tag{3.1.5}$$

There is also a contribution from the diagram having a spin-orbit vertex on one fermion line and the $\mathbf{p}\cdot\mathbf{A}$ interaction on the other fermion line, Fig.(3.1(c)). This contribution reads

$$\begin{aligned}
\Delta E_c &= \int \frac{d^3p' d^3p}{(2\pi)^6}\psi^*(\mathbf{p}')\Big[\Big(\frac{e(\mathbf{p}+\mathbf{p}')_i}{2m_a}\Big)\ \Big(\frac{iZe(-\mathbf{p}'+\mathbf{p})\times\sigma_b)_j}{2m_b}\Big) \\
&\quad \frac{-1}{(\mathbf{p}-\mathbf{p}')^2}\Big(\delta_{ij} - \frac{(\mathbf{p}-\mathbf{p}')_i(\mathbf{p}-\mathbf{p}')_j}{(\mathbf{p}-\mathbf{p}')^2}\Big)\Big]\psi(\mathbf{p}) \\
&= \frac{iZe^2}{4m_a m_b}\int \frac{d^3p' d^3p}{(2\pi)^6}\psi^*(\mathbf{p})\Big(\frac{2\boldsymbol{\sigma}_b\cdot\mathbf{p}\times\mathbf{p}'}{(\mathbf{p}-\mathbf{p}')^2}\Big)\Big)\psi(\mathbf{p}') \\
&= \frac{Z\alpha}{m_a m_b} < \frac{\mathbf{s}_b\cdot\mathbf{L}}{r^3} >,
\end{aligned} \tag{3.1.6}$$

where $\mathbf{L}$ is the total angular momentum. If we add the result of Fig.(3.1(b)) to Eq.(3.1.6), we have

$$\begin{aligned}
\Delta E_b + \Delta E_c &= \frac{Z\alpha}{m_a m_b} < \frac{(\mathbf{s}_b+\mathbf{s}_a)\cdot\mathbf{L}}{r^3} > \\
&= \frac{Z\alpha}{m_a m_b} < \frac{\mathbf{S}\cdot\mathbf{L}}{r^3} > \\
&= \frac{(1-\delta_{l,0})\mu^3(Z\alpha)^4\delta_{S,1}}{2m_a m_b \ell(\ell+1)(1/2+\ell)n^3}\begin{cases} \frac{2}{(\ell+1)} & \text{if } J=\ell+1 \\ \frac{-2}{\ell(\ell+1)} & \text{if } J=\ell, \\ \frac{-2}{\ell} & \text{if } J=\ell-1 \end{cases}
\end{aligned} \tag{3.1.7}$$

where $\mathbf{S}$ is the total spin. The contribution of Fig.(3.1(g)) is similar to Fig.(3.1(b)). The results is

$$\Delta E_g = \frac{Z\alpha}{2m_b^2} < \frac{\mathbf{s}_b\cdot\mathbf{L}}{r^3} > . \tag{3.1.8}$$

Therefore we conclude that

$$\Delta E_f + \Delta E_g = \frac{Z\alpha}{2m_b^2} < \frac{\mathbf{s}_b \cdot \mathbf{L}}{r^3} > + \frac{Z\alpha}{2m_a^2} < \frac{\mathbf{s}_a \cdot \mathbf{L}}{r^3} > . \tag{3.1.9}$$

Now, let's compute the contribution of diagram in Fig.(3.1(i))

$$\begin{aligned} \Delta E_i &= \int \frac{d^3p' d^3p}{(2\pi)^6} \psi^*(\mathbf{p}') \Big[\frac{-p^4 (2\pi)^3 \delta(\mathbf{p} - \mathbf{p}')}{8m_a^3} \Big] \psi(\mathbf{p}) \\ &= \frac{-\mu^4 (Z\alpha)^4}{2m_a^3 n^3 (l + 1/2)} + \frac{3\mu^4 (Z\alpha)^4}{8m_a^3 n^4}, \end{aligned} \tag{3.1.10}$$

For the Fig.(3.1(j)), we just need to replace m_a with m_b in Eq.(3.1.10).

Now, if we put $m_a = m_b$, then for Fig.(3.1(h)) we have

$$\begin{aligned} \Delta E_h &= \int \frac{d^3p' d^3p}{(2\pi)^6} \psi^*(\mathbf{p}') \Big[\Big(\frac{-ie(\mathbf{p}' - \mathbf{p}) \times \boldsymbol{\sigma}_a}{2m} \Big)_i \Big(\frac{iZe(-\mathbf{p}' + \mathbf{p}) \times \boldsymbol{\sigma}_b}{2m} \Big)_j \\ &\qquad \frac{-1}{(\mathbf{p} - \mathbf{p}')^2} \Big(\delta_{ij} - \frac{(\mathbf{p} - \mathbf{p}')_i (\mathbf{p} - \mathbf{p}')_j}{(\mathbf{p} - \mathbf{p}')^2} \Big) \Big] \psi(\mathbf{p}) \\ &= \frac{Ze^2}{4m^2} \int \frac{d^3p' d^3p}{(2\pi)^6} \psi^*(\mathbf{p}') \Big[\frac{((\mathbf{p}' - \mathbf{p}) \times \boldsymbol{\sigma}_a) \cdot ((\mathbf{p}' - \mathbf{p}) \times \boldsymbol{\sigma}_b)}{(\mathbf{p} - \mathbf{p}')^2} \Big] \psi(\mathbf{p}) \\ &= \frac{2Ze^2}{3m^2} |\psi(0)|^2 < \mathbf{s}_a \cdot \mathbf{s}_b > + \frac{(1 - \delta_{\ell,0})(Z\alpha)^4 \mu^3 \ < Y > \ \delta_{S,1}}{m^2 n^3 \ell(\ell + 1)(\ell + 1/2) 2\ell + 3)(2\ell - 1)}, \end{aligned} \tag{3.1.11}$$

where Y has the following form:

$$Y = 2\mathbf{L}^2 (\mathbf{s}_a \cdot \mathbf{s}_b) - 3[(\mathbf{s}_a \cdot \mathbf{L})(\mathbf{s}_b \cdot \mathbf{L}) + (\mathbf{s}_b \cdot \mathbf{L})(\mathbf{s}_a \cdot \mathbf{L})]. \tag{3.1.12}$$

The final $\mathcal{O}(\alpha^4)$ contribution comes from the annihilation diagram in Fig.(3.1(k)):

$$\Delta E_k = \frac{e^2}{4m^2} < \mathbf{S}^2 > |\psi(0)|^2 = \frac{m\alpha^4 \delta_{\ell,0}}{4n^3}. \tag{3.1.13}$$

If we put all contributions together, we obtain the full $\mathcal{O}(\alpha^4)$ energy shift for the spin $\frac{1}{2}$-spin $\frac{1}{2}$ bound state [1] which is given in Ref.[9].

$$\Delta E_{f-f}(\alpha^4) = \frac{m\alpha^4}{2} \Big(\frac{11}{32n^4} - \frac{1}{n^3(2\ell + 1)} + \epsilon^s_{J,\ell} \Big), \tag{3.1.14}$$

[1] Here, the particles are antiparticle of one another. When we have two spin 1/2 particles with equal mass which are not antiparticles of one another, we only need to subtract Eq.(3.1.13) from Eq.(3.1.14).

where s is the total spin of system and $\epsilon^0_{J,\ell} = 0$ and

$$\epsilon^1_{J,\ell} = \frac{7}{6n^3}\delta_{\ell,0} + \frac{1-\delta_{\ell,0}}{2n^3(2\ell+1)} \begin{cases} \frac{3\ell+4}{(\ell+1)(2\ell+3)} & \text{if } J = \ell+1 \\ \frac{-1}{\ell(\ell+1)} & \text{if } J = l, \\ \frac{-(3\ell-1)}{\ell(2\ell-1)} & \text{if } J = \ell-1 \end{cases} \tag{3.1.15}$$

If we ignore the spin of one the particles, then after some algebra we can recover the result of Ref.[15].

3.2 Scalar-Fermion and Scalar-Scalar Bound State Energy Shift to Order α^4.

Let us now turn our attention to scalar quantum electrodynamics. The situation is here much simpler than QED because of the absence of spin. The propagator is the same as derived above and so is the rule for the $\mathbf{p}^4/m^3$ interaction. The vertex rules are easily found by expanding the scalar-electromagnetic vertex $q(p_\mu + p'_\mu)$. Again, we divide the interaction by a factor of $\sqrt{2E}\sqrt{2E'}$ to obtain the nonrelativistic normalization. The zeroth component of the vertex is then given by

$$q\frac{p_0 + p'_0}{2\sqrt{EE'}} = q\frac{E+E'}{2\sqrt{EE'}} \tag{3.2.16}$$

which, to lowest order, gives simply q. The next order interaction is given by $q(\mathbf{p}^4 + \mathbf{p}'^4 + 4\mathbf{p}^2\mathbf{p}'^2)/16m^4$ (the $\mathcal{O}(\mathbf{p}^2/m^2)$ corrections can easily be seen to drop out). The three-vector part of the vertex is equal to

$$q\frac{\mathbf{p}+\mathbf{p}'}{2\sqrt{EE'}} = q\frac{\mathbf{p}+\mathbf{p}'}{2m} + q\frac{1}{2m^2}\left(\frac{\mathbf{p}+\mathbf{p}'}{2m}\right)^3 + \ldots \tag{3.2.17}$$

This completes the Feynman rules we are going to need in this case.

One remark must be made about perturbation theory in non-relativistic scalar QED. Because of the similarity between the non-relativistic scalar

QED and NRQED we can use the result of previous section. In the case of Scalar- Scalar bound state, there are only three diagrams which contribute to the α^4 energy correction, Figs(3.1(a)), (3.1(e)) and (3.1(f)). If we add $\Delta E_a + \Delta E_e + \Delta E_f$ we obtain the result of Ref.[18]:

$$\begin{aligned}\Delta E_{s-s}(\alpha^4) &= \frac{-\mu^4(Z\alpha)^4}{2n^4}\Big(\frac{1}{m_1^3}+\frac{1}{m_2^3}\Big)\Big(\frac{n}{(\ell+1/2)}-\frac{3}{4}\Big) \\ &+\frac{\mu^3(Z\alpha)^4\delta_{\ell,0}}{n^3 m_1 m_2}+\frac{\mu^3(Z\alpha)^4}{m_1 m_2 n^4}-\frac{3\mu^3(Z\alpha)^4}{2m_1 m_2 n^3(\ell+1/2)},\end{aligned} \tag{3.2.18}$$

where m_1 and m_2 are the scalar particle masses. For the case of spin $\frac{1}{2}$-spin0, we just need to consider diagrams (a), (b), (c), (d), (e) and (f) in Fig.(3.1). Since there is no Darwin term on scalar line, we can easily get the result in Ref.[18].

$$\begin{aligned}\Delta E_{f-s}(\alpha^4) &= \frac{-\mu^4(Z\alpha)^4}{2n^4}\Big(\frac{1}{m_f^3}+\frac{1}{m_b^3}\Big)\Big(\frac{n}{\ell+1/2}-\frac{3}{4}\Big) \\ &+\frac{\mu^3(Z\alpha)^4\delta_{\ell,0}}{n^3 m_f m_b}+\frac{\mu^3(Z\alpha)^4}{m_f m_b n^4}-\frac{3\mu^3(Z\alpha)^4}{2m_f m_b n^3(\ell+1/2)} \\ &+\frac{\mu^3(Z\alpha)^4\delta_{\ell,0}}{2m_f^2 n^3}+\frac{\mu^3(Z\alpha)^4}{n^3}\Big(\frac{1}{m_f m_b}+\frac{1}{2m_f^2}\Big) \\ &\times\frac{(1-\delta_{\ell,0})}{(2\ell+1)}\Big(\frac{\delta(j-(\ell+1/2))}{\ell+1}-\frac{\delta(j-(\ell-1/2))}{\ell}\Big),\end{aligned} \tag{3.2.19}$$

where m_b and m_f are boson and fermion masses respectively.

In this chapter, we have calculated the simplest NRQED diagrams which contribute to the lowest order, $\mathcal{O}(\alpha^4)$, of the bound state systems. In the next chapter, we consider the order α^5 calculations. To do that we are faced with one-loop NRQED diagrams which lead to UV divergences in some cases. We should not worry about this because at this order we also need to perform a matching procedure at NLO which renormalizes the NRQED coefficients.

The UV cutoff, Λ, appearing in some of these coefficients cancels the UV divergences of the one-loop NRQED diagrams. In the following chapters we discuss these points in detail.

Chapter 4

Next-to-Leading Order Bound State Energy Shift.

So far we have done tree level matching[1] to get the rules of the effective theory. It is clear that this tree level matching is equal to a series expansion in powers of $\mathbf{p}^2/m^2$. The relativistic physics must be put back into the non-relativistic theories in order to obtain sensible results. Since relativistic effects take place at a length scale much shorter than the scale probed by the low energy theory, it can be incorporated in the effective theory by renormalizing the coupling constants of the latter. To do so, all one has to do is to compute a specific process up to a given number of loops in both NRQED and QED, for example, and then require that the two results agree. Doing this at tree level would only reproduce the interactions derived before. However, when loops are taken into account, the NRQED coefficients will acquire corrections in the form of a series expansion in α. For example, the coefficient of the spin dependent interaction of Eq.(2.2.2), c_1 becomes $(e/2m)(1+\alpha/2\pi)$ [16], to take into account the correction to the anomalous magnetic moment.[2]

It is important to notice that this "matching procedure" can be done with

[1] Only tree level QED diagrams were involved.

[2] For more detailed explanations, the reader is referred to Ref.[8].

scattering amplitudes, and that no bound state physics needs to enter at this stage. Once the coefficients are fixed to a certain order in the fine structure constant, the low energy theory can be applied to bound state calculations without any further need of the full theory. This is the crucial feature that makes NRQED much simpler than the traditional Bethe-Salpeter approach, as it completely decouples the high energy contributions from the low energy contributions. The high energy contributions can be systematically incorporated by calculating scattering amplitudes only. Only the low energy theory (with its parameters renormalized) enters when the time comes to evaluate bound state properties. This is to be contrasted with the Bethe-Salpeter approach in which one must deal simultaneously with both the high and low energy contributions.

The $\mathcal{O}(\alpha^5)$ energy corrections can be divided into two parts. The first part is spin independent and contributes to the Lamb shift, and the second part which is spin dependent, should be considered in calculation of hyperfine splitting (HFS) in a bound state system. In section(4.1.1), we calculate the Lamb shift in the hydrogen atom using NRQED as an effective field theory. We then concentrate on scalar-scalar bound state in section(4.1.2). In section(4.2.1), we calculate the well-known HFS result for the ground state of hydrogen atom and then extend the formula to arbitrary n and ℓ, producing a new result. All these calculations will show how we can systematically reproduce the old results while gaining the power to extend them very easily. Those who are familiar with traditional calculation of the Lamb shift and hyperfine splitting in the hydrogen atom will surely appreciate NRQED and hopefully will consider NRQED more seriously.

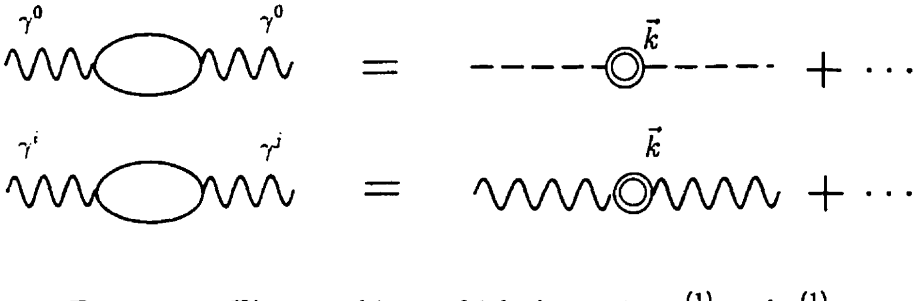

Figure 4.1: The matchings which determine $c_9^{(1)}$ and $c_{10}^{(1)}$.

4.1 Matching at Next-to-Leading Order for Two-Fermi Operators

More accurate calculations, such as those of interest in this chapter, require the next-to-leading corrections to the coefficients of Eqs.(2.1.1). In this section we discuss higher-order corrections to the coefficients appearing in both $\mathcal{L}_{photon}$ and $\mathcal{L}_{2-Fermi}$. We write $c_i = c_i^{(0)} + c_i^{(1)} + \ldots$ with $c_i^{(0)}$ as given in the section(2.2), and now concentrate on computing the next corrections, $c_i^{(1)}$.

Among the simplest higher-order corrections to the NRQED Lagrangian, Eq.(2.1.1), are the contributions to $\mathcal{L}_{photon}$. To lowest order these are produced by vacuum polarization, Fig.(4.1), which gives:

$$c_9^{(1)} = c_{10}^{(1)} = \frac{\alpha}{15\pi}. \tag{4.1.1}$$

Similarly, QED one-loop vertex corrections modify the couplings in $\mathcal{L}_{2-Fermi}$, to give [7], [12]:

$$\begin{aligned} c_2^{(1)} &= -\frac{q}{8m^2}\left(\frac{\alpha}{\pi}\right)\left[\frac{8}{3}\ln\left(\frac{2\Lambda}{m}\right) - \frac{20}{9}\right], \\ c_1^{(1)} &= \frac{q}{2m}\left(\frac{\alpha}{2\pi}\right), \\ c_3^{(1)} &= \frac{iq}{8m^2}\left(\frac{\alpha}{\pi}\right). \end{aligned} \tag{4.1.2}$$

Here Λ is the ultraviolet cutoff used to regulate NRQED loop graphs which arise when matching. In any calculation of physical properties, such di-

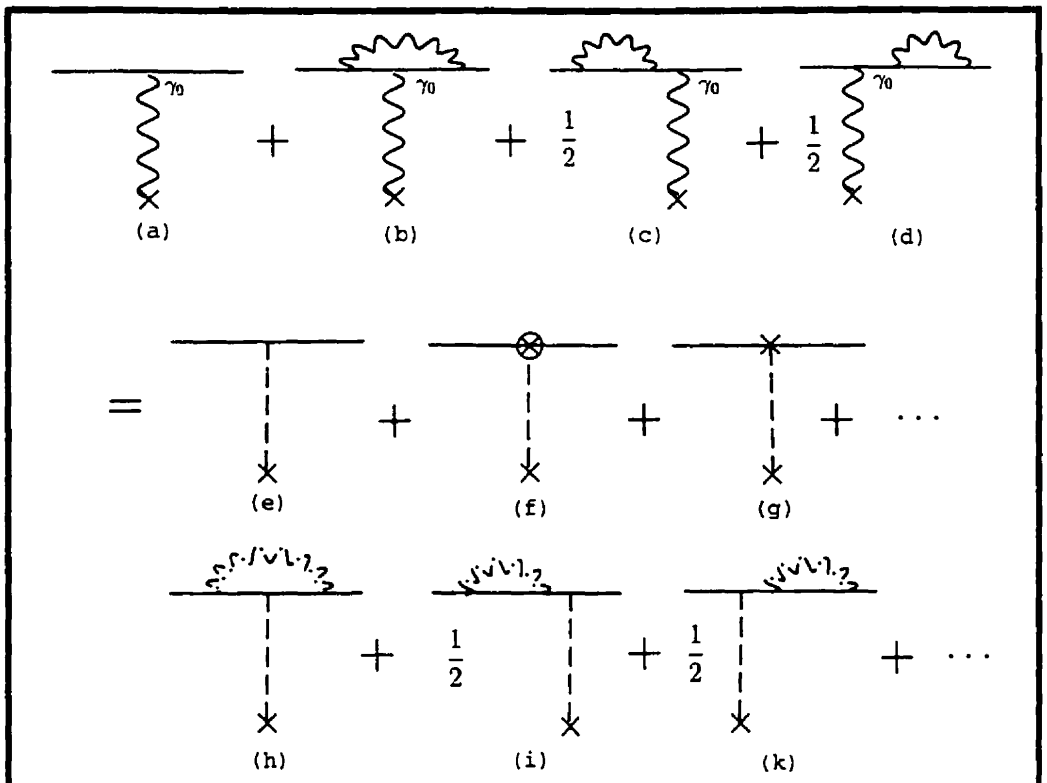

Figure 4.2: One-loop matching for the NRQED vertices.

vergences cancel amongst themselves, or against explicit cutoff dependence which arises from divergences in NRQED loop graphs.

To calculate Eqs.(4.1.2), we impose the relation illustrated in Fig.(4.2). This matching was performed in [12] but, even though our final result is of course the same, our derivation differs sufficiently to be presented it here. The QED scattering amplitude (the left hand side of Fig.(4.2)) can be expressed in terms of the usual form factors $F_1(Q^2)$ and $F_2(Q^2)$ in the following way (to be consistent, we use a non-relativistic normalization for the Dirac spinors):

$$-e\frac{\bar{u}(\mathbf{p}',\mathbf{s}')}{\sqrt{2E'}}\Big[\gamma_0 A^0(\mathbf{Q})F_1(Q^2) - \frac{i}{2m}\sigma^{0j}A^0(\mathbf{Q})\,Q^j\,F_2(Q^2)\Big]\frac{u(\mathbf{p},\mathbf{s})}{\sqrt{2E}} =$$
$$F_1(Q^2)\xi'^{\dagger}\Big[-eA^0 + \frac{e}{8m^2}\mathbf{Q}^2A^0 - \frac{ie}{4m^2}\boldsymbol{\sigma}\cdot(\mathbf{p}'\times\mathbf{p})A^0 + \ldots\Big]\xi +$$
$$F_2(Q^2)\xi'^{\dagger}\Big[\frac{e}{4m^2}\mathbf{Q}^2A^0 - \frac{ie}{2m^2}\boldsymbol{\sigma}\cdot(\mathbf{p}'\times\mathbf{p})A^0 + \ldots\Big]\xi, \qquad (4.1.3)$$

where $\mathbf{Q} = \mathbf{p}' - \mathbf{p}$, s and $\mathbf{s}'$ are the initial and final spin of the electron, respectively, and ξ, ξ' are the corresponding initial and final two component Pauli spinors normalized to unity. We choose the convention that e is positive so that the charge of the electron is $-e$. In Eq.(4.1.3), as in the rest of this section, we use m to represent the mass of the electron. Notice that the matching involves a double expansion. One expansion is in the coupling constant α and the other is the non-relativistic expansion in $\mathbf{Q}/m$ which leads to renormalization of different NRQED operators. The non-relativistic expansions of the form factors are [12]

$$\begin{aligned} F_1(Q^2) &= 1 - \frac{\alpha}{3\pi}\left[\frac{\mathbf{Q}^2}{m^2}\left(\ln(\frac{m}{\lambda}) - \frac{3}{8}\right)\right] + \ldots \\ F_2(Q^2) &= a_e - \frac{\alpha}{\pi}\frac{\mathbf{Q}^2}{12m^2} + \ldots . \end{aligned} \tag{4.1.4}$$

where a_e is the electron anomalous magnetic moment which, to the order of interest, can be taken to be $\alpha/(2\pi)$. In Eq.(4.1.4), since $Q^0 = E' - E$ is of order of v^2 and $|\mathbf{Q}|$ is of order v, we have ignored Q^0 respect to $\mathbf{Q}$. If we substitute (4.1.4) in (4.1.3) we obtain

$$\begin{aligned} \xi'^{\dagger}(-eA^0)\xi &+ \frac{e}{8m^2}\xi'^{\dagger}\mathbf{Q}^2A^0\xi\left[1 + \frac{8\alpha}{3\pi}\left(\ln(\frac{m}{\lambda}) - \frac{3}{8}\right) + \frac{\alpha}{\pi} + \ldots\right] \\ &- \frac{ie}{4m^2}\xi'^{\dagger}\boldsymbol{\sigma}\cdot(\mathbf{p}'\times\mathbf{p})A^0\,\xi\left[1 + \frac{\alpha}{\pi} + \ldots\right] + \mathcal{O}(\mathbf{Q}^4/m^4). \end{aligned} \tag{4.1.5}$$

We must now compute the right-hand side of Fig.(4.2) to complete the calculation of the one-loop renormalized NRQED coefficients. Since we are dealing with ultra-soft photons in Figs.(4.2(h)), (4.2(i)) and (4.2(k)), we use the Feynman rules for the ultra-soft photon. Working at the zeroth order of the multipole expansion, Fig.(4.2(h)) corresponds to

$$\xi'^{\dagger}(\frac{2ep_i}{2m})(\frac{2ep'_j}{2m}) \quad \int \frac{d^3k}{(2\pi)^3}\frac{\delta_{ij} - \frac{k_ik_j}{\mathbf{k}^2+\lambda^2}}{2\sqrt{\mathbf{k}^2+\lambda^2}}\,\frac{1}{-\sqrt{\mathbf{k}^2+\lambda^2}}\,(-eA_0)$$

$$
\begin{aligned}
&\times \frac{1}{\frac{\mathbf{p}^2}{2m} - \frac{\mathbf{p}'^2}{2m} - \sqrt{\mathbf{k}^2+\lambda^2}}\,\xi \\
\approx\ & \xi'^{\dagger}(-eA_0)\xi\,(\frac{e}{m})^2\,\frac{\mathbf{p}'\cdot\mathbf{p}}{3}\int\frac{dk\ \mathbf{k}^2}{2\pi^2}\ \frac{2\mathbf{k}^2+3\lambda^3}{\mathbf{k}^2+\lambda^2} \\
&\times \frac{1}{2\sqrt{\mathbf{k}^2+\lambda^2}}\frac{1}{\mathbf{k}^2+\lambda^2} \\
=\ & -\frac{8\alpha}{3\pi}\Big[\ln(\frac{2\Lambda}{\lambda})-\frac{5}{6}\Big]\,\xi'^{\dagger}eA_0\xi\,\frac{\mathbf{p}\cdot\mathbf{p}'}{4m^2} \qquad (4.1.6)
\end{aligned}
$$

where, in the second line, we have used the fact that the integral is already proportional to $\mathbf{p}\cdot\mathbf{p}'$ to justify approximating $\mathbf{p}^2 \approx \mathbf{p}'^2 \approx 0$ in the propagators. The corrections to these expressions will lead to higher order operators.

Notice that we are only working with scattering diagrams when performing the matching, no bound state physics enters this stage of the calculation. To compute the amplitudes in Figs.(4.2(i)) and (4.2(k)), we just need to evaluate the first one and then obtain the second one by replacing $\mathbf{p}$ by $\mathbf{p}'$. For Fig.(4.2(i)), we can write

$$
\frac{1}{2}\xi'^{\dagger}(\frac{2ep_i}{2m})(\frac{2ep_j}{2m})\int\frac{d^3k}{(2\pi)^3}\frac{\delta_{ij}-\frac{k_ik_j}{\mathbf{k}^2+\lambda^2}}{2\sqrt{\mathbf{k}^2+\lambda^2}}\ \frac{1}{E-\frac{\mathbf{p}^2}{2m}-\sqrt{\mathbf{k}^2+\lambda^2}}\ \frac{1}{E-\frac{\mathbf{p}^2}{2m}}\ (-eA_0)\ \xi. \qquad (4.1.7)
$$

Here, E represents the on-shell energy $\mathbf{p}^2/2m$. Of course, in that limit, the propagator $1/(E-\mathbf{p}^2/2m)$ is divergent, which signals the need for a mass renormalization. In NRQED, we perform mass renormalization exactly as in QED, *i.e.* we start by keeping $E \neq \mathbf{p}^2/2m$ and subtract the mass counterterm:

$$
\begin{aligned}
-\frac{1}{2}\xi'^{\dagger}eA_0(\frac{e}{m})^2\,\frac{\mathbf{p}^2}{3}\ &\int\frac{dk\ \mathbf{k}^2}{2\pi^2}\ \frac{2\mathbf{k}^2+3\lambda^3}{\mathbf{k}^2+\lambda^2}\ \frac{1}{2\sqrt{\mathbf{k}^2+\lambda^2}} \\
&\Big(\frac{1}{E-\frac{\mathbf{p}^2}{2m}-\sqrt{\mathbf{k}^2+\lambda^2}}-\frac{1}{-\sqrt{\mathbf{k}^2+\lambda^2}}\Big)\ \frac{1}{E-\frac{\mathbf{p}^2}{2m}}\,\xi. \qquad (4.1.8)
\end{aligned}
$$

Expanding the term in the parenthesis around $E-\frac{\mathbf{p}^2}{2m}$, we get a series which, by construction, starts at order $(E-\mathbf{p}^2/2m)^1$, which cancels the propagator

$1/(E-\mathbf{p}^2/2m)$ in Eq.(4.1). One can then finally take the limit $E \to \mathbf{p}^2/2m$ with the result for the sum of Figs.(4.2(i)) and (4.2(k)):

$$-\frac{1}{2}\xi'^{\dagger}\, eA_0\, \frac{\alpha}{3\pi m^2}(\mathbf{p}^2+\mathbf{p}'^2)\int d\!k\mathbf{k}^2 \frac{2\mathbf{k}^2+3\lambda^2}{\mathbf{k}^2+\lambda^2}\,\frac{1}{\sqrt{\mathbf{k}^2+\lambda^2}}\,\frac{-1}{\mathbf{k}^2+\lambda^2}\xi$$
$$= -\frac{8\alpha}{3\pi}\Big[\ln(\frac{2\Lambda}{\lambda})-\frac{5}{6}\Big]\Big(\frac{-\xi'^{\dagger}eA_0\xi}{8m^2}(\mathbf{p}^2+\mathbf{p}'^2)\Big). \quad (4.1.9)$$

Putting everything together, the complete right-hand side of Fig.(4.2) is obtained by adding Eqs.(4.1.6) and (4.1.9) to tree-level diagrams:

$$\begin{aligned}\xi'^{\dagger}(-eA^0)\xi \;&+\; \xi'^{\dagger}\mathbf{Q}^2A^0\xi\Big[-c_2+(\frac{e}{8m^2})\frac{8\alpha}{3\pi}\Big(\ln(\frac{2\Lambda}{\lambda})-\frac{5}{6}\Big)\Big]\\ &+\; 2c_3\,\xi'^{\dagger}\boldsymbol{\sigma}\cdot(\mathbf{p}'\times\mathbf{p})A^0\xi \qquad (4.1.10)\end{aligned}$$

Now, by equating (4.1.5) and (4.1.10), we can evaluate $c_3^{(1)}$ and $c_2^{(1)}$ to get Eq.(4.1.2).

4.1.1 Lamb Shift in Hydrogen Atom.

Having completed $c_i^{(1)}$ we now turn to some applications. The Lamb shift, the shift between the hydrogen $2S_{1/2}$ and $2P_{1/2}$ states, is without any doubt the most well-known bound state application of radiative corrections. It has the form $m_e\alpha^5(\ln\alpha + \text{finite})$ where the finite piece contains the Bethe logarithm, a state dependent term that must be evaluated numerically. The log term is relatively easy to extract and its calculation is presented in many quantum mechanics textbooks. The finite contribution is much more difficult to evaluate because it requires the application of QED to a bound state. In this section, we rederive the complete $\mathcal{O}(\alpha^5)$ corrections in the non-recoil limit[3] of hydrogen atom (*i.e.*, $m_e/m_P = 0$) using NRQED. In section(4.1.2), the Lamb shift for scalar-scalar bound state will be presented.

[3]In the literature, these corrections are also referred to as the Lamb shift. We will also adopt this notation in the rest of the thesis.

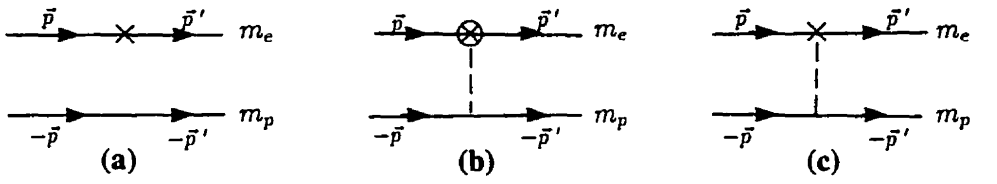

Figure 4.3: Diagrams contributing to order α^4 of hydrogen atom in the non-recoil limit.

In our case, we first need to isolate the NRQED diagrams contributing to order α^5 in the non-recoil limit, *i.e.* we neglect corrections suppressed by powers of m_e/m_p. To warm up, we first isolate the diagrams contributing to order α^4 in the non-recoil limit (the full NRQED calculation of the $\mathcal{O}(\alpha^4)$ energy shift for arbitrary masses is presented in Ref.[14]). In that limit, the only relevant diagrams are shown in Fig.(4.3). This can easily be checked by using the NRQED counting rules derived in Ref.[2]. Since soft and ultra-soft photons obey different counting rules, we consider their contribution in turn. Soft photons contribute to order :

$$\frac{\mu^{\kappa+\rho+1}}{m_e^{\kappa} m_p^{\rho}} Z^{\eta} \alpha^{\zeta} \approx \frac{m_e^{\rho+1}}{m_p^{\rho}} \alpha^{\zeta}, \tag{4.1.11}$$

where μ is the reduced mass and ρ and κ are, respectively, the total number of inverse powers of m_p and m_e appearing in the NRQED vertices. In Eq.(4.1.11), we approximated $\mu \approx m_e$ which is exact in the non-recoil limit. The coefficient ζ is defined by

$$\zeta = 1 + \kappa + \rho - N + \sum_i n_i, \tag{4.1.12}$$

as was discussed in section(2.4).

Now, to obtain the correction of order $m_e\alpha^4$, we need to have $\rho = 0$ and $\zeta = 4$ (see Eq.(4.1.11)). The only way to have $\rho = 0$ is to either have a Coulomb interaction on the nucleus line or no interaction at all. This

already reduces greatly the number of possible diagrams. Turning now to the condition $\zeta = 4$, we obtain from Eq.(4.1.12)

$$\kappa - N + \sum_i n_i = 3. \tag{4.1.13}$$

Recalling our previous result that no $\mathcal{O}(\alpha^4)$ diagrams have $N \geq 1$, we set $N = 0$. We are then left with the condition $\kappa + \sum_i n_i = 3$. One possibility is $\kappa = 3$ and $\sum n_i = 0$ which corresponds to the relativistic kinetic energy vertex on the electron line. Another possibility is $\kappa = 2$ and $\sum a_i = 1$ which can be fulfilled with the Coulomb vertex on the proton line and either the Darwin or the Spin-Orbit interaction on the electron line. There are no Coulomb interactions with only one inverse mass, so the condition $\kappa = 1$ and $\sum n_i = 2$ cannot be satisfied. The three possible diagrams are illustrated in Fig.(4.3).

To order α^5, starting first with $N = 0$, we must either increase κ or $\sum n_i$ by one. It is not possible to increase the number of inverse electron masses κ by one, but there are two ways to increase $\sum n_i$ by one. One way is to include the one-loop corrections to the coefficients c_i's of the vertices in Fig.(4.3), so requiring the matching of these interactions to $\mathcal{O}(\alpha)$. The other possibility, with $\kappa = 2$ and $\sum n_i = 2$, is to consider the new interaction corresponding to the vacuum polarization correction to the Coulomb propagator which is depicted in Fig.(4.4(a)).

We now turn to diagrams for which $N = 1$. It can easily be verified that ζ, Eq.(4.1.12), cannot be made equal to 5. We have now uncovered all the diagrams containing only soft photons which contribute to order α^5. The only remaining possibility is to consider diagrams with ultra-soft photons which lead to a contribution of the form given by Eq.(4.1.11) but now with:

$$\tilde{\zeta} = \sum_i n_i + 1 + \rho + \kappa - N + 2N_\gamma + \sum_i \mathcal{M}_i. \tag{4.1.14}$$

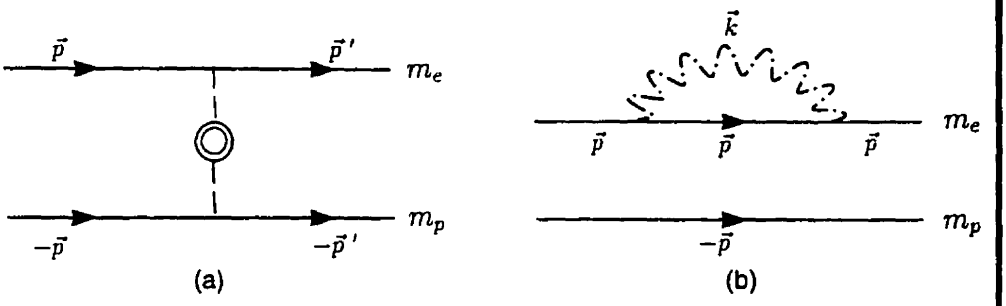

Figure 4.4: (a): Order α^5 contribution from the Uehling potential. (b): Order α^5 from ultra-soft photon(any number of Coulomb lines in the intermediate state are understood.)

As before, we set $\tilde{\zeta} = 5$ and $\rho = 0$ to obtain non-recoil corrections of order α^5. For diagrams containing ultra-soft photons, the minimum value of N is 1, because these photons propagate in the time direction (we again refer the reader to Ref.[2] for more details). Working at the zeroth order of the multipole expansion ($\mathcal{M}_i = 0$) and considering only one ultra-soft photon ($N_\gamma = 1$), we then have the condition $\kappa + \sum n_i = 3$. Since the ultra-soft photon is necessarily transverse and transverse vertices contain at least one power of inverse mass (see Fig.(2.1)), κ is bigger or equal to 2. In addition, $\sum n_i$ is at least equal to one (*i.e.* there at least one factor of α in the vertices). Thus, the condition $\kappa + \sum n_i = 3$ is satisfied by the simplest diagram which corresponds to an ultra-soft photon connected to two $\mathbf{p} \cdot \mathbf{A}$ vertices, as represented in Fig.(4.4(b)).There are no other possibilities. Having identified all diagrams contributing to the order of interest, we now turn to the matching. From the above discussion, we see that we need to match to one loop the coefficients of the interactions contributing to order α^4.

We are now ready for the third and last step of the calculation, the computation of the bound state diagrams *per se*. Since only c_2 and c_3 receive

an $\mathcal{O}(\alpha)$ correction, only Figs.(4.3b, c) are needed for the $\mathcal{O}(\alpha^5)$ calculation. Let us now start with Fig.(4.3(b)).

$$\begin{aligned}\Delta E_{(b)} &= 2c_3(Ze)\int \frac{d^3p'd^3p}{(2\pi)^6}\Psi^*(\mathbf{p})\Big(\frac{\boldsymbol{\sigma}_e\cdot\mathbf{p}'\times\mathbf{p}}{(\mathbf{p}'-\mathbf{p})^2}\Big)\Psi(\mathbf{p}') \\ &= c_3\,\frac{i\,Ze}{\pi}<\frac{\mathbf{s}_e\cdot\mathbf{L}}{r^3}> \\ &= c_3\Big(\frac{iZe}{2\pi}\Big)\frac{Z^3\mu^3\alpha^3}{n^3(\ell+1/2)}\Big(\frac{\delta(j-(\ell+1/2))}{(\ell+1)}-\frac{\delta(j-(\ell-1/2))}{\ell}\Big)(1-\delta_{\ell,0}),\end{aligned} \tag{4.1.15}$$

where $\Psi(\mathbf{p})$ is the Schrödinger wavefunction including the electron spin[4] corresponding to the quantum numbers n, j and ℓ.

In Eq.(4.1.15) we used

$$\int\frac{d^3p'}{(2\pi)^3}e^{i\mathbf{p}'\cdot\mathbf{r}'}\frac{\boldsymbol{\sigma}\cdot\mathbf{p}\times\mathbf{p}'}{\mathbf{p}'^2}=i\frac{\boldsymbol{\sigma}\cdot\mathbf{p}\times\mathbf{r}'}{4\pi r'^3}. \tag{4.1.16}$$

For the diagram of Fig.(4.3(c)), we find

$$\begin{aligned}\Delta E_{(c)} &= \int\frac{d^3p'd^3p}{(2\pi)^6}\Psi^*(\mathbf{p}')\Big(-c_2(\mathbf{p}'-\mathbf{p})^2\,Ze\,\frac{1}{(\mathbf{p}'-\mathbf{p})^2}\Big)\Psi(\mathbf{p}) \\ &= -c_2\,Ze\int\frac{d^3p'd^3p}{(2\pi)^6}\Psi^*(\mathbf{p}')\Psi(\mathbf{p}) \\ &= -c_2\,Ze|\Psi(0)|^2=-c_2\,Ze\,\frac{m^3Z^3\,\alpha^3}{\pi n^3}\delta_{\ell,0}.\end{aligned} \tag{4.1.17}$$

Using the counting rules, we also found that the diagram depicted in Fig.(4.4(a)) would contribute to $\mathcal{O}(m\alpha^5)$. This diagram corresponds to the well-known Uehling potential and is found to be

$$\begin{aligned}\Delta E_{(a)} &= \int\frac{d^3p'd^3p}{(2\pi)^3}\Psi^*(\mathbf{p}')\Big(-e\,\frac{1}{(\mathbf{p}'-\mathbf{p})^2}c_9\frac{-(\mathbf{p}'-\mathbf{p})^4}{m^2} \\ &\qquad\qquad \frac{1}{(\mathbf{p}'-\mathbf{p})^2}\,Ze\Big)\Psi(\mathbf{p}) \\ &= -c_9\,Ze^2\frac{1}{m^2}|\Psi(0)|^2=-4c_9\,\frac{m(Z\alpha)^4}{n^3}\delta_{\ell,0}.\end{aligned} \tag{4.1.18}$$

[4]In the non-recoil limit, the spin of the proton completely decouples from the problem.

We finally turn our attention to the only remaining diagram, which is represented in Fig.(4.4(b)). The corresponding integral is (as shown in Ref.[2] , in zeroth order of the multipole expansion we set $\mathbf{p}\,' = \mathbf{p}$ on the vertices):

$$\begin{aligned}\Delta E_{(b)} &= \int \frac{d^3k d^3p}{(2\pi)^6}\Psi^*(\mathbf{p})\,\frac{2ep_i}{2m}\frac{2ep_j}{2m}\frac{1}{2k}\frac{1}{E_n-\frac{\mathbf{p}^2}{2m}-k}(\delta_{ij}-\frac{k_ik_j}{\mathbf{k}^2})\,\Psi(\mathbf{p}) \\ &= \frac{e^2}{2m^2(2\pi)^3}\int\frac{d^3p}{(2\pi)^3}\Psi^*(\mathbf{p})\int dk\;k d\Omega\frac{(\mathbf{p}^2-\frac{(\mathbf{p}\cdot\mathbf{k})^2}{\mathbf{k}^2})}{E_n-\frac{\mathbf{p}^2}{2m}-k}\Psi(\mathbf{p}) \\ &= \frac{2\alpha}{3\pi}\int\frac{d^3p}{(2\pi)^3}\int dk\,k\;\Psi^*(\mathbf{p})\,(\frac{\mathbf{p}^2/m^2}{E_n-\frac{\mathbf{p}^2}{2m}-k})\,\Psi(\mathbf{p}). \qquad (4.1.19)\end{aligned}$$

In a bound state, beyond tree level, one must include an infinite number of Coulomb lines in the intermediate state. This can easily be seen from the counting rules, Eq.(4.1.14). Indeed, adding a Coulomb line will not change ζ because this increases both N and $\sum_i n_i$ by one, which has no overall effect. Because of this, one must use the Coulomb Green's function for the intermediate state. Using the bra and ket notation, Eq.(4.1.19) must then be replaced by the well-known expression:

$$\frac{2\alpha}{3\pi}\sum_{n'}\int dk\;k\;\frac{<n|\mathbf{v}_{op}|n'><n'|\mathbf{v}_{op}|n>}{E_n-E_{n'}-k}. \qquad (4.1.20)$$

This part of the calculation is well known and is carried out in many textbooks (see for example Ref.[9]). The result is

$$\Delta E = m\frac{4\alpha}{3\pi}\frac{(Z\alpha)^4}{n^3}\begin{cases}\ln\frac{\Lambda}{<E_n>} & \text{if } \ell=0 \\ \ln\frac{Z^2m\alpha^2}{2<E_n>} & \text{if } \ell\neq 0,\end{cases} \qquad (4.1.21)$$

where $< E_n >$ is the Bethe logarithm which can be evaluated numerically [15], and is defined in the following equations:

$$\ln < E_n >= \frac{\sum_{n'}|<n|\mathbf{v}_{op}|n'>|^2(E'_n-E_n)\ln|E'_n-E_n|}{\sum_{n'}|<n|\mathbf{v}_{op}|n'>|^2(E'_n-E_n)}\ ,\ \text{for}\ \ell=0$$

$$\frac{4\alpha}{3\pi}m\ln\left(\frac{mZ^2\alpha^2}{<E_n>}\right)=\frac{2\alpha}{3\pi}\sum_{n'}|<n|\mathbf{v}_{op}|n'>|^2(E'_n-E_n)\ln\left(\frac{1}{E'_n-E_n}\right)\ ,\ \text{for}\ \ell\neq 0$$

Now, by using Eqs.(4.1.2), (4.1.1) we can add the α^5 contributions from Eqs.(4.1.15), (4.1.17) and (4.1.18) to Eq.(4.1.21) to obtain

$$\Delta E = m\frac{4\alpha}{3\pi}\frac{(Z\alpha)^4}{n^3}\begin{cases} ln\frac{m}{2<E_{n,0}>} + \frac{19}{30} & \text{if } \ell = 0 \\ \ln\frac{Z^2m\alpha^2}{2<E_{n,\ell}>} + \frac{3}{8(2\ell+1)}C_{j\ell} & \text{if } \ell \neq 0, \end{cases} \tag{4.1.22}$$

where $C_{j\ell}$ is given by:

$$C_{j\ell} = \Big(\frac{\delta(j-(\ell+1/2))}{(\ell+1)} - \frac{\delta(j-(\ell-1/2))}{\ell}\Big). \tag{4.1.23}$$

Eq.(4.1.22) is the well-known Lamb shift.

4.1.2 Lamb Shift in the Scalar-Scalar Bound State.

Let us consider the scalar-scalar bound state which is made of two non-relativistic particles with masses m and M respectively. We assume the non-recoil limit namely, $\frac{m}{M} = 0$. As shown in previous chapter that the coulomb and Dipole vertices in non-relativistic scalar QED are the same as NRQED. There is no Darwin vertex at leading order and obviously no spin dependent vertex. Although there is no Darwin vertex at the leading order, there is no guarantee that this vertex does not contribute at the NLO in α. To check this possibility we match NRQED with scalar QED at the one loop order. We follow the same steps as we did in section(4.1.1). First of all we calculate the modified vertex function of scalar QED (SQED) [5]:

$$\frac{-e(p'_\mu + p_\mu)A^\mu}{2\sqrt{EE'}}\Big[1 - \frac{\alpha\mathbf{Q}^2}{3\pi m^2}\Big(\ln(\frac{m}{\lambda}) - \frac{3}{4}\Big) + \ldots\Big] \tag{4.1.24}$$

The next step consists of imposing the relation shown in Fig(4.5) for the external static coulomb field $A^0(\mathbf{q})$. The left hand side of Fig(4.5)(scalar

[5]The charge of particles are taken to be $-e$ and Ze for light and heavy mass respectively.

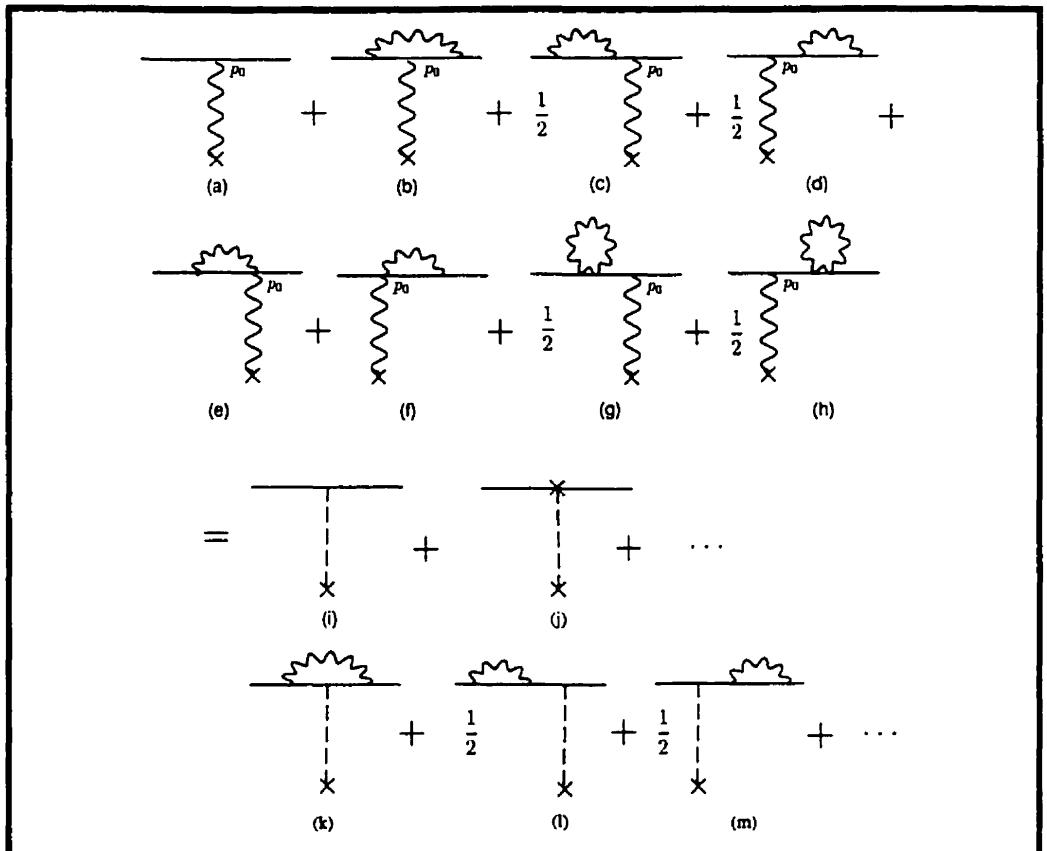

Figure 4.5: One-loop matching for the scalar non-relativistic QED vertices.

QED scattering amplitude) can be written as follows

$$\frac{-e(p_0'+p_0)A^0}{2\sqrt{EE'}}\Big[1-\frac{\alpha\mathbf{Q}^2}{3\pi m^2}\Big(\ln(\frac{m}{\lambda})-\frac{3}{4}\Big)+\ldots\Big] \;=\; -eA^0+\frac{e}{8m^2}\mathbf{Q}^2A^0\Big[\frac{8\alpha}{3\pi}\Big(\ln(\frac{m}{\lambda})-\frac{3}{4}\Big)+\ldots\Big]+\mathcal{O}(\mathbf{Q}^4/m^4), \tag{4.1.25}$$

where $\mathbf{Q}=\mathbf{p}'-\mathbf{p}$. The right hand side of Fig.(4.5) has been calculated in Ref[16]. The result is

$$-eA^0+\mathbf{Q}^2A^0\Big[-(c_2)_{SQED}+\frac{e}{8m^2}\frac{8\alpha}{3\pi}\Big(\ln(\frac{2\Lambda}{\lambda})-\frac{5}{6}\Big)\Big]. \tag{4.1.26}$$

Now, by equating Eqs. (4.1.25) and (4.1.26), we can evaluate $(c_2)_{SQED}$:

$$(c_2)_{SQED} \;=\; \frac{e}{8m^2}\frac{\alpha}{\pi}\frac{8}{3}\Big[\ln\Big(\frac{2\Lambda}{m}\Big)-\frac{2}{9}\Big]+\mathcal{O}(\alpha^2). \tag{4.1.27}$$

We see from Eq.(4.1.27) that $(c_2)_{SQED}$ starts at $\mathcal{O}(\alpha)$ which differs from QED case.

Consider next the Uehling potential coming from the vacuum polarization of scalar particles as well as the electron. If the $m_e \sim m$ then we cannot ignore the effect of scalar particle in this vertex. Therefore we should calculate the vacuum polarization in SQED and do the similar matching shown in Fig.(4.1) at the lowest order to the non-relativistic SQED, we obtain:

$$(c_9^{(1)})_{SQED} = (c_{10}^{(1)})_{SQED} = \frac{\alpha}{120\pi} \tag{4.1.28}$$

It is important to mention that when $m \gg m_e$, the $\frac{\mathbf{p}}{m_e}$ expansion of the electron part of the one-loop vacuum polarization can not be used, since m_e is small compared to $\mathbf{p} \sim \gamma = \mu\alpha \sim m\alpha$. To see this fact, consider the first term of the $\frac{\mathbf{p}}{m_e}$ expansion, which is refered to as the Uehling potential. The diagram of this potential is proportional to $\frac{\alpha^2}{m_e^2}$. To obtain the dimension of energy for the whole diagram, the integral over three momentum should lead to $\gamma^3 = (Z\mu\alpha)^3 \sim (Zm\alpha)^3$. As a result the whole diagram becomes proportional to $\frac{m^3\alpha^2}{m_e^2}$. Now, if we consider the second term of the $\frac{\mathbf{p}}{m_e}$ expansion, it has an extra factor of $\frac{1}{m_e^2}$ with respect to the first term of expansion. This means it should be multiplied by an extra factor γ^2. Therefore the second term in expansion will be suppressed by a factor of $\frac{\alpha^2 m^2}{m_e^2}$ with respect to the first term (the Uehling potential). Now, if $m \gg m_e$, then $\frac{\alpha^2 m^2}{m_e^2}$ will not be suppressed. This means that we cannot simply keep the first term in Taylor expansion of the electron vacuum polarization. On the other hand, if $m \sim m_e$ then $\frac{\alpha^2 m^2}{m_e^2} \sim \alpha^2$ is a small number, which assures that the higher order corrections in the Taylor expansion will be suppressed.

Now we are ready to look at bound state diagrams. By using the counting rules in previous chapter, we find that Figs.(4.6), (4.4) are the diagrams that

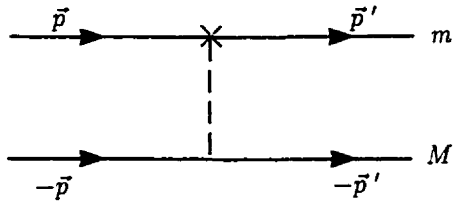

Figure 4.6: Diagram contributing to order α^4 of scalar-scalar bound state in the non-recoil limit.

contribute to the $\mathcal{O}(\alpha^5)$. Similar to what we have calculated in chapter(3), these bound states diagrams can be evaluated:

$$\Delta E_{Darwin} = -(c_2)_{SQED}\ Ze\ \frac{(mZ\alpha)^3}{\pi n^3}\delta_{l,0} \tag{4.1.29}$$

$$\Delta E_{Uehling} = -4c_9^{(1)}\frac{\mu^3(Z\alpha)^4}{m_e^2 n^3}\delta_{\ell,0} - 4(c_9^{(1)})_{SQED}\frac{\mu^3(Z\alpha)^4}{m^2 n^3}\delta_{\ell,0} \tag{4.1.30}$$

$$\Delta E_{self\ energy} = m\frac{4\alpha}{3\pi}\frac{(Z\alpha)^4}{n^3}\begin{cases} \ln\frac{\Lambda}{<E_n>} & \text{if } \ell = 0 \\ \ln\frac{Z^2 m\alpha^2}{2<E_n>} & \text{if } \ell \neq 0, \end{cases} \tag{4.1.31}$$

where $< E_n >$ is the Bethe logarithm which can be evaluated numerically [15] and m_e is the mass of the electron. Now, by using Eqs.(4.1.1), (4.1.27) and (4.1.28), we can add the α^5 contributions from Eqs.(4.1.29) , (4.1.30) to Eq.(4.1.31) to obtain:

$$\Delta E = m\frac{4\alpha}{3\pi}\frac{(Z\alpha)^4}{n^3}\begin{cases} \ln\frac{m}{2<E_{n,0}>} + \frac{71}{360} - \frac{m^2}{5m_e^2} & \text{if } \ell = 0 \\ \ln\frac{Z^2 m\alpha^2}{2<E_{n,\ell}>} & \text{if } \ell \neq 0, \end{cases} \tag{4.1.32}$$

Eq(4.1.32) is the Lamb shift for scalar-scalar bound state. Unfortunately we do not have a scalar particle with $m \sim m_e$, so these calculations do not have a physical application. When $m_e \ll m$, the terms appearing in the $\frac{\mathbf{p}}{m}$ expansion of the vacuum polarization are not suppressed for higher powers of $\frac{\mathbf{p}}{m}$, requiring one to sum all these terms. The resulting integral is still under investigation.

4.2 Matching at Next-to-Leading Order for Four-Fermi Operators.

We now turn to the next-to-leading corrections to $\mathcal{L}_{4-Fermi}$. These corrections can be divided into the following three classes according to the topology of the one-loop QED graphs which are involved:

- One-Photon Annihilation

  These corrections consist of QED graphs which describe one-loop corrections to the tree-level process of the s-channel exchange of a single virtual photon. As before, t-channel exchange of a single virtual photon does not contribute corrections to $\mathcal{L}_{4-Fermi}$.

- Two-Photon Annihilation

  These consist of the QED 'box' graphs which describe the s-channel exchange of two virtual photons.

- t-Channel Two-Photon Exchange

  The final class consists of QED box graphs which describe the t-channel exchange of two virtual photons. Although t-channel one-photon exchange does not contribute to NRQED four-fermion interactions, t-channel two-photon exchange *does* contribute because there is a region of phase space for which the loop momentum is larger than the electron mass, and so does not appear in the corresponding two-photon exchange graphs of NRQED. The corresponding physics is therefore put back into the effective field theory by renormalizing the coefficients of the NRQED four-fermi interactions.

We now describe, in turn, the matching due to each of these classes of graphs. While the contributions to $c_4^{(1)}$ and $c_5^{(1)}$ due to the first two of these

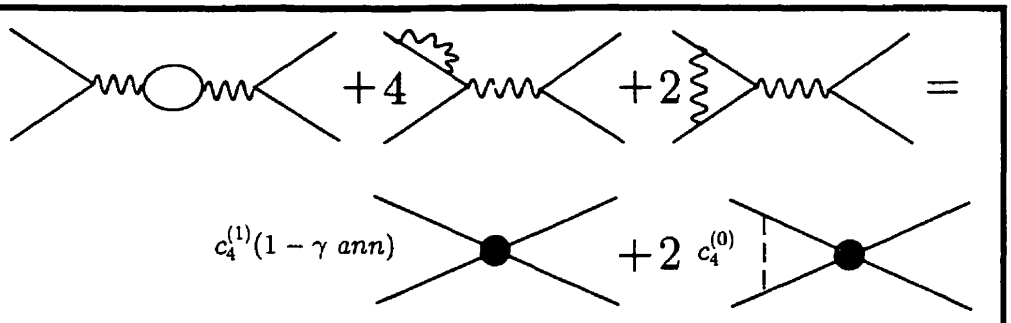

Figure 4.7: The graphs which give the one-photon annihilation contribution to $c_4^{(1)}$.

may be found in the literature [7], [12], those due to the third class we present here for the first time.

Matching due to one-loop corrections to single-photon annihilation are described by the graphs of Figure (4.7). The contributions to the scattering amplitude of electrons and positrons at threshold from the QED graphs on the left-hand side of the equality in this figure must be equated to the contributions of the NRQED graphs on the right-hand side. Evaluating all the graphs for a spin-triplet e^+e^- state, and solving for $c_4^{(1)}$ then gives [7], [12]:

$$c_4^{(1)}(1\text{-}\gamma\ \text{ann}) = \frac{44\alpha^2}{9m^2}. \tag{4.2.33}$$

The same matching can be performed for the coefficient $c_5^{(1)}$ by using the spin-0 annihilation vertex for the NRQED four-fermi interaction and evaluating all diagrams in a state of total spin equal to zero. The result is trivially

$$c_5^{(1)}(1\text{-}\gamma\ \text{ann}) = 0 \tag{4.2.34}$$

by charge conjugation invariance.

Although all possible one-loop s-channel single-photon exchange QED graphs appear on the left-hand side of Fig.(4.7), all NRQED one-loop corrections to the four-fermi interaction do *not* appear on the right-hand side.

An important issue is therefore how to determine which NRQED graphs must be included to any given order in the matching process. The simplest way to do this is to imagine performing the matching slightly off-threshold, *i.e.* with the external particles having a small velocity in the center of mass frame. As mentioned earlier, this does not affect the value of the NRQED coefficients. Which NRQED diagram must be kept is then decided by counting powers of α and v, with $v \sim \alpha$ kept in mind for bound-state applications.

For example, for the present purposes of computing the $\mathcal{O}(m\alpha^5)$ hyperfine splitting, we show in section(4.2.1) that we require both c_4 and c_5 to next-to-leading order, $\mathcal{O}(\alpha^2)$. This implies that this coupling must be matched to QED with an accuracy of up to order $\alpha^2 v^0$. The loop diagram involving the exchange of one Coulomb photon contributes to order [6] α^2/v and cancels a similar term in the QED one loop vertex correction. At threshold, the $1/v$ contribution becomes [7] a $1/\lambda$ infrared divergence which cancels a similar term in the QED diagram[8]. All other NRQED loop graphs which could appear on the right-hand side necessarily involve additional powers of the electron or positron velocity, v, and so give contributions to c_4 which are smaller than $\mathcal{O}(\alpha^2)$. For example, consider the diagram containing the four-fermi operator followed by a transverse photon connected to two dipole vertices. Since each dipole vertex is proportional to $e\mathbf{p}/m \sim ev$, the total contribution of this diagram would be $\sim \alpha(ev)^2/v$, where the factor of α comes from the coefficient $c_4^{(0)}$ and the $1/v$ has a similar origin as the $1/v$ encountered in the Coulomb diagram. The total contribution of this diagram is therefore $\sim \alpha^2 v$

[6] This diagram is proportional to $\alpha^2 \int d^3k/((\mathbf{p}^2 - \mathbf{k}^2 + i\epsilon)(\mathbf{k} - \mathbf{p})^2) \simeq \alpha^2/\mathbf{p}$ where $\mathbf{p} = m\mathbf{v}$ is the external momentum.

[7] We regulate all such infrared divergences by including a photon mass, λ, into photon propagators.

[8] Because the coefficients of the effective theory describes only high-energy virtual effects in QED, it is a general result that these coefficients are always infrared finite.

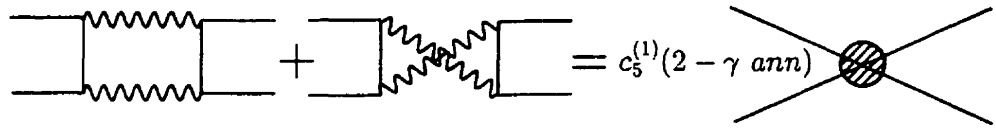

Figure 4.8: Diagrams which contribute to two-photon annihilation contributions to $c_5^{(1)}$.

which is of higher order than required for the $\mathcal{O}(m\alpha^5)$ hyperfine splitting. In this way it may be seen that only the Coulomb-exchange NRQED loop need be kept in Fig.(4.7).

We next turn to the QED box graphs describing s-channel electron-positron annihilation into two virtual photons, Figure (4.8) (notice that there is no diagram with a one Coulomb correction to the four-Fermi operator because $c_5^{(0)} = 0$). The matching appropriate for these graphs gives [7], [12]:

$$c_5^{(1)}(2\text{-}\gamma \text{ ann}) = \left(\frac{\alpha^2}{m^2}\right)\left(2 - 2\ln 2 + i\pi\right). \tag{4.2.35}$$

This time charge conjugation invariance forbids a contribution to the spin-triplet operator and one finds

$$c_4^{(1)}(2\text{-}\gamma \text{ ann}) = 0. \tag{4.2.36}$$

Notice that in Eq.(4.2.35), the one-loop contribution to c_5, has both a real and imaginary part. This imaginary part causes the low-energy hamiltonian not to be hermitian. The resulting loss of unitarity in the time evolution is just what is required to describe the depletion of electrons and positrons due to their mutual annihilation into real photons. Since annihilation is a high-energy effect, it appears in NRQED as an effective four-fermi operator. This imaginary part may be used to compute the decay rate for positronium bound states by calculating the imaginary part it implies for the bound state

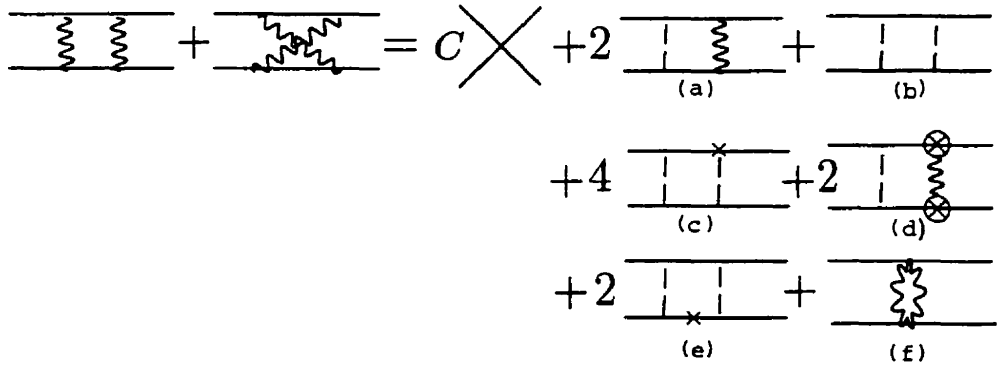

Figure 4.9: The one-loop t-channel matching diagrams.

energy eigenvalue, E. The decay rate for bound state is then given by the familiar relation, $\Gamma = -2\ \mathrm{Im}(E)$.

We now turn to the contribution to c_4 and c_5 due to the t-channel two-photon QED exchange graphs, given in Figure (4.9). Here C is meant to represent $c_4^{(1)}$ when the diagrams are evaluated in a spin 1 state, and $c_5^{(1)}$ when the diagram is evaluated in a spin 0 state. Similarly, the four-fermi interaction represents either the spin 1 or spin 0 annihilation vertex. It is straightforward to verify that only the given NRQED graphs can contribute to these coefficients up to $\mathcal{O}(\alpha^2 v^0)$.

In order to determine $c_4^{(1)}$ and $c_5^{(1)}$ separately, we must include all of the spin-independent NRQED diagrams in the matching. This is actually more work than is required purely for the purposes of calculating the hyperfine splitting, because only the difference $c_4^{(1)} - c_5^{(1)}$ enters into this quantity. Since the spin-independent graphs cancel in this difference, it suffices to only compute spin-dependent graphs if one is strictly interested only in the hyperfine splitting. However, we present here the separate matching for both c_4 and c_5, since these two coefficients must be known separately for other applications, such as the complete $\mathcal{O}(m\alpha^5)$ shift of the positronium energy

levels.

Evaluating the left-hand side of Fig.(4.9) (the QED graphs) for a spin-triplet electron-positron configuration gives, after a straightforward calculation:

$$(\mathrm{QED})_{S=1} = \alpha^2 \left[\frac{-2\pi m}{\lambda^3} + \frac{11\pi}{12\lambda m} + \frac{4}{3m^2} + \frac{2}{m^2}\ln\left(\frac{\lambda}{m}\right)\right]. \qquad (4.2.37)$$

Using the NRQED Feynman rules to calculate the right-hand side of Fig.(4.9) gives the following contributions. The only spin-dependent NRQED diagram, part (d) of Figure(4.9), gives:

$$\begin{aligned}(\mathrm{NRQED})_{S=1}(d) &= 2\int \frac{d^3\mathbf{p}}{(2\pi)^3}\left(\frac{-ie\mathbf{p}\times\boldsymbol{\sigma}_1}{2m}\right)_i\left(\frac{-ie\mathbf{p}\times\boldsymbol{\sigma}_2}{2m}\right)_j\left(\frac{-1}{\mathbf{p}^2+\lambda^2}\right)\\ &\qquad\times\left(\delta_{ij}-\frac{\mathbf{p}_i\mathbf{p}_j}{\mathbf{p}^2+\lambda^2}\right)\left(\frac{-m}{\mathbf{p}^2}\right)\left(\frac{-e^2}{\mathbf{p}^2+\lambda^2}\right)\\ &= \frac{8\alpha^2}{3m}\left(\int\frac{dp\,\mathbf{p}^2}{(\mathbf{p}^2+\lambda^2)^2}\right)\\ &= \frac{2\pi\alpha^2}{3m\lambda}, \qquad (4.2.38)\end{aligned}$$

where the overall factor of 2 in the first line takes into account the two possible ways in which the NRQED diagram can be drawn.

Similarly, diagram (f) of Fig.(4.9) gives:

$$\begin{aligned}(\mathrm{NRQED})_{S=1}(f) &= \int\frac{d^3\mathbf{p}}{(2\pi)^3}\left(\frac{e^2}{2m}\right)\left(\frac{e^2}{2m}\right)\frac{1}{\sqrt{\mathbf{p}^2+\lambda^2}}\left(\delta_{ij}-\frac{\mathbf{p}_i\mathbf{p}_j}{\mathbf{p}^2+\lambda^2}\right)\\ &\qquad\times\frac{-1}{2\sqrt{\mathbf{p}^2+\lambda^2}}\frac{1}{\sqrt{\mathbf{p}^2+\lambda^2}}\left(\delta^{ij}-\frac{\mathbf{p}^i\mathbf{p}^j}{\mathbf{p}^2+\lambda^2}\right)\\ &= \frac{\alpha^2}{m^2}\left[\frac{28}{15}-2\ln 2+\ln\left(\frac{\lambda}{\Lambda}\right)\right]. \qquad (4.2.39)\end{aligned}$$

All the other NRQED diagrams can be calculated in a similar manner. The final result for the sum of the NRQED diagrams, evaluated in a spin-triplet state is:

$$(\mathrm{NRQED})_{S=1} = -2\,c_4^{(1)}(t\text{-ch}) \;+\; \alpha^2\left[\frac{-2\pi m}{\lambda^3}+\frac{11\pi}{12\lambda m}+\frac{28}{15m^2}\right.$$

$$-\frac{2}{m^2}\ln 2+\frac{2}{m^2}\ln\left(\frac{\lambda}{\Lambda}\right)\Bigg]. \quad (4.2.40)$$

Solving for $c_4(t\text{-ch})$ then gives the result:

$$c_4^{(1)}(t\text{-}ch) = -\left(\frac{\alpha^2}{m^2}\right)\left[\ln\left(\frac{\Lambda}{m}\right)-\frac{4}{15}+\ln 2\right]. \quad (4.2.41)$$

An identical procedure applies to the $S=0$ state. The QED graphs are then found to give:

$$(\text{QED})_{S=0} = \alpha^2\left[\frac{-2\pi m}{\lambda^3}-\frac{21\pi}{12\lambda m}+\frac{16}{3m^2}+\frac{2}{m^2}\ln\left(\frac{\lambda}{m}\right)\right]. \quad (4.2.42)$$

For $S=0$, part (d) of Fig.(4.9) now equals

$$(\text{NRQED})_{S=0}(d) = -\frac{2\pi\alpha^2}{\lambda m} \quad (4.2.43)$$

whereas the other NRQED diagrams are left unchanged because they are spin independent. The sum of the NRQED diagrams is then found to be

$$(\text{NRQED})_{S=0} = -2\,c_5^{(1)}(t\text{-ch}) \;+\; \alpha^2\left[\frac{-2\pi m}{\lambda^3}-\frac{21\pi}{12\lambda m}+\frac{28}{15m^2} -\frac{2}{m^2}\ln(2)+\frac{2}{m^2}\ln\left(\frac{\lambda}{\Lambda}\right)\right]. \quad (4.2.44)$$

The complete matching result from Fig.(4.9) then is

$$c_5^{(1)}(t\text{-ch}) = -\left(\frac{\alpha^2}{m^2}\right)\left[\ln\left(\frac{\Lambda}{m}\right)+\frac{26}{15}+\ln 2\right]. \quad (4.2.45)$$

The complete one-loop contributions to the coefficients c_4 and c_5 are then given by combining the results from all three classes of graphs:

$$\begin{aligned} c_4^{(1)} &= c_4^{(1)}(1\text{-}\gamma\text{ ann}) + c_4^{(1)}(t\text{-ch}) = \frac{\alpha^2}{m^2}\left[-\ln\left(\frac{\Lambda}{m}\right)+\frac{232}{45}-\ln 2\right] \\ c_5^{(1)} &= c_5^{(1)}(2\text{-}\gamma\text{ ann}) + c_5^{(1)}(t\text{-}ch) = \frac{\alpha^2}{m^2}\left[-\ln\left(\frac{\Lambda}{m}\right)+\frac{4}{15}-3\ln 2+i\pi\right]. \end{aligned} \quad (4.2.46)$$

With the NRQED Lagrangian now in hand, we next proceed with the determination of which graphs can contribute to the $\mathcal{O}(m\alpha^5)$ hyperfine splitting in positronium.

4.2.1 Hyperfine Splitting in Positronium to Order α^5.

In this section, we present an NRQED calculation of the complete contributions to the positronium hyperfine structure at next-to-leading order, $\mathcal{O}(m\alpha^5)$. The result we obtain for the ground state hyperfine splitting agrees with previous results [40]. However our results are easily extended to the hyperfine splitting of excited states having arbitrary quantum numbers n and ℓ. These agree with previous results [20] for arbitrary n but $\ell = 0$, but to our knowledge ours is the first calculation[9] which is applicable to general n and ℓ. We may now apply these power-counting arguments to the hyperfine splitting. An important simplifying feature appears in this specific application, since the hyperfine splitting compares the energies of two states having different net spin. As a result it suffices to consider only graphs for which at least one of the vertices involves a spin-dependent coupling.

To proceed, we start by recapping the power counting which leads to the graphs which contribute to the $O(m\alpha^4)$ hyperfine splitting [14]. In this case we require $\zeta = 4$, so $\kappa + \rho + \sum_i n_i - N = 3$. Consider first the case $N = 0$. In this case we require all possible graphs containing a single instantaneous photon exchange, subject to the following two conditions: (i) at least one vertex is spin dependent; and (ii) $\kappa + \rho + \sum_i n_i = 3$. The five classes of graphs which satisfy these two conditions are displayed in Figure(4.10). The coupling which appears in part (a) of this figure is c_1, which appears twice, so inspection of Eq.(2.2.2) shows that the tree-level contribution, $c_1^{(0)}$, gives $\kappa + \rho = 2$ and $\sum_i n_i = 1$, as required. The same is true for parts (b) — which is linear in $c_1^{(0)}$ — and (c) — which is proportional to $c_3^{(0)}$. Finally,

[9]The authors of ref.[21] have presented all the potentials necessary to calculate the order α^5 shift of the positronium energy levels but explicit numbers are only given, in a numerical form, for the $n = 2$ level. Our formula agrees with these numbers.

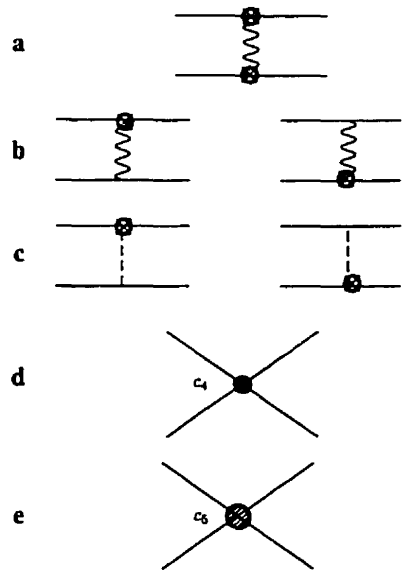

Figure 4.10: The NRQED graphs which contribute to the hyperfine structure at order $m\alpha^4$.

parts (d) and (e) involve the four-fermi couplings, c_4 and c_5, the largest of which also arises at tree-level, proportional to α/m^2, again giving $\kappa + \rho = 2$, $\sum_i n_i = 1$. It follows that these graphs contribute to $\mathcal{O}(m\alpha^4)$ provided we use the leading-order contribution to their couplings. It is noteworthy that only the graphs of parts (a), (d) and (e) of Figure (4.10) contribute to the hyperfine splitting of the ground state, since all of the others vanish when evaluated in an s-wave configuration.

It now remains to consider the case $N > 0$. Having $N = 1$ implies including one more interaction in addition to the diagrams shown in Figure (4.10). It can be easily verified that any additional interaction (excluding, of course, the Coulomb interaction) increases the combination $\kappa + \rho + \sum_i n_i$ by at least 3. For example, one can add a transverse photon coupled to two dipole vertices, introducing the square of the coefficient $c_1^{(0)} = q/(2m)$. This increases κ by 2 and n by 1. The net change in ζ is therefore $3 - 1 = 2$ and

the diagram contributes only to order $m\alpha^6$. Similarly, adding a Coulomb photon connected to a Coulomb and Darwin vertex increases $\kappa+\rho$ by 2 and $\sum_i n_i$ by 1, whereas adding a relativistic kinetic vertex doesn't change $\sum_i n_i$ but increases $\kappa+\rho$ by 3. Adding other interactions necessarily leads to, at best, $\mathcal{O}(m\alpha^6)$.

This last argument has immediate implications for calculating the $\mathcal{O}(m\alpha^5)$ hyperfine structure. To this order all of the relevant graphs must still have $N=0$. The next-to-leading result is therefore obtained from the *same* graphs, Figure (4.10), but using the next-to-leading order — *i.e.* $\mathcal{O}(\alpha^2)$ — contributions to the coefficients, c_i. In section(4.2), We have shown in detail how these corrections are computed for the case of the coefficients of the four-fermi interactions, $c_4^{(1)}$ and $c_5^{(1)}$. To compute the hyperfine splitting we evaluate the graphs of Figure(4.10) using Coulomb wavefunctions to describe the initial and final electron-positron lines. Consider, first, the hyperfine splitting for s-wave states. In this case only graphs (a), (d) and (e) of Fig.(4.10) contribute since the other two graphs contain one vector, $\boldsymbol{\sigma}$, which can't be dotted into any other vector if $\ell=0$. We find

$$\begin{aligned}
\delta E_n(a) &= 2\left(\frac{\alpha}{2\pi}\right)\int\frac{d^3\mathbf{p}\,d^3\mathbf{k}}{(2\pi)^3}\,\Psi^*(\mathbf{p})\left(\frac{-ie(\mathbf{p}-\mathbf{k})\times\boldsymbol{\sigma}_1}{2m}\right)_i\frac{-1}{(\mathbf{p}-\mathbf{k})^2}\\
&\qquad\left(\frac{-ie((\mathbf{p}-\mathbf{k})\times\boldsymbol{\sigma}_2}{2m}\right)_j\left(\delta_{ij}-\frac{(\mathbf{p}-\mathbf{k})_i(\mathbf{p}-\mathbf{k})_j}{(\mathbf{p}-\mathbf{k})^2}\right)\Psi(\mathbf{k})\\
&= 2\left(\frac{\alpha}{2\pi}\right)\frac{2\pi\alpha}{3m^2}<\boldsymbol{\sigma}_1\cdot\boldsymbol{\sigma}_2>|\Psi(0)|^2\\
&= 2\left(\frac{\alpha}{2\pi}\right)\left(\frac{m\alpha^4}{6n^3}\left[S(S+1)-\frac{3}{2}\right]\delta_{\ell,0}\right)\\
\delta E_n(d) &= -\frac{m^3\alpha^3}{8\pi n^3}\left(c_4^{(1)}\,S(S+1)\right)\delta_{\ell,0}\\
&= -\left(\frac{m^3\alpha^3}{8\pi n^3}\right)\left(\frac{\alpha}{m}\right)^2\left(-\ln\left(\frac{\Lambda}{m}\right)+\frac{232}{45}-\ln 2\right)\;S(S+1)\,\delta_{\ell,0}\\
\delta E_n(e) &= -\frac{m^3\alpha^3}{8\pi n^3}\left(c_5^{(1)}\,[2-S(S+1)]\,\delta_{\ell,0}\right)
\end{aligned}$$

$$= -\left(\frac{m^3\alpha^3}{8\pi n^3}\right)\left(\frac{\alpha}{m}\right)^2\left(-\ln\left(\frac{\Lambda}{m}\right)+\frac{4}{15}-3\ln 2+i\pi\right)\times$$
$$[2-S(S+1)]\ \delta_{\ell,0} \qquad (4.2.47)$$

where n and $\ell = 0$ are the principal and orbital quantum number of the positronium state of interest, and $S = 0$ or 1 is the net intrinsic spin of the e^+e^- state.

Using the formula $\Gamma = -2\ \mathrm{Im}(E)$, we obtain from $\delta E_n(e)$ the $\mathcal{O}(m\alpha^5)$ decay rate of the s-wave state of parapositronium ($S = 0$):

$$\Gamma(n,\alpha^5) = \frac{m\alpha^5}{2n^3}\,\delta_{\ell,0} \quad . \qquad (4.2.48)$$

In the rest of the chapter, we concentrate on the hyperfine splitting so we drop the imaginary part contained in $\delta E_n(e)$. Adding the contributions of diagrams (a), (d) and (e) of Fig.(4.10), and taking the difference between $S = 1$ and $S = 0$ finally gives:

$$\begin{aligned}\Delta E_{hfs}(n,\alpha^5) &\equiv \delta E_n(S=1)-\delta E_n(S=0)\\ &= -\left(\frac{m\alpha^5}{2\pi n^3}\right)\left[\ln 2+\frac{16}{9}\right]\delta_{\ell,0} \quad , \qquad (4.2.49)\end{aligned}$$

in agreement with standard results [40][20].

The hyperfine splitting for arbitrary quantum numbers is computed by modifying the previous calculation in two ways. First, diagram (a) of Fig.(4.10) must be computed for $\ell \neq 0$ states. Notice that diagrams (d) and (e) of this figure are nonzero only for s-wave states since they represent contact interactions. Secondly, diagrams (b) and (c), which contribute only to $\ell \neq 0$ states, must be computed. Since the calculation of these latter contributions is presented in chapter(3) [14], we present here just the final result[22] for the splitting $\delta E_n(S=1,\ell,j) - \delta E_n(S=0,\ell,j'=\ell)$:

$$\Delta E_{\mathrm{hfs}}(n,\ell,\alpha^5) = -\left(\frac{m\alpha^5}{2\pi n^3}\right)\ \left[\ \left(\ln 2+\frac{16}{9}\right)\delta_{\ell 0}\right.$$

$$- \frac{C_{j\ell}}{4(\ell+\frac{1}{2})}\left(1-\delta_{\ell 0}\right)\Big], \quad (4.2.50)$$

where j is the total angular momentum quantum number of the triplet state ($S=1$), and the coefficients $C_{j\ell}$ are given explicitly by:

$$C_{j\ell} = \begin{cases} \frac{4\ell+5}{2(\ell+1)(2\ell+3)} & \text{if } j=\ell+1 \\ \frac{-1}{2\ell(\ell+1)} & \text{if } j=\ell \\ \frac{-4\ell+1}{2\ell(2\ell-1)} & \text{if } j=\ell-1 \end{cases} \quad (4.2.51)$$

To summarize, we see that the hyperfine splitting to $\mathcal{O}(m\alpha^5)$ is hardly more difficult to obtain in NRQED than is the $\mathcal{O}(m\alpha^4)$ result. The only extra effort required is obtaining the complete matching of all spin-dependent effective operators to next-to-leading order in α. We have performed the required $\mathcal{O}(\alpha^2)$ matchings for those four-fermi operators which had not been previously given in the literature. Furthermore, results for the hyperfine splitting for general n and ℓ are obtained with very little effort.

Summary

In this chapter we have performed four different calculations.

- Rederivation of the Lamb shift of the hydrogen atom in the non-recoil limit, $\frac{m_e}{m_p}=0$, using NRQED as an effective theory.
- Derivation of the Lamb shift of a scalar-scalar bound state in the non-recoil limit, $\frac{m}{M}=0$, using NRQED as an effective field theory.
- Rederivation of HFS of positronium in its ground state to the α^5 order using NRQED as an effective field theory. This result is the second term in Eq.(1.0.1).

- Extension of the HFS of the positronium at $O(\alpha^5)$ order to the general excited state, n and ℓ .

In brief, throughout chapters(3) and (4), we have obtained, respectively, the first two terms of Eq.(1.0.1). We are now ready to calculate the unknown coefficient, K_1(1-γ ann), in Eq.(1.0.1).

Chapter 5

Next-to-Next-Leading Order Bound State Energy Shift.

In this chapter we calculate the analytical expression for the HFS of positronium in its ground state coming from the one photon annihilation diagram to order $m\alpha^6$. Let us recall the results of chapter(4.2), where the coefficient of spin-1 annihilation vertex, c_4(1-γ ann), was derived at Next-to-Leading order (NLO) in α, Eq.(4.2), and then by using $c_4^{(1)}$(1-γ ann) we were able to get the contribution of the HFS in positronium to order α^5. Therefore, to achieve our goal in this chapter we should proceed one step further and perform a matching at two loop level to get $c_4^{(2)}$(1-γ ann). Fig(5.1) shows the relation that we can use to accomplish this goal. Since we have already obtained the coefficient $c_4^{(0)}$ from the matching of NRQED with QED at tree level (see section (2.2.1)) then in Fig(5.1), the first term on the left-hand side cancels the first term of the right-hand side. The same cancellation happens for the second terms with the coefficient $c_4^{(1)}$(1-γ ann) recalculated at one-loop matching taking into account all one-loop NRQED diagrams. Therefore Fig(5.1) reduces to a simpler form, Fig(5.2), which is our basic relation for matching at Next-to-Next-Leading order (NNLO). From now on the match-

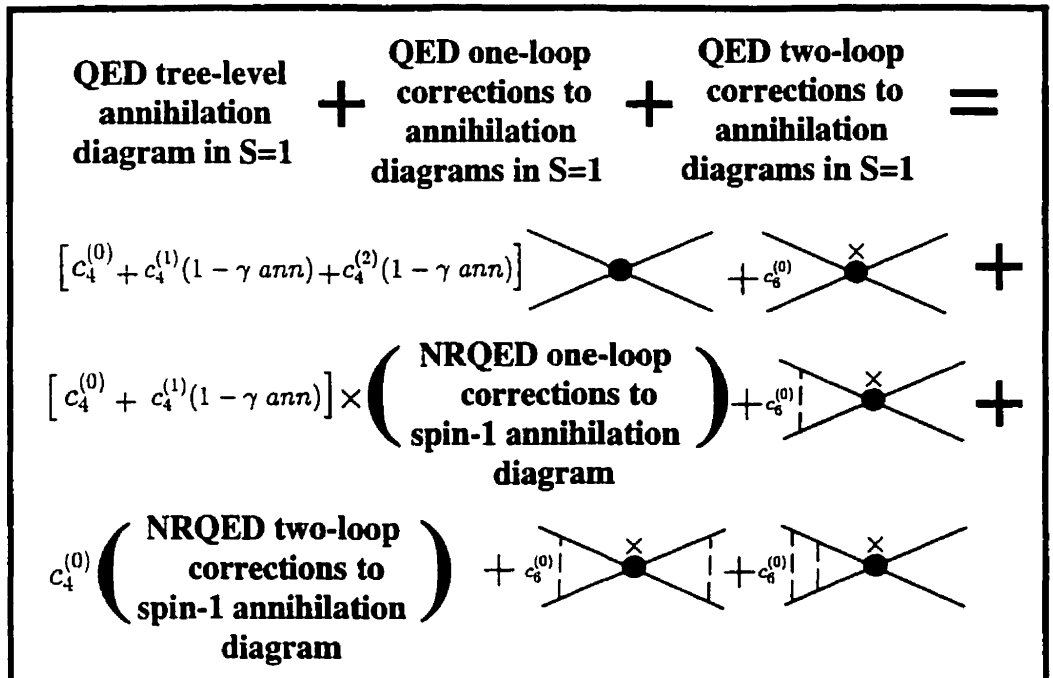

Figure 5.1: The general form of matching for the annihilation diagrams in a triplet state up to two loops.

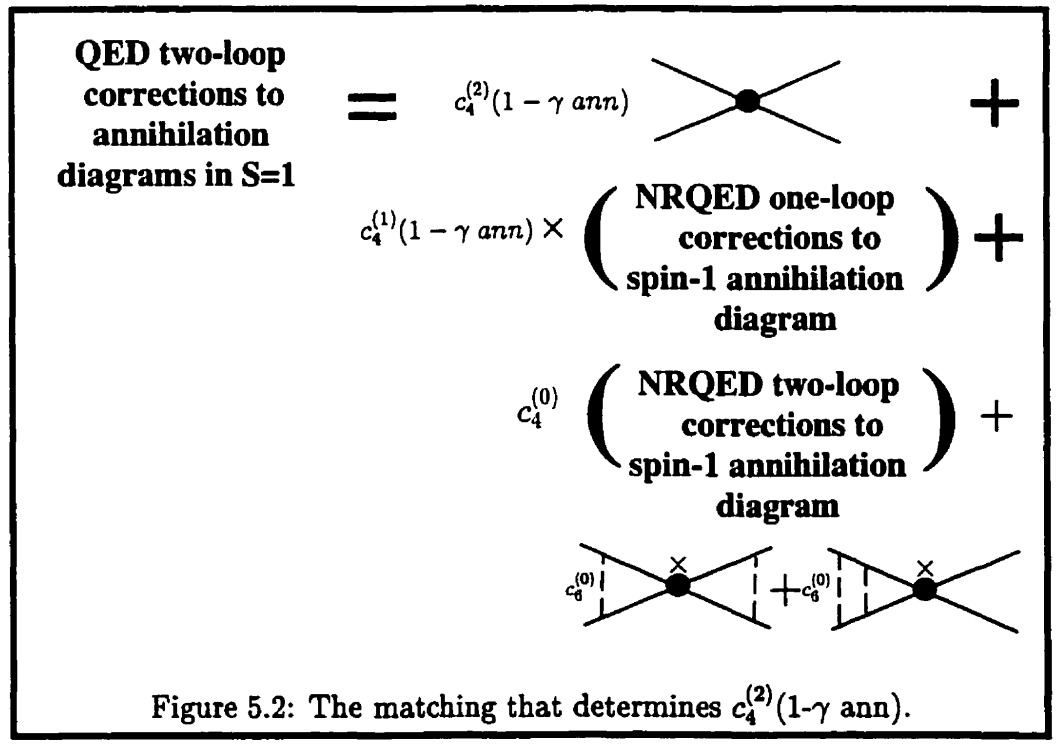

Figure 5.2: The matching that determines $c_4^{(2)}$(1-γ ann).

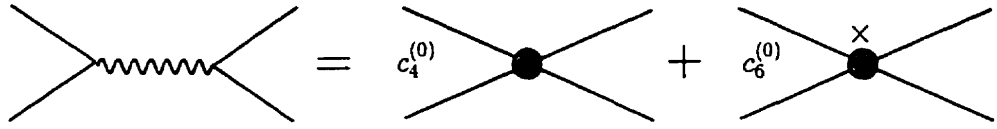

Figure 5.3: The matching above the threshold which determines $c_4^{(0)}$ and $c_6^{(0)}$.

ing is done above the threshold where the external particle are NOT at rest: $\lambda/m \ll \alpha \ll v \ll 1$ (where λ is IR-regulating, photon mass). This is contrary to the previous chapter where we took all the external particles at threshold: $v = 0 \ll \lambda/m \ll \alpha \ll 1$.

Before we embark on the two-loop matching, we need to introduce the concept of Derivative interaction. We also need to redo one-loop matching with all the NRQED diagrams which are relevant for the two-loop calculation.

5.1 Derivative Interaction

As we have shown in section(2.2.2) the threshold amplitude of the one photon annihilation gives a four-fermi interaction at tree level, $c_4^{(0)}$. To obtain the NNLO precision we need the correction to this diagram up to p_0^2/m^2, where p_0 is the three-momentum of the fermions. In other words, we need to do the matching above the threshold, as shown in Fig.(5.3). We denote by $c_6^{(0)}$ the coefficient of the new four-fermi interaction, which we call the Derivative interaction. $c_6^{(0)}$ is derived in Ref.[7] and is equal to

$$c_6^{(0)} = \frac{-2\pi\alpha}{3m^4}. \tag{5.1.1}$$

It is important to mention that 3/4 of the Derivative vertex, $\frac{-\pi\alpha}{m^4}(\mathbf{p}^2+\mathbf{q}^2) = \frac{-2\pi\alpha}{m^4}(\mathbf{p}^2)$, comes from the photon propagator correction[1]. To see this fact,

[1] $\mathbf{p}^2$ and $\mathbf{q}^2$ are the momentum squares of incoming and outgoing of particles in the center of mass frame ($\mathbf{p}^2 = \mathbf{q}^2$).

let us look at the photon propagator in the one photon annihilation diagram:

$$\begin{aligned}\frac{e^2}{q^2} &= \frac{e^2}{(p_1+p_2)^2} \\ &= \frac{e^2}{[(m+\frac{\mathbf{p}^2}{m},\mathbf{p})+(m+\frac{\mathbf{p}^2}{m},-\mathbf{p})]^2} \\ &= \frac{e^2}{(2m+\frac{\mathbf{p}^2}{m})^2} = \frac{e^2}{4m^2(1+\frac{\mathbf{p}^2}{m^2})^2} \\ &\approx \frac{\pi\alpha}{m^2}\Big(1-\frac{\mathbf{p}^2}{m^2}\Big), \end{aligned} \tag{5.1.2}$$

where we should still multiply Eq.(5.1.2) by a factor 2 due to the spin average of triplet state. Further, it is shown in [7] that 1/8 of the Derivative vertex comes from the Taylor expansion of each vertex of the one photon annihilation diagram.

5.2 Revisiting One-Loop Matching

Although we have shown one-loop matching in the $\mathcal{O}(\alpha^5)$ calculation, for higher precision we should redo the matching, this time keeping some higher order diagrams that were previously left out (the diagrams with the insertions of interactions relevant at the NNLO). The one-loop matching is shown in Fig.(5.4), and we start with the NRQED diagrams.

The NRQED Part.

In all NRQED diagrams in this chapter, we use the Table of Integrals given in Refs.[7] and [38] (see Appendices A, B). Throughout this chapter the hierarchy $\lambda \ll p_0$ is understood. We start with the diagram which has one Coulomb line.

$$Fig.(5.4(a)) = \Big(\frac{2\pi\alpha}{m^2}\Big)\int\frac{d^3p}{(2\pi)^3}(-e^2)\Big(\frac{-m}{p^2-p_0^2-i\epsilon}\Big)\frac{1}{(\mathbf{p}_0-\mathbf{p})^2+\lambda^2}$$

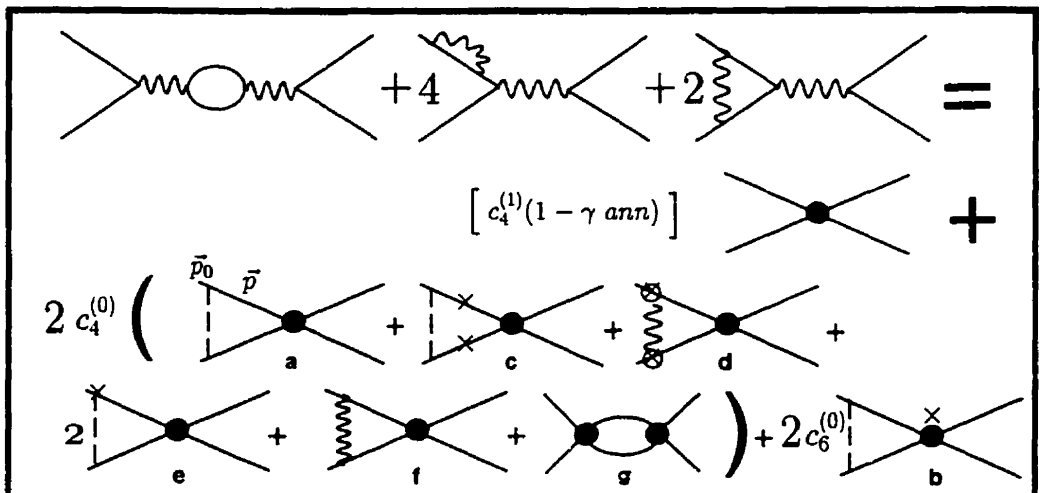

Figure 5.4: One-loop matching required for two-loop calculation.

$$= \left(\frac{\alpha^2}{mp_0}\right) \int dp \frac{p}{p^2 - p_0^2 - i\epsilon} \ln\left(\frac{(p_0+p)^2+\lambda^2}{(p_0-p)^2+\lambda^2}\right)$$
$$= \left(\frac{\alpha^2}{mp_0}\right)\left[\frac{\pi^2}{2} + i\pi \ln\left(\frac{2p_0}{\lambda}\right)\right] \qquad (5.2.3)$$

where p_0 is the momentum of external particle.

The analytic expression for the NRQED diagram with the insertion of the Transverse interaction, Fig.(5.4(f)), reads:

$$\begin{aligned} Fig.(5.4(f)) &= \left(\frac{2\pi\alpha}{m^2}\right) \int \frac{d^3p}{(2\pi)^3} \left(\frac{e(\mathbf{p}_0+\mathbf{p})_i}{2m}\right) \frac{e(\mathbf{p}_0+\mathbf{p})_j}{2m} \\ &\quad \frac{-1}{(\mathbf{p}_0-\mathbf{p})^2+\lambda^2} \left(\delta_{ij} - \frac{(\mathbf{p}_0-\mathbf{p})_i(\mathbf{p}_0-\mathbf{p})_j}{(\mathbf{p}_0-\mathbf{p})^2+\lambda^2}\right) \left(\frac{-m}{p^2-p_0^2-i\epsilon}\right) \\ &= \left(\frac{-\alpha^2}{2m^3}\right)\Big[\int -2\frac{dpp^2}{(p^2-p_0^2-i\epsilon)} \\ &\qquad + \int \frac{dpp(2p_0^2+2p^2+\lambda^2)}{2p_0(p^2-p_0^2-i\epsilon)} \ln\left(\frac{(p+q)^2+\lambda^2}{(p-q)^2+\lambda^2}\right) \\ &\qquad - \int \frac{dpp^2 2(p^2-p_0)^2}{((p^2+p_0^2+\lambda^2)^2-4p^2p_0^2)(p^2-p_0^2-i\epsilon)}\Big] \\ &= \left(\frac{\pi p_0 \alpha^2}{m^3}\right)\left[\frac{-i}{2} + \frac{\pi}{2} + i\ln\left(\frac{2p_0}{\lambda}\right)\right] \qquad (5.2.4) \end{aligned}$$

The diagram with the Spin-Spin interaction is the next one-loop NRQED

diagram

$$
\begin{aligned}
Fig.(5.4(d)) &= \int \frac{d^3p}{(2\pi)^3}\Big(\frac{-ie(\mathbf{p}-\mathbf{p}_0)\times\boldsymbol{\sigma}}{2m}\Big)_i\Big(\frac{-ie(\mathbf{p}-\mathbf{p}_0)\times\boldsymbol{\sigma}}{2m}\Big)_j \\
&\quad \frac{-1}{(\mathbf{p}-\mathbf{p}_0)^2+\lambda^2}\Big(\delta_{ij}-\frac{(\mathbf{p}-\mathbf{p}_0)_i(\mathbf{p}-\mathbf{p}_0)_j}{(\mathbf{p}-\mathbf{p}_0)^2+\lambda^2}\Big) \\
&\quad \Big(\frac{2\pi\alpha}{m^2}\Big)\Big(\frac{-m}{p^2-p_0^2-i\epsilon}\Big) \\
&= \Big(\frac{-\alpha^2}{2\pi m^3}\Big)\int \frac{d^3p\ \ 2/3(\mathbf{p}-\mathbf{p}_0)^2}{((\mathbf{p}-\mathbf{p}_0)^2+\lambda^2)(p^2-p_0^2-i\epsilon)} \\
&= \Big(\frac{-2\alpha^2}{3m^3}\Big)\Big[\Lambda+\frac{i\pi p_0}{2}\Big] \qquad (5.2.5)
\end{aligned}
$$

where Λ is the ultraviolet cutoff coming from the loop integral. Diagrams containing the Darwin interaction can be obtained from the diagrams with the Spin-Spin interaction. To see this fact, we calculate the diagram in the Fig.(5.4(e)).

$$
\begin{aligned}
Fig.(5.4(e)) &= \int \frac{d^3p}{(2\pi)^3}(-e)\frac{1}{(\mathbf{p}-\mathbf{p}_0)^2+\lambda^2}\Big(\frac{2\pi\alpha}{m^2}\Big) \\
&\quad \Big(\frac{-m}{p^2-p_0^2-i\epsilon}\Big)\Big(\frac{-e(\mathbf{p}-\mathbf{p}_0)^2}{8m^2}\Big) \\
&= \frac{3}{4}\Big(Fig.(5.8(d))\Big) \qquad (5.2.6)
\end{aligned}
$$

Using the Feynman rules given in Fig.(2.1), we find:

$$
\begin{aligned}
Fig.(5.4(b)) &= \int \frac{d^3p}{(2\pi)^3}(-e^2)\frac{1}{(\mathbf{p}-\mathbf{p}_0)^2+\lambda^2} \\
&\quad \Big(\frac{-m}{p^2-p_0^2-i\epsilon}\Big)\Big(\frac{-4\pi\alpha(p^2+p_0^2)}{3m^4}\Big) \\
&= \Big(\frac{-2\alpha^2}{3m^3}\Big)\Big[p_0\pi^2+4\Lambda+2i\pi p_0\ln\Big(\frac{2p_0}{\lambda}\Big)\Big] \qquad (5.2.7)
\end{aligned}
$$

We should mention an important fact: in all NRQED calculations, we are allowed to put the cutoff either on the momentum flowing through the fermion line, or on the Coulomb line, or on the contact interaction. As it is shown in Ref. [7], whatever routing we choose for one diagram, we can

not change it for the other diagrams in the middle of the calculation. That means we have to calculate all the scattering diagrams, as well as bound state diagrams, with one type of routing. In this chapter we always put the cutoff on the fermion line. The last two diagrams contain the Relativistic Kinetic and the Double Annihilation interactions:

$$\begin{aligned} Fig.(5.4(c)) &= \int \frac{d^3p}{(2\pi)^3}(-e^2)\frac{1}{(\mathbf{p}-\mathbf{p}_0)^2+\lambda^2}\Big(\frac{-m}{p^2-p_0^2-i\epsilon}\Big)^2 \times \\ &\qquad \Big(-\frac{p^4-p_0^4}{4m^3}\Big)\Big(\frac{2\pi\alpha}{m^2}\Big) \\ &= \Big(\frac{\alpha^2}{4m^3}\Big)\Big[4\Lambda + p_0\pi^2 + 2i\pi p_0 \ln\Big(\frac{2p_0}{\lambda}\Big)\Big] \qquad (5.2.8) \\ Fig.(5.4(g)) &= \int \frac{d^3p}{(2\pi)^3}(\frac{2\pi\alpha}{m^2})^2\Big(\frac{-m}{p^2-p_0^2-i\epsilon}\Big) \\ &= \frac{-\alpha^2}{m^3}\Big(2\Lambda + ip_0\pi\Big) \qquad (5.2.9) \end{aligned}$$

The QED Part

The QED diagrams for one- and two-loop vacuum polarization and vertex correction have been calculated in Refs. [32] [33][31]. In Refs. [37] [36] these calculation have been implemented into the threshold regime. The expansion of one-loop vacuum polarization above the threshold is :

$$\Pi_1 = \frac{-8\alpha}{9\pi} - \frac{ip_0\alpha}{2m}. \qquad (5.2.10)$$

The spin average ($S = 1$) of the one-loop vertex correction above threshold, expanded in terms of the center of mass velocity is:

$$G_1 = \Big(\frac{\alpha}{\pi}\Big)\Big[\frac{\pi^2 m}{4p_0} - 2 + \frac{\pi^2 p_0}{3m} + \frac{i\pi m}{2p_0}\ln\Big(\frac{2p_0}{\lambda}\Big) + \frac{2ip_0\pi}{3m}\ln\Big(\frac{2p_0}{\lambda}\Big) - \frac{2i\pi p_0}{3m}\Big] \qquad (5.2.11)$$

To get the QED part, the left-hand side of Fig.(5.4), we should use Π_1 and G_1[36][37]:

$$QED = \Big[\Pi_1 + 2G_1\Big(1 + \frac{-p_0^2}{m^2} + \frac{-p_0^2}{6m^2}\Big)\Big]\Big(\frac{2\pi\alpha}{m^2}\Big), \qquad (5.2.12)$$

where we have seen before that $-p_0^2/m^2$ comes from the expansion of photon propagator and $-p_0^2/(6m^2)$ comes from the expansion of each vertex. Therefore for the QED part we obtain:

$$QED = \left[\Pi_1 \ + 2G_1\left(1+\frac{-7p_0^2}{6m^2}\right)\right]\left(\frac{2\pi\alpha}{m^2}\right). \tag{5.2.13}$$

Now if we put everything back into the relation shown in Fig.(5.4), we obtain

$$c_4^{(1)}(\text{1-}\gamma \text{ ann}) \ = \ \frac{44\alpha^2}{9m^2} - \frac{13\Lambda\alpha^2}{3m^3} \tag{5.2.14}$$

If we performed the $c_4^{(1)}(\text{1-}\gamma \text{ ann})$ matching for the vacuum and the vertex separately we would obtain the following result

$$c_4^{(1)}(\text{1-}\gamma \text{ ann}) \ = \ [c_4^{(1)}(\text{1-}\gamma \text{ ann})]_{PC} + [c_4^{(1)}(\text{1-}\gamma \text{ ann})]_{VC} \tag{5.2.15}$$

where

$$\begin{aligned} [c_4^{(1)}(\text{1-}\gamma \text{ ann})]_{PC} \ &= \ \frac{8\alpha^2}{9m^2} - \frac{\alpha^2\Lambda}{m^3} \\ [c_4^{(1)}(\text{1-}\gamma \text{ ann})]_{VC} \ &= \ \frac{4\alpha^2}{m^2} - \frac{10\alpha^2\Lambda}{3m^3}, \end{aligned} \tag{5.2.16}$$

where PC and VC stand for the propagator and vertex corrections.

5.3 Matching at NNLO for Four-Fermi Operators Coming from Propagator Corrections.

To compute $c_4^{(2)}(\text{1-}\gamma \text{ ann})$ we proceed in analogy to the calculation of $c_4^{(1)}(\text{1-}\gamma \text{ ann})$ in the previous section, and determine the contributions of the vertex correction and vacuum polarization to $c_4^{(2)}(\text{1-}\gamma \text{ ann})$ separately:

$$c_4^{(2)}(\text{1-}\gamma \text{ ann}) = [c_4^{(2)}(\text{1-}\gamma \text{ ann})]_{PC} + [c_4^{(2)}(\text{1-}\gamma \text{ ann})]_{VC}, \tag{5.3.17}$$

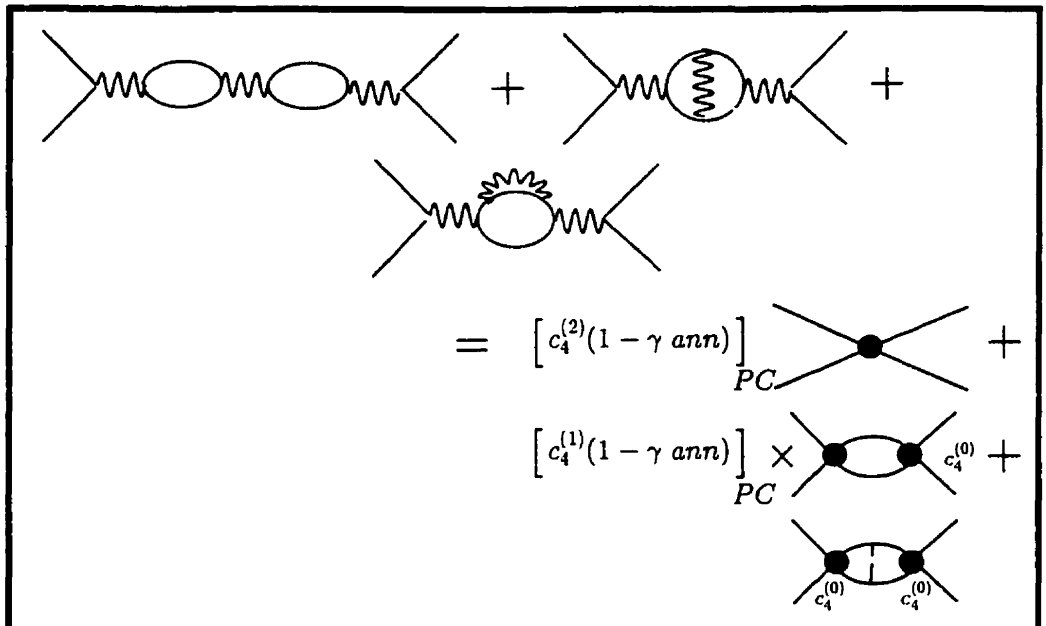

Figure 5.5: The matching which determines $[c_4^{(2)}(1\text{-}\gamma\ \text{ann})]_{PC}$.

We start with the calculation of $[c_4^{(2)}(1\text{-}\gamma\ \text{ann})]_{PC}$ from the relation displayed in Fig(5.5). As may be seen from this figure, the QED part (left-hand side of Fig.(5.5)) requires calculation of the vacuum polarization function up to two loops. We then need to expand these functions for small velocities. The corresponding expression suitable for our task can be found in Ref.[37]. The result is as follows:

$$\Pi_2 = \left[\frac{-\alpha^2}{4\pi^2}\left(3-\frac{21}{2}\zeta_3\right)-\frac{11\alpha^2}{32} + \frac{3\alpha^2}{4}\ln(2)+\frac{\alpha^2}{2}\ln\left(\frac{-ip_0}{m}\right)\right] \tag{5.3.18}$$

The final form of the QED part (left-hand side of Fig.(5.5)) is thus:

$$QED = \left(\frac{2\pi\alpha}{m^2}\right)\left(\Pi_1^2+\Pi_2\right) \tag{5.3.19}$$

To compute the NRQED part (the right hand-side of Fig.(5.5)) we start with the next NRQED diagram shown in Fig.(5.6):

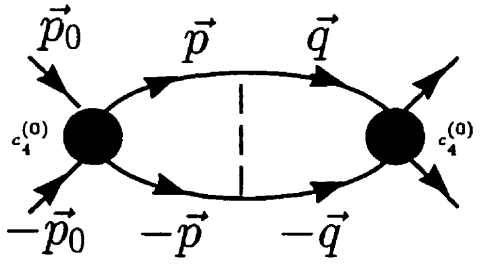

Figure 5.6: Double annihilation diagram with one Coulomb line inside.

$$
\begin{aligned}
Fig.(5.6) &= \int \frac{d^3p d^3q}{(2\pi)^6}\Big(\frac{1}{\frac{p_0^2}{m}-\frac{p^2}{m}+i\epsilon}\Big)(e)(-e)\Big(\frac{1}{\frac{p_0^2}{m}-\frac{q^2}{m}+i\epsilon}\Big) \\
&\quad (\frac{2\pi\alpha}{m^2})^2\frac{1}{((\mathbf{p}-\mathbf{q})^2+\lambda^2)} \\
&= \frac{-\alpha^3}{m^2\pi}\int dpdq\frac{pq}{(q^2-p_0^2-i\epsilon)(p^2-p_0^2-i\epsilon)}\ln\Big(\frac{(p+q)^2+\lambda^2}{(p-q)^2+\lambda^2}\Big) \\
&= \frac{-\alpha^3\pi}{m^2}\Big[\ln\Big(\frac{\Lambda}{2p_0}\Big)+\frac{i\pi}{2}\Big] \qquad (5.3.20)
\end{aligned}
$$

Now, we put all terms into the equation shown in Fig.(5.5), and then solve for $[c_4^{(2)}(\text{1-}\gamma\text{ ann})]_{PC}$:

$$
[c_4^{(2)}(\text{1-}\gamma\text{ ann})]_{PC} = \Big(\frac{-\alpha^3}{2m^2}\Big)\Big[\frac{128}{81\pi}-\frac{1}{2\pi}\Big(3-\frac{21}{2}\zeta_3\Big)-\frac{11\pi}{16}+\frac{\pi}{2}\ln(2)+\pi\ln(\frac{\Lambda}{m})\Big], \qquad (5.3.21)
$$

where we have ignored the terms proportional to $\frac{1}{m^4}$ and the terms with higher inverse powers of the electron mass because they would contribute to the HFS at higher order (more than α^6).

5.3.1 Hyperfine Splitting in Positronium to Order α^6 Coming from Propagator Correction.

Before we start the bound state calculation, we would like to recall an essential element of NRQED. As we have shown by using the counting rules, adding a Coulomb line does not change the order of a diagram, which in-

dicates the nonperturbative nature of the Coulomb interaction in a bound state. Therefore, there are an infinite number of diagrams, each with a different number of Coulomb lines that should be added up. These Coulomb lines can occur in two places, in external lines or in intermediate states. Fortunately, in external lines, Coulomb lines are already considered in the Schrödinger wave function of the external particles. Furthermore, we are lucky because even for the intermediate states, the sum of Coulomb ladder diagrams (full propagator) has been calculated before. Therefore, an analytical expression exists both in coordinate space [24] and in momentum space [25]. Because in this thesis we work exclusively in momentum space, only the expressions of [25] are used. In summary, the full propagator in momentum space, due to Schwinger [25], consists of three pieces: a piece with no Coulomb terms, one with one Coulomb term, and another with two and more Coulomb lines. The term with no Coulomb lines is the usual electron-positron propagator used so far, whereas the one Coulomb term has been used, for example, in the calculation of the diagram depicted in Fig.(5.6). The term with two or more Coulomb lines, called the $\mathbf{R}(\mathbf{p},\mathbf{q})$ term, is

$$\begin{aligned}\mathbf{R}(\mathbf{p},\mathbf{q}) &= \frac{-64\pi\gamma^4}{\alpha(\mathbf{p}^2+\gamma^2)^2(\mathbf{q}^2+\gamma^2)^2}\Big(\frac{5}{2}-\frac{4\gamma^2}{\mathbf{p}^2+\gamma^2}-\frac{4\gamma^2}{\mathbf{q}^2+\gamma^2}+\frac{1}{2}\ln(A)\\ &\quad+\frac{2A-1}{(4A-1)^{1/2}}tan^{-1}(4A-1)^{1/2}\Big), \qquad (5.3.22)\end{aligned}$$

where A is defined to be

$$A=\frac{(\mathbf{p}^2+\gamma^2)(\mathbf{q}^2+\gamma^2)}{4\gamma^2(\mathbf{q}-\mathbf{p})^2}. \qquad (5.3.23)$$

When we use Schwinger's expression to calculate a diagram consisting of an intermediate state, the diagram can only diverge for the no Coulomb and one Coulomb case. This UV divergence will then be canceled with four-Fermi interactions coming from the matching of NRQED with QED. On the other

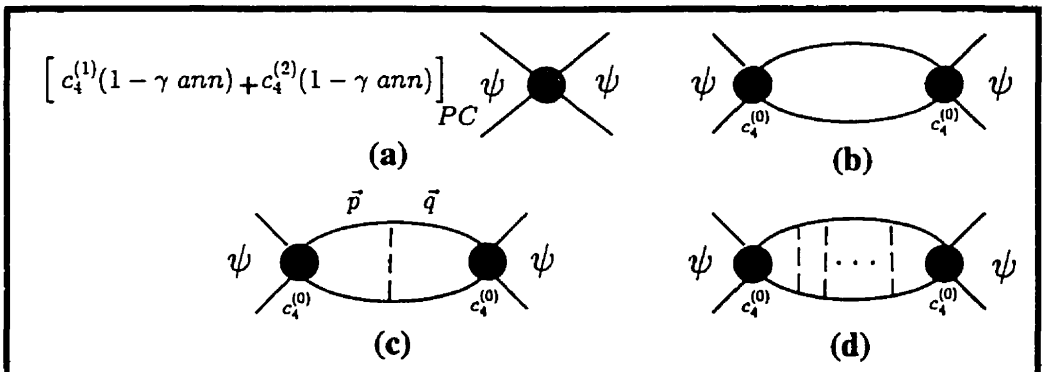

Figure 5.7: The whole double annihilation bound state diagrams.

hand, all the contributions coming from the **R** term are finite (there are no UV divergences).

We can now concentrate on all bound state diagrams which are shown in Fig.(5.7). (We have to include $c_4^{(1)}$(1-γ ann) in this diagram because it has been changed by the rematching procedure shown in Fig.(5.4))

$$\begin{aligned} Fig.(5.7(a)) &= -\Big[c_4^{(1)}(1\text{-}\gamma\ \text{ann}) + c_4^{(2)}(1\text{-}\gamma\ \text{ann})\Big]_{PC}\Big(S(S+1)\Big)|\psi(0)|^2 \\ &= 2\Big(\frac{m^3\alpha^3}{8\pi}\Big)\Big[\frac{\alpha^2\Lambda}{m^3} - \frac{8\alpha^2}{9m^2}\Big] + \\ &\quad \Big(\frac{m^3\alpha^3}{8\pi}\Big)\Big(\frac{\alpha^3}{m^2}\Big)\Big[\frac{128}{81\pi} - \frac{1}{2\pi}\Big(3 - \frac{21}{2}\zeta_3\Big) \\ &\qquad -\frac{11\pi}{16} + \frac{\pi}{2}\ln(2) + \pi\ln\big(\frac{\Lambda}{m}\big)\Big] \end{aligned} \tag{5.3.24}$$

The linear divergent term in the above equation coming from the rematching of $c_4^{(1)}$(1-γ ann) cancels the linear divergence appearing in the bound state, Fig(5.7(b)).

$$\begin{aligned} Fig.(5.7(b)) &= \Big(\frac{\gamma^3}{\pi}\Big)\int\frac{d^3p}{(2\pi)^3}\Big(\frac{-m}{p^2+\gamma^2}\Big) \\ &= \frac{-m\alpha^5}{4\pi}\frac{\Lambda}{m} + \frac{m\alpha^6}{16} \end{aligned} \tag{5.3.25}$$

$$Fig.(5.7(c)) = \Big(\frac{\gamma^3}{\pi}\Big)\int\frac{d^3pd^3q}{(2\pi)^6}\Big(\frac{-m}{p^2+\gamma^2}\Big)\Big(\frac{-m}{q^2+\gamma^2}\Big)(e)(-e)\Big(\frac{2\pi\alpha}{m^2}\Big)^2$$

$$= -\frac{m\alpha^6}{32\pi^4}\int d^3p d^3q \frac{1}{(p^2+\gamma^2)(q^2+\gamma^2)(\mathbf{p}-\mathbf{q})^2}$$

$$= -\frac{m\alpha^6}{8}\ln\left(\frac{\Lambda}{\gamma}\right) + \frac{m\alpha^6}{8}\ln(2) \qquad (5.3.26)$$

$$Fig.(5.7(d)) = \left(\frac{\gamma^3}{\pi}\right)\left(\frac{2\pi\alpha}{m^2}\right)^2 \int \frac{d^3p d^3q}{(2\pi)^6}\mathbf{R}(\mathbf{p},\mathbf{q}) = \frac{-3}{16}m\alpha^6 \qquad (5.3.27)$$

Now if we add Eqs.(5.3.24), (5.3.27), (5.3.25) and (5.3.26) together, we arrive at the HFS of positronium coming from the two-loop correction of the photon propagator up to $\mathcal{O}(\alpha^6)$.

$$\Big[\Delta E_{hfs}(1\text{-}\gamma \text{ ann})\Big]_{PC} = -\frac{2}{9}m\alpha^5 + \frac{m\alpha^6}{4}\Big[-\frac{27}{32} + \frac{1}{4\pi^2}\Big(\frac{13}{81} + \frac{21}{2}\zeta_3\Big) + \frac{1}{4}\ln(2) + \frac{1}{2}\ln(\alpha)\Big] \qquad (5.3.28)$$

where the first term in the above equation is a part of α^5 contribution to HFS of positronium that we have calculated in the previous chapter. It is worth nothing that the terms involving Λ and $\ln(\Lambda)$ have been canceled, showing that in NRQED the physics is independent of the choice of momentum cutoff, Λ.

5.4 Matching at NNLO for Four-Fermi Operators Coming from Vertex Corrections.

To obtain the complete form of $c_4^{(2)}(1\text{-}\gamma \text{ ann})$, we start with the basic relation shown in Fig.(5.2), whose full form is depicted in Fig.(5.8).

NRQED Calculation

We begin by considering the NRQED part of Fig.(5.2). We note momentum is routed through the fermion line, which is always kept as shown in Fig.(5.8(g)), and secondly, the momentum of any external line is taken to be $\mathbf{p}_0$. For one loop and two loop NRQED diagrams, the momenta are always

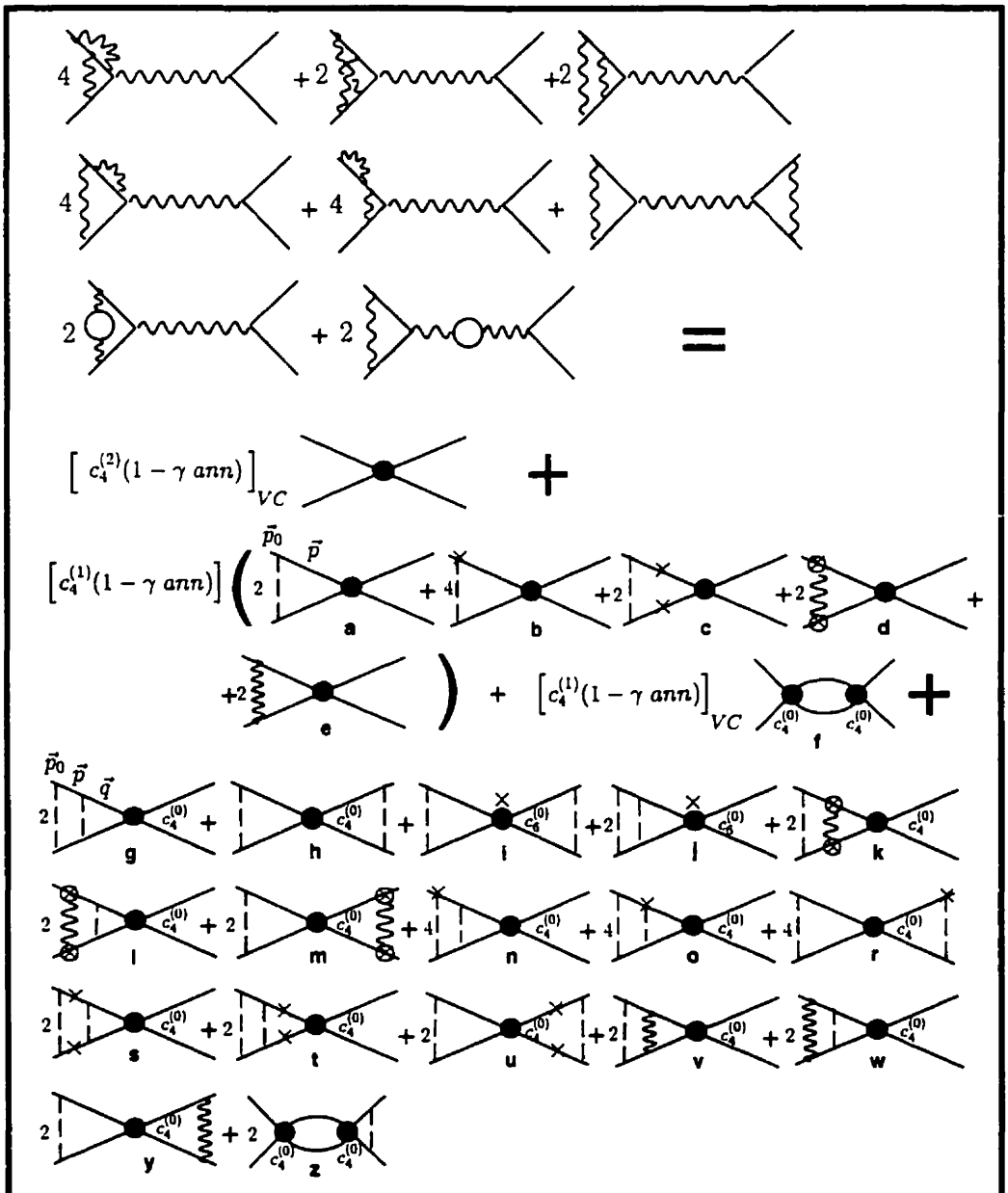

Figure 5.8: The matching which determines $[c_4^{(2)}(1\text{-}\gamma\ \text{ann})]_{VC}$

shown as in Fig.(5.8(a)) and Fig.(5.8(g)) respectively. It is easy to show that Figs.(5.8, b, c, d, e, f) will not contribute to the order α^6 in bound state calculations. Let us look at one of these figures, Fig.(5.8(b)): If we count all the factors of α and m in this diagram we find that this contribution is proportional to $(\frac{\alpha^2}{m^2})(\frac{\alpha}{m})$. Therefore in the bound state this diagram should be multiplied by $\gamma^4 = \frac{m^4\alpha^4}{16}$ to have the dimensions of energy. That means this figure will contribute to $m\alpha^7$, which is irrelevant to our calculation. Since the only relevant one-loop NRQED diagram, Fig.(5.8(a)), has been calculated before, we only need to concentrate on the two-loop diagrams.

Coulomb Interaction

Let us begin with Fig.(5.8(h)), which is an easy diagram to calculate since we need only to square Fig.(5.8(a)) and then divide it by factor $2\pi\alpha/m^2$:

$$Fig.(5.8(h)) = \left(\frac{\alpha^3}{2\pi p_0^2}\right)\left[\frac{\pi^2}{2} + i\pi \ln\left(\frac{2p_0}{\lambda}\right)\right]^2 \qquad (5.4.29)$$

The next diagram is shown in Fig.(5.8(g))

$$\begin{aligned} Fig.(5.8(g)) &= \left(\frac{2\pi\alpha}{m^2}\right)\int \frac{d^3p d^3q}{(2\pi)^6}(-e^2)\frac{1}{(\mathbf{p}_0-\mathbf{p})^2+\lambda^2}\left(\frac{-m}{p^2-p_0^2-i\epsilon}\right) \\ &\qquad (-e^2)\frac{1}{(\mathbf{p}-\mathbf{q})^2+\lambda^2}\left(\frac{-m}{q^2-p_0^2-i\epsilon}\right) \\ &= \left(\frac{\alpha^3}{2\pi p_0}\right)\int dpdq \frac{q}{(p^2-p_0^2-i\epsilon)(q^2-p_0^2-i\epsilon)} \\ &\quad \ln\left(\frac{(p+p_0)^2+\lambda^2}{(p-p_0)^2+\lambda^2}\right)\ln\left(\frac{(q+p)^2+\lambda^2}{(q-p)^2+\lambda^2}\right) \\ &= \left(\frac{\alpha^3}{2\pi p_0^2}\right)\left[\frac{\pi^4}{24} - \frac{\pi^2}{2}\ln\left(\frac{2p_0}{\lambda}\right)^2 + \frac{i\pi^3}{2}\ln\left(\frac{2p_0}{\lambda}\right)\right]. \qquad (5.4.30) \end{aligned}$$

Transverse Interaction

There are three two-loop diagrams in Fig.(5.8) which have a transverse photon: (v), (w) and (y). Let us start with (w):

$$\begin{aligned} Fig.(5.8(w)) &= \int \frac{d^3p d^3q}{(2\pi)^3}\Big(\frac{e(\mathbf{p}_0+\mathbf{p})_i}{2m}\Big)\Big(\frac{e(\mathbf{p}_0+\mathbf{p})_j}{2m}\Big)\Big(\frac{-m}{p^2-p_0^2-i\epsilon}\Big) \\ &\quad \frac{-1}{(\mathbf{p}_0-\mathbf{p})^2+\lambda^2}\Big(\delta_{ij}-\frac{(\mathbf{p}_0-\mathbf{p})_i(\mathbf{p}_0-\mathbf{p})_j}{(\mathbf{p}_0-\mathbf{p})^2+\lambda^2}\Big) \\ &\quad (-e^2)\frac{1}{(\mathbf{p}-\mathbf{q})^2+\lambda^2}\Big(\frac{-m}{q^2-p_0^2-i\epsilon}\Big) \\ &= \frac{\pi\alpha^3}{48m^2}\Big[6i\pi+48-12\ln\Big(\frac{2p_0}{\lambda}\Big)^2+12i\pi\ln\Big(\frac{2p_0}{\lambda}\Big) \\ &\quad +\pi^2+12p_0\ln\Big(\frac{\lambda}{p_0}\Big)\Big] \end{aligned} \tag{5.4.31}$$

$$\begin{aligned} Fig.(5.8(v)) &= \int \frac{d^3p d^3q}{(2\pi)^3}(-e^2)\frac{1}{(\mathbf{p}_0-\mathbf{p})^2+\lambda^2}\Big(\frac{-m}{p^2-p_0^2-i\epsilon}\Big) \\ &\quad \Big(\frac{-m}{q^2-p_0^2-i\epsilon}\Big)\Big(\frac{e(\mathbf{p}+\mathbf{q})_i}{2m}\Big)\Big(\frac{e(\mathbf{p}+\mathbf{q})_j}{2m}\Big) \\ &\quad \frac{-1}{(\mathbf{p}-\mathbf{q})^2+\lambda^2}\Big(\delta_{ij}-\frac{(\mathbf{p}-\mathbf{q})_i(\mathbf{p}-\mathbf{q})_j}{(\mathbf{p}-\mathbf{q})^2+\lambda^2}\Big) \\ &= \frac{\pi\alpha^3}{48m^2}\Big[-12\ln\Big(\frac{2p_0}{\lambda}\Big)^2-48\ln\Big(\frac{p_0}{\Lambda}\Big)-36\ln(2) \\ &\quad +12i\pi\ln\Big(\frac{2p_0}{\lambda}\Big)+\pi^2+24\pi\ln\Big(\frac{p_0}{\lambda}\Big)+12i\pi+72\Big] \end{aligned} \tag{5.4.32}$$

To calculate Fig.(5.8(y)), we can multiply Eq.(5.2.3) by Eq.(5.2.4) and then divide it by the factor $2\pi\alpha/m^2$.

$$Fig.(5.8(y)) = \Big(\frac{\alpha^3}{2m^2}\Big)\Big[\frac{\pi^2}{2}+i\pi\ln\Big(\frac{2p_0}{\lambda}\Big)\Big]\times\Big[\frac{-i}{2}+\frac{\pi}{2}+i\ln\Big(\frac{2p_0}{\lambda}\Big)\Big] \tag{5.4.33}$$

Spin-Spin Interaction

The two loops diagrams are

$$Fig.(5.8(k)) = \int \frac{d^3p d^3q}{(2\pi)^6}(-e^2)\frac{1}{(\mathbf{p}-\mathbf{p}_0)^2+\lambda^2}\Big(\frac{-m}{p^2-p_0^2-i\epsilon}\Big)$$

$$\left(\frac{-ie(\mathbf{q}-\mathbf{p})\times\boldsymbol{\sigma}}{2m}\right)_i\left(\frac{-ie(\mathbf{q}-\mathbf{p})\times\boldsymbol{\sigma}}{2m}\right)_j$$
$$\left(\frac{-m}{q^2-p_0^2-i\epsilon}\right)\left(\frac{2\alpha\pi}{m^2}\right)$$
$$= \left(\frac{-\alpha^3}{12m^2p_0}\right)\left[\pi+2i\ln\left(\frac{2p_0}{\lambda}\right)\right]\left(2\Lambda+i\pi p_0\right) \quad (5.4.34)$$

With a similar calculation we can show that

$$Fig.(5.8(l)) = \left(\frac{-\alpha^3}{6m^2}\right)\left[2\ln\left(\frac{\Lambda}{\lambda}\right)-2\ln\left(\frac{2p_0}{\lambda}\right)+i\pi\right] \quad (5.4.35)$$

$$Fig.(5.8(m)) = \left(\frac{-\alpha^3}{12m^2p_0}\right)\left[\pi+2i\ln\left(\frac{2p_0}{\lambda}\right)\right]\left(2\Lambda+i\pi p_0\right) \quad (5.4.36)$$

Darwin Interaction

For the Darwin contribution, as showed in the previous section, we need to multiply the corresponding diagrams with the Spin-Spin interaction by a factor 3/4:

$$Fig.(5.8(o)) = \left(\frac{-\alpha^3}{16m^2p_0}\right)\left[\pi+2i\ln\left(\frac{2p_0}{\lambda}\right)\right]\left(2\Lambda+i\pi p_0\right) \quad (5.4.37)$$

$$Fig.(5.8(n)) = \left(\frac{-\alpha^3}{16m^2p_0}\right)\left[2\ln\left(\frac{\Lambda}{\lambda}\right)-2\ln\left(\frac{2p_0}{\lambda}\right)+i\pi\right] \quad (5.4.38)$$

$$Fig.(5.8(r)) = \left(\frac{\alpha^3}{32m^2p_0}\right)\left[\pi+2i\ln\left(\frac{2p_0}{\lambda}\right)\right]\left(2\Lambda+i\pi p_0\right) \quad (5.4.39)$$

Derivative Interaction

There are two two-loop diagrams with the derivative interaction, Fig.(5.8j, i):

$$Fig.(5.8(j)) = \int\frac{d^3pd^3q}{(2\pi)^6}(-e^2)\frac{1}{(\mathbf{p}-\mathbf{p}_0)^2+\lambda^2}\left(\frac{-m}{p^2-p_0^2-i\epsilon}\right)$$
$$(-e^2)\frac{1}{(\mathbf{q}-\mathbf{p})^2+\lambda^2}\left(\frac{-m}{q^2-p_0^2-i\epsilon}\right)\left(\frac{-4\pi\alpha(q^2+p_0^2)}{3m^4}\right)$$
$$= \left(\frac{-\alpha^3}{3\pi m^2p_0}\right)\int\frac{dp\,dq\,q(q^2+p_0^2)}{(q^2-p_0^2-i\epsilon)(p^2-p_0^2-i\epsilon)}\ln\left(\frac{(p+p_0)^2+\lambda^2}{(p-p_0)^2+\lambda^2}\right)$$
$$\ln\left(\frac{(p+q)^2+\lambda^2}{(p-q)^2+\lambda^2}\right)$$

$$= \left(\frac{-\alpha^3}{36m^2p_0}\right)\left[p_0\pi^3 - 12p_0\pi\ln\left(\frac{2p_0}{\lambda}\right)^2 + 12ip_0\pi^2\ln\left(\frac{2p_0}{\lambda}\right)\right.$$
$$\left. +24\Lambda\pi + 48i\Lambda\ln\left(\frac{2p_0}{\lambda}\right) - 24p_0\pi\right] \qquad (5.4.40)$$

$$Fig.(5.8(i)) = \int\frac{d^3pd^3q}{(2\pi)^6}(-e^2)\frac{1}{(\mathbf{p}-\mathbf{p}_0)^2+\lambda^2}\left(\frac{-m}{p^2-p_0^2-i\epsilon}\right)$$
$$(-e^2)\frac{1}{(\mathbf{q}-\mathbf{p}_0)^2+\lambda^2}\left(\frac{-m}{q^2-p_0^2-i\epsilon}\right)\left(\frac{-4\pi\alpha(q^2+p^2)}{3m^4}\right)$$
$$= \left(\frac{-\alpha^3}{6m^2p_0}\right)\left[\pi + 2i\ln\left(\frac{2p_0}{\lambda}\right)\right]\times$$
$$\left[p_0\pi^2 + 8\Lambda + +2i\pi p_0\ln\left(\frac{2p_0}{\lambda}\right)\right] \qquad (5.4.41)$$

Relativistic Kinetic Correction

The next class of NRQED diagrams contain a Relativistic vertex.

$$Fig.(5.8(t)) = \left(-\frac{\alpha^3}{96m^2p_0}\right)\left[-p_0\pi^3 + 12p_0\ln\left(\frac{2p_0}{\lambda}\right)^2\right.$$
$$\left. -12ip_0\pi^2\ln\left(\frac{2p_0}{\lambda}\right) - 24\Lambda\pi - 48i\Lambda\ln\left(\frac{2p_0}{\lambda}\right) + 24p_0\pi\right]$$
$$Fig.(5.8(s)) = \left(\frac{\alpha^3}{96m^2p_0}\right)\left[48p_0 - 48p_o\ln\left(\frac{2p_0}{\lambda}\right)\right.$$
$$\left. +24i\pi p_0 + \pi^2p_0 - 12p_0\ln\left(\frac{2p_0}{\lambda}\right)^2 + 12ip_0\ln\left(\frac{2p_0}{\lambda}\right)\right]$$
$$(5.4.42)$$

Similar to Fig.(5.4.33), Fig.(5.8(u)) is just the product of two one-loop diagrams:

$$Fig.(5.8(u)) = \left(\frac{\alpha^3}{16m^2p_0}\right)\left[\pi + 2i\ln\left(\frac{2p_0}{\lambda}\right)\right]\times$$
$$\left[p_0\pi^2 + 4\Lambda + +2i\pi p_0\ln\left(\frac{2p_0}{\lambda}\right)\right] \qquad (5.4.43)$$

Double Annihilation

The last diagram in the NRQED part is shown in Fig.(5.9), which reads:

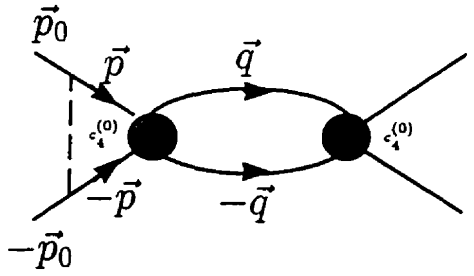

Figure 5.9: Double annihilation diagram with one Coulomb line outside.

$$\begin{aligned} Fig.(5.8(z)) &= \int \frac{d^3p d^3q}{(2\pi)^6}(e)\left(\frac{-m}{p^2-p_0^2-i\epsilon}\right)(-e)\left(\frac{-m}{q^2-p_0^2-i\epsilon}\right)\left(\frac{2\pi\alpha}{m^2}\right)^2 \\ &= \left(\frac{-4\pi\alpha^3}{m^2}\right)\left[\frac{\Lambda}{4p_0\pi}+\frac{i}{8}\right]\left(\frac{\pi}{2}+i\ln\left(\frac{2p_0}{\lambda}\right)\right) \end{aligned} \tag{5.4.44}$$

Now if we add all the NRQED diagrams in Fig.(5.8) which contribute to the $\mathcal{O}(\alpha^6)$ HFS, *i.e.*, (a), (g), (h), (i), (j), (k), (l), (m), (n), (o), (r), (s), (t), (u), (v), (w), (x), (y) and (z), we obtain:

$$\begin{aligned} NRQED &= \frac{\alpha^3\pi^3}{6p_0^2}+\frac{i\alpha^3\pi^2}{p_0^2}\ln\left(\frac{2p_0}{\lambda}\right)-\frac{\alpha^3\pi}{p_0^2}\ln\left(\frac{2p_0}{\lambda}\right)^2-\frac{5\alpha^3\pi}{3m^2}\ln\left(\frac{2p_0}{\lambda}\right)^2 \\ &+ \frac{5}{18}\frac{\alpha^3\pi^3}{m^2}+\frac{i5\alpha^3\pi^2}{3m^2}\ln\left(\frac{2p_0}{\lambda}\right)+\frac{29}{6}\frac{\alpha^3\pi}{m^2}-\frac{7i\pi^2\alpha^3}{6m^2} \\ &+ \frac{7\alpha^3\pi}{3m^2}\ln\left(\frac{2p_0}{\lambda}\right)+\frac{4\alpha^3\pi^3}{3m^2}\ln\left(\frac{\Lambda}{\lambda}\right)-\frac{44}{9}\frac{\alpha^3\pi}{mp_0}-\frac{88i\alpha^3}{mp_0}\ln\left(\frac{2p_0}{\lambda}\right) \end{aligned} \tag{5.4.45}$$

QED Calculation

To calculate the left-hand side of Fig.(5.8), we use the spin average ($S=1$) of the one- and two-loop vertex correction above the threshold expanded in terms of c.m. velocity. This calculation has been carried out in Ref.[37] with the following result:

$$G_2 = \left(\frac{\alpha^3}{288p_0^2\pi m^2}\right)\left[6m^2\pi^4-72m^2\pi^2\ln\left(\frac{2p_0}{\lambda}\right)^2-288m\pi^2p_0\right.$$

$$-204\pi^2 p_0^2 \ln\left(\frac{2p_0}{\lambda}\right)^2 + 192 p_0^2\pi^2 \ln\left(\frac{2p_0}{\lambda}\right) - 192\pi^2 p_0^2 \ln\left(\frac{p_0}{m}\right)$$
$$+3064 p_0^2 - 688 p_0^2\pi^2 + 17\pi^4 p_0^2 + 384 p_0^2\pi^2 \ln(2) - 288\zeta_3 p_0^2$$
$$+72 i\pi^3 m^2 \ln\left(\frac{2p_0}{\lambda}\right) - 576 i\pi m p_0 \ln\left(\frac{2p_0}{\lambda}\right) + 204 i\pi^3 p_0^2 \ln\left(\frac{2p_0}{\lambda}\right)\Big] \tag{5.4.46}$$

Using G_1(Eq.(5.2.11) and G_2, for the QED part we obtain

$$\begin{aligned} QED &= \left(\frac{2\pi\alpha}{m^2}\right)\left[G_1^2\left(1+\frac{-p_0^2}{m^2}\right) + 2G_2\left(1+\frac{-p_0^2}{m^2}+\frac{-p_0^2}{6m^2}\right)\right] \\ &= \left(\frac{2\pi\alpha}{m^2}\right)\left[G_1^2 + G_1^2\left(\frac{-p_0^2}{m^2}\right) + 2G_2 + G_2\left(\frac{-7p_0^2}{3m^2}\right)\right]. \end{aligned} \tag{5.4.47}$$

Solving the relation shown in Fig.(5.8) for $[c_4^{(2)}(1\text{-}\gamma \text{ ann})]_{VC}$, we obtain

$$[c_4^{(2)}(1\text{-}\gamma \text{ ann})]_{VC} = NRQED - QED, \tag{5.4.48}$$

where QED and $NRQED$ terms were given in Eqs.(5.4.47) and (5.4.45):

$$[c_4^{(2)}(1\text{-}\gamma \text{ ann})]_{VC} = \left(\frac{-\alpha^3\pi}{2m^2}\right)\left[\frac{1}{\pi^2}\left(\frac{655}{18}-2\zeta_3\right) - \frac{173}{18} + 4\ln(2) - \frac{4}{3}\ln\left(\frac{\Lambda}{m}\right)\right] \tag{5.4.49}$$

5.4.1 Hyperfine Splitting in Positronium to Order α^6 Coming From Vertex Correction.

With the help of counting rules, we find all the diagrams which contribute to α^6. They are shown in Fig.(5.10). We begin by calculating the diagram(a)

$$\begin{aligned} Fig.(5.10(a)) &= -[c_4^{(1)}(1\text{-}\gamma \text{ ann}) + c_4^{(2)}(1\text{-}\gamma \text{ ann})]_{VC}\Big(S(S+1)\Big)|\psi(0)|^2 \\ &= m\alpha^5\left[\frac{5\Lambda}{6\pi} - 1\right] + \\ &\quad m\alpha^6\left[\frac{1}{\pi^2}\left(\frac{655}{144}-\frac{\zeta_3}{4}\right) - \frac{173}{144} + \frac{1}{2}\ln(2) - \frac{1}{6}\ln\left(\frac{\Lambda}{m}\right)\right] \end{aligned} \tag{5.4.50}$$

As we see from Fig.(5.10), except for the Derivative interaction, we have three different types of NRQED bound states for each interaction. In our

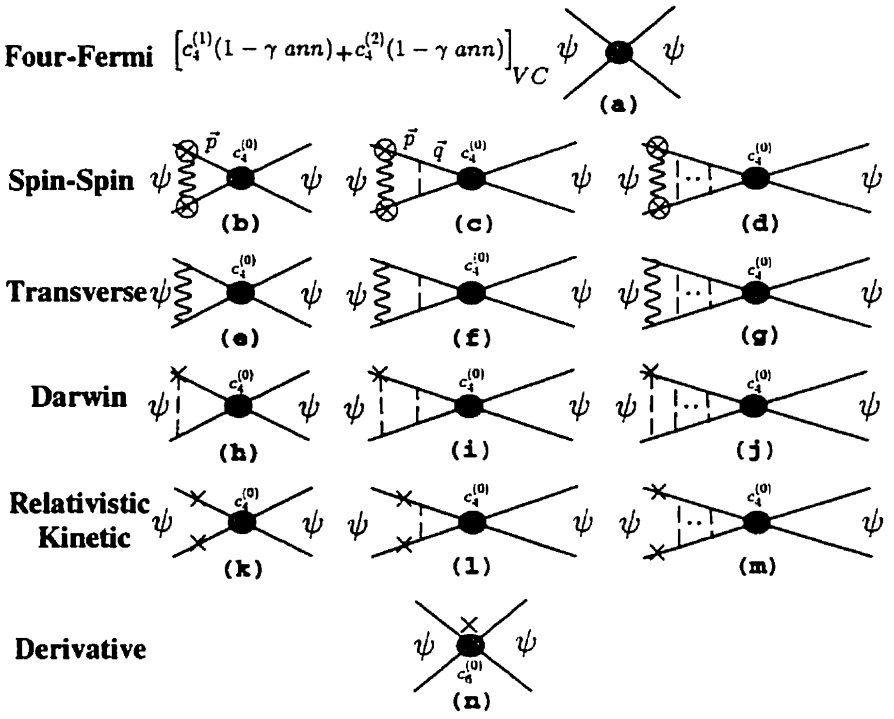

Figure 5.10: All the bound state diagrams which contribute to α^6 except the diagrams with the Double Annihilation interaction.

calculation we use the ground state wave function which has the following property:

$$\int \frac{d^3p}{(2\pi)^3}\Psi(\mathbf{p}) = \int \frac{d^3p}{(2\pi)^3}\frac{8\pi^{1/2}\gamma^{5/2}}{(\mathbf{p}^2+\gamma^2)^2} = \left(\frac{\gamma^3}{\pi}\right)^{1/2} . \tag{5.4.51}$$

We label all the bound state diagrams with momenta $\mathbf{p}$ and $\mathbf{q}$, as shown in Fig.(5.10b, c). Once again we should mention that we have to put the cutoff on the fermion line (fermion routing) in all the bound state calculations.

The next diagram has the Spin-Spin interaction:

$$Fig.(5.10(b)) = \left(\frac{\gamma^3}{\pi}\right)^{1/2}\int \frac{d^3pd^3q}{(2\pi)^6}\frac{8\pi^{1/2}\gamma^{5/2}}{(\mathbf{p}^2+\gamma^2)^2}\left(\frac{2\pi\alpha}{m^2}\right)\left(\frac{1}{-\frac{\gamma^2}{m}-\frac{q^2}{m}}\right)\left(\frac{-ie(\mathbf{q}-\mathbf{p})\times\boldsymbol{\sigma}_1}{2m}\right)_i\left(\frac{-ie(\mathbf{q}-\mathbf{p})\times\boldsymbol{\sigma}_2}{2m}\right)_j$$

$$\frac{-1}{(\mathbf{p}-\mathbf{q})^2+\lambda^2}\Big(\delta_{ij}-\frac{(\mathbf{p}-\mathbf{q})_i(\mathbf{p}-\mathbf{q})_j}{(\mathbf{p}-\mathbf{q})^2+\lambda^2}\Big)$$

$$= \Big(-\frac{m\alpha^6}{64\pi^4}\Big)\int\frac{2/3(\mathbf{q}-\mathbf{p})^2\boldsymbol{\sigma}_1\cdot\boldsymbol{\sigma}_2}{(\mathbf{q}-\mathbf{p})^2(p^2+\gamma^2)(q^2+\gamma^2)}$$

$$= \frac{-m\alpha^5}{12\pi}\frac{\Lambda}{m}+\frac{m\alpha^6}{48} \tag{5.4.52}$$

$$\begin{aligned} Fig.(5.10(c)) &= \Big(\frac{\gamma^3}{\pi}\Big)^{1/2}\int\frac{d^3pd^3qd^3k}{(2\pi)^9}\frac{8\pi^{1/2}\gamma^{5/2}}{(\mathbf{p}^2+\gamma^2)^2}\Big(\frac{2\pi\alpha}{m^2}\Big)\Big(\frac{-m}{-\gamma^2-q^2}\Big) \\ &\quad \Big(\frac{-ie(\mathbf{q}-\mathbf{p})\times\boldsymbol{\sigma}_1}{2m}\Big)_i\Big(\frac{-ie(\mathbf{q}-\mathbf{p})\times\boldsymbol{\sigma}_2}{2m}\Big)_j \\ &\quad \frac{-1}{(\mathbf{p}-\mathbf{q})^2}\Big(\delta_{ij}-\frac{(\mathbf{p}-\mathbf{q})_i(\mathbf{p}-\mathbf{q})_j}{(\mathbf{p}-\mathbf{q})^2}\Big) \\ &\quad \Big(\frac{-m}{-\gamma^2-q^2}\Big)(-e^2)\frac{-1}{(\mathbf{q}-\mathbf{k})^2} \\ &= \Big(\frac{-m^2\alpha^7}{96}\Big)\int\frac{d^3pd^3q}{(2\pi)^6}\frac{1\cdot}{(p^2+\gamma^2)^2(q^2+\gamma^2)}\frac{tan^{-1}(\frac{q}{\gamma})}{q} \\ &= \frac{-m\alpha^6}{24}\Big(\ln\Big(\frac{\Lambda}{\gamma}\Big)-\ln(2)\Big), \end{aligned} \tag{5.4.53}$$

Eq.(5.4.53) is 1/3 of contribution of the Double Annihilation bound state with one Coulomb line, Eq.(5.3.25). Therefore, we can multiply Eq.(5.3.26) by factor 1/3 to get the **R** term for spin-spin interaction.

$$Fig.(5.10(d)) = \frac{-m\alpha^6}{16}. \tag{5.4.54}$$

Since the diagram with a Darwin interaction and one with a spin-spin interaction differs by a factor 3/4 we can write down the result of the Darwin bound state diagrams easily:

$$\begin{aligned} Fig.(5.10(h)) &= \frac{-m\alpha^5}{16\pi}\frac{\Lambda}{m}+\frac{m\alpha^6}{64} \\ Fig.(5.10(i)) &= \frac{-m\alpha^6}{32}\Big(\ln\Big(\frac{\Lambda}{\gamma}\Big)-\ln(2)\Big) \\ Fig.(5.10(j)) &= \frac{-3m\alpha^6}{64}. \end{aligned} \tag{5.4.55}$$

The next set is the Transverse bound state diagrams

$$
\begin{aligned}
Fig.(5.10(e)) &= \left(\frac{\gamma^3}{\pi}\right)^{1/2}\int\frac{d^3pd^3q}{(2\pi)^6}\frac{8\pi^{1/2}\gamma^{5/2}}{(\mathbf{p}^2+\gamma^2)^2}\left(\frac{2\pi\alpha}{m^2}\right)\\
&\quad\left(\frac{e(\mathbf{q}+\mathbf{p})_i}{2m}\right)\left(\frac{e(\mathbf{q}+\mathbf{p})_j}{2m}\right)\left(\frac{-m}{q^2+\gamma^2}\right)\\
&\quad\frac{-1}{(\mathbf{q}-\mathbf{p})^2+\lambda^2}\left(\delta_{ij}-\frac{(\mathbf{q}-\mathbf{p})_i(\mathbf{q}-\mathbf{p})_j}{(\mathbf{q}-\mathbf{p})^2}\right)\\
&= \left(\frac{m\alpha^6}{64\pi^4}\right)\int\frac{d^3pd^3q\ [(\mathbf{p}+\mathbf{q})^2-\frac{(p^2-q^2)^2}{(\mathbf{q}-\mathbf{p})^2}]}{(\mathbf{q}-\mathbf{p})^2(p^2+\gamma^2)(q^2+\gamma^2)}\\
&= m\alpha^6\left[\frac{1}{4}\ln\left(\frac{\Lambda}{\gamma}\right)-\frac{1}{4}\ln(2)-\frac{1}{8}\right]\\
Fig.(5.10(f)) &= \left(\frac{\gamma^3}{\pi}\right)^{1/2}\int\frac{d^3pd^3qd^3k}{(2\pi)^9}\frac{8\pi^{1/2}\gamma^{5/2}}{(\mathbf{p}^2+\gamma^2)^2}\left(\frac{2\pi\alpha}{m^2}\right)\\
&\quad\left(\frac{e(\mathbf{q}+\mathbf{p})_i}{2m}\right)\left(\frac{e(\mathbf{q}+\mathbf{p})_j}{2m}\right)\left(\frac{-m}{q^2+\gamma^2}\right)\\
&\quad\frac{-1}{(\mathbf{q}-\mathbf{p})^2+\lambda^2}\left(\delta_{ij}-\frac{(\mathbf{q}-\mathbf{p})_i(\mathbf{q}-\mathbf{p})_j}{(\mathbf{q}-\mathbf{p})^2}\right)\\
&\quad\left(\frac{-m}{k^2+\gamma^2}\right)\frac{1}{(\mathbf{q}-\mathbf{k})^2}(-e^2)\\
&= \frac{m\alpha^6}{16}\left(\frac{\pi^2}{3}-1\right) \qquad (5.4.56)
\end{aligned}
$$

For the $\mathbf{R}$ term of Transverse interaction, we have

$$
\begin{aligned}
Fig.(5.10(g)) &= \left(\frac{\gamma^3}{\pi}\right)^{1/2}\int\frac{d^3pd^3qd^3k}{(2\pi)^9}\frac{8\pi^{1/2}\gamma^{5/2}}{(\mathbf{p}^2+\gamma^2)^2}\left(\frac{2\pi\alpha}{m^2}\right)\\
&\quad\left(\frac{e(\mathbf{q}+\mathbf{p})_i}{2m}\right)\left(\frac{e(\mathbf{q}+\mathbf{p})_j}{2m}\right)\\
&\quad\frac{-1}{(\mathbf{q}-\mathbf{p})^2}\left(\delta_{ij}-\frac{(\mathbf{q}-\mathbf{p})_i(\mathbf{q}-\mathbf{p})_j}{(\mathbf{q}-\mathbf{p})^2}\right)\mathbf{R}(\mathbf{q},\mathbf{k})\\
&= \left(\frac{2\alpha}{\pi^{1/6}m^4}\right)\int\frac{d^3pd^3q\ [(\mathbf{p}+\mathbf{q})^2-\frac{(p^2-q^2)^2}{(\mathbf{q}-\mathbf{p})^2}]\mathbf{R}(\mathbf{q},\mathbf{k})}{(\mathbf{q}-\mathbf{p})^2(p^2+\gamma^2)(q^2+\gamma^2)}\\
&= \frac{m\alpha^6}{16}\left(\frac{9}{2}-\frac{\pi^2}{3}\right) \qquad (5.4.57)
\end{aligned}
$$

The next set is related to those diagrams which have Relativistic Kinetic vertex

$$
Fig.(5.10(k)) = \left(\frac{\gamma^3}{\pi}\right)^{1/2}\int\frac{d^3}{(2\pi)^3}\frac{8\pi^{1/2}\gamma^{5/2}}{(\mathbf{p}^2+\gamma^2)^2}\left(-\frac{p^2-\gamma^2}{4m^3}\right)
$$

$$\left(\frac{-m}{p^2+\gamma^2}\right)\left(\frac{2\pi\alpha}{m^2}\right)$$

$$= \frac{m\alpha^5}{8\pi}\frac{\Lambda}{m} - \frac{m\alpha^6}{16}$$

$$Fig.(5.10(l)) = \frac{m\alpha^6}{16}\left(\ln\left(\frac{\Lambda}{\gamma}\right) - \ln(2) - \frac{1}{2}\right)$$

$$Fig.(5.10(m)) = \frac{56}{256}m\alpha^6 \qquad (5.4.58)$$

The last diagram contains Derivative interaction:

$$Fig.(5.10(n)) = \int \frac{d^3p d^3q}{(2\pi)^6}\frac{8\pi^{1/2}\gamma^{5/2}}{(\mathbf{p}^2+\gamma^2)^2}\left(\frac{-4\pi\alpha(p^2+q^2)}{3m^4}\right)\frac{8\pi^{1/2}\gamma^{5/2}}{(\mathbf{q}^2+\gamma^2)^2}$$

$$= \frac{-2m\alpha^5}{3\pi}\frac{\Lambda}{m} + \frac{m\alpha^6}{4} \qquad (5.4.59)$$

Now, we add all the contributions coming from the diagrams of Fig.(5.10)[2]with the result:

$$\left[\Delta E_{hfs}(1\text{-}\gamma \text{ ann})\right]_{VC} = -m\alpha^5 + \frac{m\alpha^6}{4}\left[-\frac{235}{72} + \frac{1}{4\pi^2}\left(\frac{655}{36} - \zeta_3\right)\right.$$

$$\left. +2\ln(2) - \frac{2}{3}\ln(\alpha)\right] \qquad (5.4.60)$$

Final Result

We will now obtain the final result by adding the order α^6 terms of Eq.(5.3.28) to that of Eq.(5.4.60)

$$\Delta E_{hfs}(1\text{-}\gamma \text{ ann}, \alpha^6) = \frac{m_e\alpha^6}{4}\left[\frac{1}{\pi^2}\left(\frac{1477}{81} + \frac{13}{8}\zeta_3\right)\right.$$

$$\left. -\frac{1183}{288} + \frac{9}{4}\ln(2) + \frac{1}{6}\ln(\alpha^{-1})\right]. \qquad (5.4.61)$$

The $\ln(\alpha^{-1})$ term was already known and is included in the $\ln(\alpha^{-1})$ contribution presented in Eq.(1.0.1). We can now easily read off the unknown

[2]There is also a numerical factor related to the permutation of some diagrams shown in Fig.(5.10): For Figs.(b, c, d, e, f, g, k, e, h), this factor is 2. For the Figs.(h, i, j), it is 4. There is no permutation factor for Fig.(n).

	Order	Specification	analytical/ numerical	Contribution in Mhz	Refs.
1.	$m_e\alpha^4$		a	204 386.7(1)	[39]
2.	$m_e\alpha^5$		a	−1 005.5	[40]
3.	$m_e\alpha^6 \ln \alpha^{-1}$		a	19.1	[29]
4.	$m_e\alpha^6$	Nonannihilation(C/L)	n	−7.2(6)	[41]+[42]+[1]
5.		Nonannihilation(Pa)	n	−3.29(4)	[41]+[42]+[43]
6.		1-γ annihilation	a	−2.34	this work
7.		2-γ annihilation	a	−0.61	[44]
8.		3-γ annihilation	a	−0.97	[45]
9.	$m_e\alpha^7 \ln^2 \alpha^{-1}$		a	−0.92	[30, 7]
		Sum (Caswell/Lepage)		203 388.3(6)	
		Sum (Pachucki)		203 392.2(1)	
		Experiment		203 389.1(7)	[28]

Table 5.1: Summary of the theoretical calculations to the HFS. Only the references with the first correct calculations are given.

coefficient K_1(1-γ ann) from the Eq.(5.4.61).

$$K_1(\text{1-}\gamma \text{ ann}) = \frac{1}{4}\left[\frac{1}{\pi^2}\left(\frac{1477}{81}+\frac{13}{8}\zeta_3\right) - \frac{1183}{288}+\frac{9}{4}\ln(2)\right] \qquad (5.4.62)$$

Our analytical result completes the calculations to order $m_e\alpha^6$ and clearly shows how amazingly[3], NRQED simplifies the bound state calculation. In Table 5.1 we have summarized the status of the theoretical calculation to the HFS of the positronium ground state including our own result. To order $m_e\alpha^6$, the logarithmic in α and constant contributions are given separately. The constant terms are further subdivided into non-annihilation, and one, two and three photon annihilation contributions. The error in the order $m_e\alpha^4$ result (1.) comes from the uncertainties in the input pa-

[3]During completion of this thesis we were informed of the work by Adkins, Fell and Mitrikov[46] using Bethe-Salpeter formalism and numerical methods. Their result agrees with ours representing an independent cross check.

rameters α, $\hbar$ and m_e and the errors in items 4. and 5. are numerical. For all other contributions the errors are negligible. The uncertainties from the ignorance of the remaining $m_e\alpha^7 \ln \alpha^{-1}$ and $m_e\alpha^7$ contributions are not taken into account. As indicated, there are two contradictory calculations for some of non-annihilation contributions based on results from Caswell and Lepage (C/L) [1] and Pachucki (Pa) [43]. The result containing the Caswell-Lepage calculation leads to perfect agreement between theory and experiment $[\Delta E_{hfs}(\text{th}) - \Delta E_{hfs}(\text{ex}) = -0.8(1.0)$ Mhz], whereas the HFS prediction based on the result by Pachucki leads to a discrepancy of more than four standard deviations $[\Delta E_{hfs}(\text{th}) - \Delta E_{hfs}(\text{ex}) = 3.1(0.7)$ Mhz]. It remains the task of future examinations to finally resolve the theoretical situation.

Chapter 6

Discussion

Having come this far, we would like to claim that the two principal goals of this thesis, as outlined in chapter(1), have been accomplished.

The first part of the thesis from the beginning until chapter(5), except sections(4.2.1) and (4.1.2), essentially proves to the reader that we can obtain all the well-known results on the properties of bound states by using NRQED as an effective field theory. These results, obtained here from NRQED for the first time, are as follows:

- Order α^4 energy shift in positronium and the Hydrogen atom[14].
- Lamb shift in the Hydrogen atom[16].
- Order α^5 hyperfine splitting of ground state of positronium[17].

By using the NRQED power counting we can isolate the diagrams that contribute to each of the above cases and then perform a matching procedure which brings the effects of high energy modes to the NRQED coefficients. Hence, we would claim that NRQED is **simple** and **systematic**. The reader is strongly urged to compare the NRQED calculations presented here to the existing calculations done using conventional methods in standard text books such as [9] to confirm our claim.

In the remainder of the thesis, we have further demonstrated the strength and elegance of the NRQED formalism by presenting the following new results:

- α^6 HFS of positronium.

  In chapter(5), for the first time, we gave an analytical result to the order α^6 of the ground state hyperfine splitting coming from one photon annihilation.

$$\Delta E_{hfs}(1\text{-}\gamma \text{ ann}, \alpha^6) = \frac{m_e \alpha^6}{4}\left[\frac{1}{\pi^2}\left(\frac{1477}{81}+\frac{13}{8}\zeta_3\right) - \frac{1183}{288}+\frac{9}{4}\ln 2+\frac{1}{6}\ln \alpha^{-1}\right]. \tag{6.0.1}$$

  To obtain the above result, we had to perform a matching procedure at the 2-loop level in order to derive the spin1-annihilation vertex coming from one-photon annihilation. The relevant contribution was:

$$c_4^{(2)}(1\text{-}\gamma \text{ ann}) = \left(\frac{-\alpha^3\pi}{m^2}\right)\left[\frac{1}{\pi^2}\left(\frac{1477}{81}+\frac{13}{8}\zeta_3\right) - \frac{1483}{288}+\frac{9}{4}\ln(2)+\frac{1}{6}\ln\left(\frac{\Lambda}{m}\right)\right] \tag{6.0.2}$$

  Our calculation completes the order α^6 HFS of positronium which proves QED, once again, is a correct theory to very high order in α. It would be very difficult, if not impossible, to obtain this analytical result using traditional methods.

- Completing the expression for $c_4^{(1)}$ and $c_5^{(1)}$ at NLO, $\mathcal{O}(\alpha^2)$.
  We have calculated the contribution to the $c_4^{(1)}$ and $c_5^{(1)}$ coming from the t-channel two-photon QED exchange graphs. This has finally com-

pleted the expression for $c_4^{(1)}$ and $c_5^{(1)}$:

$$\begin{aligned} c_4^{(1)} &= \frac{\alpha^2}{m^2}\left[-\ln\left(\frac{\Lambda}{m}\right)+\frac{232}{45}-\ln 2\right] \\ c_5^{(1)} &= \frac{\alpha^2}{m^2}\left[-\ln\left(\frac{\Lambda}{m}\right)+\frac{4}{15}-3\ln 2+i\pi\right]. \end{aligned} \tag{6.0.3}$$

- Order α^5 HFS of positronium

  Another new result is the order α^5 HFS of positronium for general n and ℓ

$$\begin{aligned} \Delta E_{\rm hfs}(n,\ell,\alpha^5) = -\left(\frac{m\alpha^5}{2\pi n^3}\right) \Bigg[& \left(\ln 2+\frac{16}{9}\right)\delta_{\ell 0} \\ & - \frac{C_{j\ell}}{4(\ell+\frac{1}{2})}\left(1-\delta_{\ell 0}\right)\Bigg], \end{aligned} \tag{6.0.4}$$

  where the coefficients $C_{j\ell}$ are given explicitly by:

$$C_{j\ell} = \begin{cases} \frac{4\ell+5}{2(\ell+1)(2\ell+3)} & \text{if } j=\ell+1 \\ \frac{-1}{2\ell(\ell+1)} & \text{if } j=\ell \\ \frac{-4\ell+1}{2\ell(2\ell-1)} & \text{if } j=\ell-1 \end{cases} \tag{6.0.5}$$

  The above result has been previously obtained for the ground state using the conventional ways.

- Scalar-Scalar bound state

  We have shown the Lamb shift for scalar-scalar bound state to be

$$\Delta E = m\frac{4\alpha}{3\pi}\frac{(Z\alpha)^4}{n^3}\begin{cases} \ln\frac{m}{2<E_{n,0}>}+\frac{71}{360}-\frac{m^2}{5m_e^2} & \text{if } \ell=0 \\ \ln\frac{Z^2m\alpha^2}{2<E_{n,\ell}>} & \text{if } \ell\neq 0, \end{cases} \tag{6.0.6}$$

  This result is valid for the scalar particle case with a mass approximately equal to that of the electron, which does not correspond to a physical case. The order α^5 of Scalar-Scalar bound state for $m_{scalar} \gg m_{electron}$ is still under investigation.

The above new results show that NRQED is not simply a method to simplify the well-known calculations, but is a **powerful** formalism which allows the derivation of new results, such as $\mathcal{O}(\alpha^6)$ HFS, previously unattainable with conventional techniques.

In summary we hope to have convinced the skeptical reader that:

NRQED is simpler, more systematic and more powerful than QED for the study of non-relativistic systems, and particularly non-relativistic bound states.

Appendix A

Table of Integrals(1)

The Integrals which are shown in Tables.(A.1, 2, 3, 4, 5) are directly copied from Ref.[7]. These are very useful integrals for the bound state calculations and scatering diagrams at threshold. Let us define the values in the Tables.

$$\mathcal{A} \equiv \frac{tan^{-1}(|\mathbf{q}|/\gamma)}{|\mathbf{q}|} \tag{A.0.1}$$

$$\mathcal{B} \equiv \frac{\gamma}{(\mathbf{q}^2+\gamma^2)} \tag{A.0.2}$$

$$\mathcal{C} \equiv \frac{\gamma}{(\mathbf{q}^2+4\gamma^2)} \tag{A.0.3}$$

$$\mathcal{D} \equiv \frac{tan^{-1}(|\mathbf{q}|/2\gamma)}{|\mathbf{q}|} \tag{A.0.4}$$

$$A \equiv \frac{|\mathbf{q}|}{\gamma} \tag{A.0.5}$$

$$B \equiv \frac{\mathbf{q}^2}{\mathbf{q}^2+\gamma^2} \tag{A.0.6}$$

f($\mathbf{p}$, $\mathbf{q}$)	$\int d^3p \frac{f(\mathbf{p},\mathbf{q})}{(\mathbf{p}-\mathbf{q})^2(\mathbf{p}^2+\gamma^2)^2}$
1	$\pi^2\mathcal{B}/\gamma^2$
$\mathbf{p}\cdot\mathbf{q}$	$\pi^2\mathcal{A}-\pi^2\mathcal{B}$
$(\mathbf{p}\cdot\mathbf{q})^2$	$\pi^2(\mathbf{q}^2-\gamma^2)\mathcal{A}+\pi^2\gamma^2\mathcal{B}$
$\mathbf{p}^2$	$2\pi^2\mathcal{A}-\pi^2\mathcal{B}$
$\mathbf{p}^2+\gamma^2$	$2\pi^2\mathcal{A}$

Table A.1: Three dimensional integrals

f($\mathbf{p}$, $\mathbf{q}$)	$\int d^3p \frac{f(\mathbf{p},\mathbf{q})}{\left((\mathbf{p}-\mathbf{q})^2+\gamma^2\right)^2(\mathbf{p}^2+\gamma^2)^2}$
1	$2\pi^2\mathcal{C}^2/\gamma^3$
$\mathbf{p}^2$	$2\pi^2\mathcal{C}^2/\gamma+\mathbf{q}^2\pi^2\mathcal{C}^2/\gamma^3$
$(\mathbf{p}\cdot\mathbf{q})$	$\pi^2\mathbf{q}^2\mathcal{C}^2/\gamma^3$
$\mathbf{p}^2\,\mathbf{p}\cdot\mathbf{q}$	$\pi^2\mathcal{C}^2(8\gamma^4+5\gamma^2\mathbf{q}^2+\mathbf{q}^4)/\gamma^3-\pi^2\mathcal{D}$
$(\mathbf{p}\cdot\mathbf{q})^2$	$\pi^2\mathcal{C}^2(8\gamma^4+4\gamma^2\mathbf{q}^2+\mathbf{q}^4)/\gamma^3-\pi^2\mathcal{D}$
$(\mathbf{p}^2)^2$	$\pi^2\mathcal{C}^2(10\gamma^4+6\gamma^2\mathbf{q}^2+\mathbf{q}^4)/\gamma^3$

Table A.2: Three dimensional integrals (continued)

Values of n,m	$4\pi/\gamma^2 \int dq\, A^n\, B^m$
$-10,5$	$35\pi^2/64\gamma$
$-8,4$	$5\pi^2/8\gamma$
$-6,2$	$4\pi/\lambda - 3\pi^2/\gamma$
$-6,3$	$3\pi^2/4\gamma$
$-6,4$	$\pi^2/8\gamma$
$-4,1$	$4\pi/q - 2\pi^2/\gamma$
$-4,2$	π^2/γ
$-4,3$	$\pi^2/4\gamma$
$-4,4$	$\pi^2/8\gamma$
$-4,5$	$5\pi^2/64\gamma$
$-3,0$	$2\pi\gamma/\lambda^2$
$-3,1$	$-4\pi \ln(\lambda/\gamma)/\gamma$
$-3,2$	$2\pi/\gamma$
$-2,0$	$4\pi/\lambda$
$-2,1$	$2\pi^2/\gamma$
$-2,2$	π^2/γ
$-2,3$	$3\pi^2/4\gamma$
$-2,4$	$5\pi^2/8\gamma$
$-1,-1$	$4\pi \ln(\Lambda/\gamma)/\gamma - 4\pi \ln(\lambda/\gamma)/\gamma + 2\pi\gamma/\lambda^2$
$-1,0$	$4\pi \ln(\Lambda/\gamma)/\gamma - 4\pi \ln(\lambda/\gamma)/\gamma$
$-1,1$	$4\pi \ln(\Lambda/\gamma)/\gamma$
$0,-1$	$4\pi\Lambda/\gamma^2 + 4\pi/\lambda$
$0,0$	$4\pi\Lambda/\gamma^2$
$0,1$	$4\pi\Lambda/\gamma^2 - 2\pi^2/\gamma$
$0,2$	$4\pi\Lambda/\gamma^2 - 3\pi^2/\gamma$
$0,3$	$4\pi\Lambda/\gamma^2 - 15\pi^2/4\gamma$
$1,-2$	$2\pi\Lambda^2/\gamma^3 + 8\pi \ln(\Lambda/\gamma)/\gamma - 8\pi \ln(\lambda/\gamma)/\gamma + 2\pi\gamma/\lambda^2$
$1,-1$	$2\pi\Lambda^2/\gamma^3 + 4\pi \ln(\Lambda/\gamma)/\gamma - 4\pi \ln(\lambda/\gamma)/\gamma$
$1,0$	$2\pi\Lambda^2/\gamma^3$
$1,1$	$2\pi\Lambda^2/\gamma^3 - 4\pi \ln(\Lambda/\gamma)/\gamma$
$1,2$	$2\pi\Lambda^2/\gamma^3 - 8\pi \ln(\Lambda/\gamma)/\gamma + 2\pi/\gamma$
$2,-2$	$4\pi\Lambda^3/3\gamma^4 + 8\pi\Lambda/\gamma^2 + 4\pi/\lambda$
$2,-1$	$4\pi\Lambda^3/3\gamma^4 + 4\pi\Lambda/\gamma^2$
$2,0$	$4\pi\Lambda^3/3\gamma^4$
$2,1$	$-4\pi\Lambda/\gamma^2 + 4\pi\Lambda^3/3\gamma^4 + 2\pi^2/\gamma$
$2,2$	$-8\pi\Lambda/\gamma^2 + 4\pi\Lambda^3/3\gamma^4 + 5\pi^2/\gamma$

Table A.3: One dimensional integrals

Values of n,m	$4\pi/\gamma^2 \int dq\, A^n\ B^m\ \mathrm{Tan}^{-1}(A)$
$-5,1$	$4\pi/\lambda - \pi^2/\gamma - 2\pi^2 \ln 2/\gamma$
$-5,2$	$-\pi^2/2\gamma + 2\pi^2 \ln 2/\gamma$
$-5,3$	$3\pi^2/16\gamma$
$-4,2$	$\pi^3/4\gamma - \pi/\gamma$
$-3,0$	$-\pi^2/\gamma + 4\pi/\lambda$
$-3,1$	$2\pi^2 \ln 2/\gamma$
$-3,2$	$\pi^2/2\gamma$
$-3,4$	$11\pi^2/48\gamma$
$-2,1$	$\pi^3/2\gamma$
$-2,2$	$\pi^3/4\gamma + \pi/\gamma$
$-1,-1$	$2\pi^2 \ln(\Lambda/\gamma)/\gamma - \pi^2/\gamma + 4\pi/\lambda$
$-1,0$	$2\pi^2 \ln(\Lambda/\gamma)/\gamma$
$-1,1$	$2\pi^2 \ln(\Lambda/\gamma)/\gamma - 2\pi^2 \ln 2/\gamma$
$-1,2$	$2\pi^2 \ln(\Lambda/\gamma)/\gamma - 2\pi^2 \ln 2/\gamma - \pi^2/2\gamma$
$-1,3$	$2\pi^2 \ln(\Lambda/\gamma)/\gamma - 2\pi^2 \ln 2/\gamma - 13\pi^2/16\gamma$
$1,-2$	$\pi^2\Lambda^2/\gamma^3 + 4\pi^2 \ln(\Lambda/\gamma)/\gamma - 4\pi\Lambda/\gamma^2 + +4\pi/\lambda$
$1,-1$	$\pi^2\Lambda^2/\gamma^3 - 2\pi\Lambda/\gamma^2 + 2\pi^2 \ln(\Lambda/\gamma)/\gamma + \pi^2/\gamma$
$1,0$	$\pi^2\Lambda^2/\gamma^3 - 4\pi\Lambda/\gamma^2 + \pi^2/\gamma$
$1,1$	$\pi^2\Lambda^2/\gamma^3 - 2\pi^2 \ln(\Lambda/\gamma)/\gamma - 4\pi\Lambda/\gamma^2 + \pi^2/\gamma + 2\pi^2 \ln 2/\gamma$
$1,2$	$\pi^2\Lambda^2/\gamma^3 - 4\pi^2 \ln(\Lambda/\gamma)/\gamma - 2\pi\Lambda/\gamma^2 + 3\pi^2/2\gamma + 4\pi^2 \ln 2/\gamma$

Table A.4: Second type of one dimensional integrals

Values of n,m	$4\pi/\gamma^2 \int dq\, A^n\ B^m\ \ln(1+A^2)$
$-4,1$	$-4\pi^2 \ln 2/\gamma + 4\pi^2/\gamma$
$-4,2$	$2\pi^2 \ln 2/\gamma - \pi^2/\gamma$
$-4,3$	$\pi^2 \ln 2/2\gamma - \pi^2/8\gamma$
$-2,0$	$4\pi^2/\gamma$
$-2,1$	$4\pi^2 \ln 2/\gamma$
$-2,2$	$2\pi^2 \ln 2/\gamma + \pi^2/\gamma$
$-2,4$	$55\pi^2/48\gamma + 5\pi^2 \ln 2/4\gamma$
$0,-1$	$8\pi \ln(\Lambda/\gamma)/\gamma - 8\pi\Lambda/\gamma^2 + 8\pi^2/\gamma$
$0,0$	$8\pi \ln(\Lambda/\gamma)/\gamma - 8\pi\Lambda/\gamma^2 + 4\pi^2/\gamma$
$0,1$	$8\pi \ln(\Lambda/\gamma)/\gamma - 8\pi\Lambda/\gamma^2 + 4\pi^2/\gamma - 4\pi^2 \ln 2/\gamma$
$0,2$	$8\pi \ln(\Lambda/\gamma)/\gamma - 8\pi\Lambda/\gamma^2 + 3\pi^2/\gamma - 6\pi^2 \ln 2/\gamma$
$0,3$	$8\pi \ln(\Lambda/\gamma)/\gamma - 8\pi\Lambda/\gamma^2 + 15\pi^2/8\gamma - 15\pi^2 \ln 2/2\gamma$

Table A.5: Third type of one dimensional integrals

Appendix B

Table of Integrals(2)

The following Integrals have been preformed by A. H. Hoang[38]. These Integrals are very useful in doing the scattering calculations above the threshold.

$$\begin{aligned} I_1 &= \int dp \frac{p^2}{p^2 - p_0^2 - i\epsilon} \\ &= \Lambda + i\pi \frac{p_0}{2} \end{aligned} \tag{B.0.1}$$

$$\begin{aligned} I_2 &= \int dp \frac{p}{p^2 - p_0^2 - i\epsilon} \ln\left(\frac{(p+p_0)^2 + \lambda^2}{(p-p_0)^2 + \lambda^2}\right) \\ &= \pi tan^{-1}\left(\frac{2p_0}{\lambda}\right) + i\frac{\pi}{2} \ln\left(1 + \frac{4p_0^2}{\lambda^2}\right) \end{aligned} \tag{B.0.2}$$

$$\begin{aligned} I_3 &= \int dp \frac{p}{p^2 - p_0^2 - i\epsilon} \ln\left(\frac{(q+p)^2 + \lambda^2}{(q-p)^2 + \lambda^2}\right) \\ &= \pi\left[tan^{-1}\left(\frac{q+p_0}{\lambda}\right) + tan^{-1}\left(\frac{q-p_0}{\lambda}\right) + \frac{i}{2} \ln\left(\frac{(q+p_0)^2 + \lambda^2}{(q-p_0)^2 + \lambda^2}\right)\right] \end{aligned} \tag{B.0.3}$$

For the following Integrals, we present the answer with the condition $\lambda \ll p_0$:

$$\begin{aligned} I_4 &= \int dq dp \frac{q}{(p^2 - p_0^2 - i\epsilon)(q^2 - p_0^2 - i\epsilon)} \ln\left(\frac{(q+p)^2 + \lambda^2}{(q-p)^2 + \lambda^2}\right) \ln\left(\frac{(p+p_0)^2 + \lambda^2}{(p-p_0)^2 + \lambda^2}\right) \\ &= \frac{1}{p_0}\left[\frac{\pi^4}{24} - \frac{1}{2}\pi^2 \ln\left(\frac{2p_0}{\lambda}\right)^2 + \frac{i\pi^3}{2} \ln\left(\frac{2p_0}{\lambda}\right)\right] \end{aligned} \tag{B.0.4}$$

$$\begin{aligned} I_5 &= \int dq dp \frac{qp}{(p^2 - p_0^2 - i\epsilon)(q^2 - p_0^2 - i\epsilon)} \ln\left(\frac{(q+p)^2 + \lambda^2}{(q-p)^2 + \lambda^2}\right) \\ &= \pi^2\left[\ln\left(\frac{\Lambda}{\lambda}\right) - \ln\left(\frac{2p_0}{\lambda}\right) + \frac{i\pi}{2}\right] \end{aligned} \tag{B.0.5}$$

$$
\begin{aligned}
I_6 &= \int dqdp \frac{q}{(q^2 - p_0^2 - i\epsilon)} \ln\left(\frac{(q+p)^2+\lambda^2}{(q-p)^2+\lambda^2}\right) \ln\left(\frac{(p+p_0)^2+\lambda^2}{(p-p_0)^2+\lambda^2}\right) \\
&= \pi^2\left[4p_0 - 4p_0 \ln\left(\frac{2p_0}{\lambda}\right) + 2i\pi p_0\right] \qquad \text{(B.0.6)} \\
I_7 &= \int dp \frac{p^3}{(p^2 - p_0^2 - i\epsilon)} \ln\left(\frac{(p+p_0)^2+\lambda^2}{(p-p_0)^2+\lambda^2}\right) \\
&= p_0\left[\frac{1}{2}p_0\pi^2 + ip_0\pi \ln\left(\frac{2p_0}{\lambda}\right) + 4\Lambda\right] \qquad \text{(B.0.7)} \\
I_8 &= \int dqdp \frac{q^3}{(q^2 - p_0^2 - i\epsilon)(p^2 - p_0^2 - i\epsilon)} \ln\left(\frac{(q+p)^2+\lambda^2}{(q-p)^2+\lambda^2}\right) \ln\left(\frac{(p+p_0)^2+\lambda^2}{(p-p_0)^2+\lambda^2}\right) \\
&= p_0^2 I_4 + 4\Lambda I_2 - 2p_0\pi^2 \qquad \text{(B.0.8)}
\end{aligned}
$$

Bibliography

[1] W.E. Caswell and G.P. Lepage, *Phys. Lett.* **167B**, 437 (1986).

[2] P. Labelle, *Effective Field Theories for QED Bound States: Extending Nonrelativistic QED to Study Retardation Effects*, preprint McGill-96/33 (hep-ph/9608491).

[3] M. Luke, A. V. Manohar, *Phys. Rev.* D **55**, 4129 (1997).

[4] M. Luke, M. Savage, *Phys. Rev.* D **57**, 413 (1998).

[5] P. Labelle, G. P. Lepage, and U. Magnea, *Phys. Rev. Lett.* **72**, 2006 (1994).

[6] B. Grinstein and I. Z. Rothstein, *Phys. Rev.* D **57**, 1 (1998).

[7] P. Labelle, Cornell University Ph.D. thesis, UMI-94-16736-mc (microfiche), 1994.

[8] NRQED was introduced in:

For pedagogical introductions, see:

"What is renormalization?", G.P. Lepage, invited lectures given at the TASI-89 Summer School, Boulder, Colorado; "Quantum Electrodynamics for Nonrelativistic Systems and High Precision Determinations of α", G.P. Lepage and T. Kinoshita, in *Quantum Electrodynamics*, T.Kinoshita ed. (World Scientific, Singapore, 1990); "NRQED in bound states: applying renormalization to an effective field theory", P. Labelle, XIV MRST Proceedings (1992).

[9] C.Itzykson and Zuber, Quantum Field Theory, McGraw-Hill,1980.

[10] I.J.R. Aitchison, A.J.G. Hey, Gauge Theories In Particle Physics, Adam-Hilger 1989.

[11] P. Labelle, "NRQED in bound states: applying renormalization to an effective field theory", proceedings of the fourteenth MRST Meeting, P.J. O'Donnell ed., University of Toronto, 1992, hep-ph/9209266.

[12] T. Kinoshita and M. Nio, *Phys. Rev.* D **53**, 4909 (1996).

[13] T. Kinoshita and M. Nio, *Phys. Rev.* D **55**, 7267 (1997).

[14] P.Labelle, S M Zebarjad, *An Effective Field Theory Approach to Nonrelativistic Bound States in QED and Scalar QED*, preprint McGill-97/01.

[15] J.R. Sapirstein and D.R. Yennie in *Quantum Electrodynamics*, ed. by T. Kinoshita (World Scientific, Singapore, 1990).

[16] P. Labelle, S. M. Zebarjad *Derivation of the Lamb Shift Using an Effective Field Theory*, preprint McGill-96/41 (hep-ph/9611313).

[17] P. Labelle, S.M. Zebarjad and C.P. Burgess, *Phys. Rev.* D **56**, 8053 (1997).

[18] D.A. Owen, *Phys. Rev.* D **42**, 3534 (1990) M. Halpert and D.A. Owen, *J. Phys.* G **20**, 51 (1994).

[19] A. Hoang, P. Labelle and S.M. Zebarjad, *Phys. Rev. Lett.* **79**, 3387 (1997).

[20] S. Gupta, W. Repko and C. Suchyta III, *Phys. Rev.* D **40**, 4100 (1989)

[21] T. Fulton and P.C. Martin, *Phys. Rev.* **95**, 811 (1954)

[22] A. Pineda and J. Soto, *Effective Field Theory for Ultrasoft Momenta in NRQCD and NRQED*, (hep-ph/9707481).

[23] A. Pineda and J. Soto, *The Lamb Shift in Dimensional Regularisation*, (hep-ph/9711292).

[24] E.H. Wichmann and C.H. Woo,J. Math. Phys. **5**, 178 (1961),
L. Hostler, J. Math Phys. **5**, 591 (1964).

[25] J Schwinger, J. Math. Phys. **5**, (1964) 1601.

[26] S. Mohorovičić, *Astron. Nachr.* **253**, 94 (1934).

[27] M. Deutsch, *Phys. Rev.* **82**, 455 (1951);
M. Deutsch and E. Dulit, *Phys. Rev.* **84**, 601 (1951).

[28] M. W. Ritter, P.O. Egan, V.W. Hughes and K.A. Woodle, *Phys. Rev.* A **30**, 1984 (1331).

[29] G.T. Bodwin and D.R. Yennie, *Phys. Reports* **43**, 267 (1978);
W.E. Caswell and G.P. Lepage, *Phys. Rev.* A **20**, 36 (1979).

[30] S.G. Karshenboĭm, *JETP Lett.* **76** (4) 1993.

[31] J. Schwinger, *Particles, Sources and Fields*, Vol II, (Addison-Wesley, New York, 1973).

[32] G. Källen and A. Sabry, *K. Dan. Vidensk. Selsk. Mat.-Fys. Medd.* **29** (1955) No. 17.

[33] R. Barbieri and E. Remiddi, *Nuovo Cim.* **13A**, 99 (1973);
D. J Broadhurst, J. Fleischer and O.V. Tarasov, *Z. Phys.* **C 60**, 287 (1993).

[34] R. Barbieri, P. Christillin and E. Remiddi, *Phys. Rev.* A **8**, 2266 (1973);
R. Barbieri and E. Remiddi, *Phys. Lett.* **65B**, 258 (1976).

[35] G.T. Bodwin, E. Braaten and G.P. Lepage, *Phys. Rev.* D **51**, 1125 (1995).

[36] A.H. Hoang, *Phys. Rev.* D **56**, 7276 (1997).

[37] A.H. Hoang, *The Vacuum Polarization function to $\mathcal{O}(\alpha^2)$ accuaracy Near Threshold and Darwin Corrections*, UCSD preprint UCSD/PTH 97-04 (hep-ph/9702331).

[38] A.H. Hoang, unpublished table of Integrals.

[39] J. Pirenne, *Arch. Sci. Phys. Nat.* **28**, 233 (1946).

[40] R. Karplus and A. Klein, *Phys. Rev.* **87**, 848 (1952).

[41] J.R. Sapirstein, E.A. Terray and D.R. Yennie, *Phys. Rev.* D **29**, 2290 (1984).

[42] A trivial correction to order $m_e\alpha^6$ is obtained by including the anomalous magnetic moment to two loops in the lowest order Fermi correction, $m_e\alpha^4/3 \to m_e\alpha^4(1+a_e)^2/3$ which leads to an $\mathcal{O}(m_e\alpha^6)$ contribution equal to $m_e\alpha^6[\frac{1}{2\pi^2}(\frac{215}{108}+\zeta_3)+\frac{1}{18}-\frac{1}{3}\ln 2] \approx -0.26$ MHz. This correction was not included in the non-annihilation contributions computed in the other references. We are grateful to G. Adkins for bringing this point to our attention.

[43] K. Pachucki, *Phys. Rev.* A **56**, 297 (1997).

[44] G.S. Adkins, Y.M. Aksu and M.H.T. Bui, *Phys. Rev.* A **47**, 2640 (1993).

[45] G.S. Adkins, M.H.T. Bui and D. Zhu, *Phys. Rev.* A **37**, 4071 (1988).

[46] G.S. Adkins, R.N. Fell and P.M. Mitrikov *Phys. Rev. Lett.* **79**, 3383 (1997).